



Mathematical Modelling and Numerical Simulation with Applications

ISSN Online : 2791-8564

Year : 2022

Volume : 2

Issue : 4



www.mmnsa.org

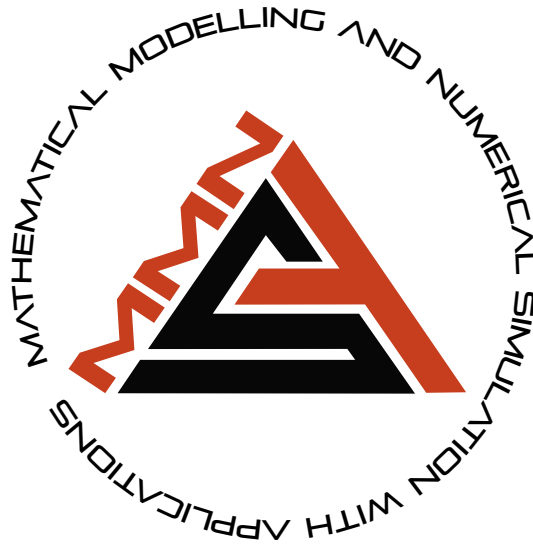
EDITOR-IN-CHIEF

Mehmet Yavuz, PhD,
Necmettin Erbakan University, Turkey

M
M
N
S
A

VOLUME: 2 ISSUE: 4
ISSN ONLINE: 2791-8564

December 2022
<https://www.mmnsa.org>



MATHEMATICAL MODELLING AND NUMERICAL SIMULATION WITH APPLICATIONS

Editor-in-Chief and Publisher

Mehmet Yavuz
Department of Mathematics and Computer Sciences,
Faculty of Science, Necmettin Erbakan University,
Meram Yeniyol, 42090 Meram, Konya / TÜRKİYE
mehmetyavuz@erbakan.edu.tr

Editorial Board

Abdeljawad, Thabet
Prince Sultan University
Saudi Arabia

Agarwal, Praveen
Anand International College of Engineering
India

Aguilar, José Francisco Gómez
CONACyT- National Center for Technological Research
and Development
Mexico

Ahmad, Hijaz
International Telematic University Uninettuno
Italy

Arqub, Omar Abu
Al-Balqa Applied University
Jordan

Asjad, Muhammad Imran
University of Management and Technology
Pakistan

Atangana, Abdon
University of the Free State
South Africa

Baleanu, Dumitru
Cankaya University, *Türkiye*;
Institute of Space Sciences, Bucharest, *Romania*

Başkonuş, Hacı Mehmet
Harran University
Türkiye

Biswas, Md. Haider Ali
Khulna University
Bangladesh

Bonyah, Ebenezer
Department of Mathematics Education
Ghana

Bulai, Iulia Martina
University of Basilicata
Italy

Cabada, Alberto
University of Santiago de Compostela
Spain

Dassios, Ioannis
University College Dublin
Ireland

Eskandari, Zohreh
Shahrekord University
Iran

Flaut, Cristina
Ovidius University of Constanta
Romania

González, Francisco Martínez
Universidad Politécnica de Cartagena
Spain

Gürbüz, Burcu
Johannes Gutenberg-University Mainz, Institute of
Mathematics, *Germany*

Hammouch, Zakia
ENS Moulay Ismail University Morocco;
Thu Dau Mot University Vietnam and China Medical
University, *Taiwan*

Hristov, Jordan
University of Chemical Technology and Metallurgy
Bulgaria

Ibadula, Denis
Ovidius University of Constanta
Romania

Jafari, Hossein
University of Mazandaran, *Iran*;
University of South Africa, *South Africa*

Jajarmi, Amin
University of Bojnord
Iran

Jain, Shilpi
Poornima College of Engineering, Jaipur
India

Kaabar, Mohammed K.A.
Washington State University
USA

Kumar, Devendra
University of Rajasthan
India

Kumar, Sunil
National Institute of Technology
India

Lupulescu, Vasile
Constantin Brâncuși University of Târgu-Jiu
Romania

Merdan, Hüseyin
TOBB University of Economy and Technology
Türkiye

Mohammed S. Abdo
Hodeidah University, Al-Hodeidah, Department of
Mathematics
Yemen

Naik, Parvaiz Ahmad
School of Mathematics and Statistics, Xi'an Jiaotong
University, *China*

Noeiaghdam, Samad
Irkutsk National Research Technical University
Russian Federation

Owolabi, Kolade
Federal University of Technology
Nigeria

Otero-Espinar, Maria Victoria
University of Santiago de Compostela
Spain

Özdemir, Necati
Balıkesir University
Türkiye

Pinto, Carla M.A.
ISEP, *Portugal*

Povstenko, Yuriy
Jan Długosz University in Czeszochowa
Poland

Qureshi, Sania
Mehran University of Engineering and Technology
Pakistan

Sabatier, Jocelyn
Bordeaux University
France

Safaei, Mohammad Reza
Florida International University
USA

Salahshour, Soheil
Bahçeşehir University
Türkiye

Sarı, Murat
Yıldız Technical University
Türkiye

Sarris, Ioannis E.
University of West Attica
Greece

Sene, Ndolane
Cheikh Anta Diop University
Senegal

Singh, Jagdev
JECRC University
India

Stamova, Ivanka
University of Texas at San Antonio
USA

Torres, Delfim F. M.
University of Aveiro
Portugal

Townley, Stuart
University of Exeter
United Kingdom

Valdés, Juan Eduardo Nápoles
Universidad Nacional del Nordeste
Argentina

Veerasha, Pundikala
Christ University
India

Weber, Gerhard-Wilhelm
Poznan University of Technology
Poland

Xu, Changjin
Guizhou University of Finance and Economics
China

Yalçınkaya, İbrahim
Necmettin Erbakan University
Türkiye

Yang, Xiao-Jun
China University of Mining and Technology
China

Yuan, Sanling
University of Shanghai for Science and Technology
China

Technical Editor

Halil İbrahim Özer
Department of Computer and Instructional Technologies
Education, Ahmet Keleşođlu Faculty of Education,
Necmettin Erbakan University, Meram Yenyol, 42090
Meram, Konya / TÜRKİYE
hiozer@gmail.com

English Editor

Abdulkadir Ünal
School of Foreign Languages, Foreign Languages, Alanya
Alaaddin Keykubat University, Antalya / TÜRKİYE
abdulkadir.unal@alanya.edu.tr

Editorial Secretariat

Fatma Özlem Coşar
Department of Mathematics and Computer Sciences,
Faculty of Science, Necmettin Erbakan University,
Meram Yenyol, 42090 Meram, Konya / TÜRKİYE

Müzeyyen Akman
Department of Mathematics and Computer Sciences,
Faculty of Science, Necmettin Erbakan University,
Meram Yenyol, 42090 Meram, Konya / TÜRKİYE

Contents

Research Articles

- 1 A model for COVID-19 and bacterial pneumonia coinfection with community- and hospital-acquired infections
Angel G. Cervantes Pérez, David Adeyemi Oluyori 197-210
- 2 A new analytical approach to the (1+1)-dimensional conformable Fisher equation
Gölnur Yel, Miraç Kayhan, Armando Ciancio 211-220
- 3 On the relations between a singular system of differential equations and a system with delays
Ioannis Dassios 221-227
- 4 Dynamics of a fractional-order COVID-19 model under the nonsingular kernel of Caputo-Fabrizio operator
Saeed Ahmad, Dong Qiu, Mati ur Rahman 228-243
- 5 Mathematical modelling of a glucose-insulin system for type 2 diabetic patients in Chad
Adam Hassan Adoum, Mahamat Saleh Daoussa Haggar, Jean Marie Ntaganda 244-251



RESEARCH PAPER

A model for COVID-19 and bacterial pneumonia coinfection with community- and hospital-acquired infections

Angel G. Cervantes Pérez ^{1,*},[†] and David Adeyemi Oluyori ^{2,†}

¹Facultad de Matemáticas, Universidad Autónoma de Yucatán, Mérida, Yucatán, Mexico, ²Department of Mathematics, School of Physical Science, Ahmadu Bello University, Zaria, Kaduna State, Nigeria

*Corresponding Author

[†]agcp26@hotmail.com (Angel G. Cervantes Pérez); oluyoridavid@gmail.com (David Adeyemi Oluyori)

Abstract

We propose a new epidemic model to study the coinfection dynamics of COVID-19 and bacterial pneumonia, which is the first model in the literature used to describe mathematically the interaction of these two diseases while considering two infection ways for pneumonia: community-acquired and hospital-acquired transmission. We show that the existence and local stability of equilibria depend on three different parameters, which are interpreted as the basic reproduction numbers of COVID-19, bacterial pneumonia, and bacterial population in the hospital. Numerical simulations are performed to complement our theoretical analysis, and we show that both diseases can persist if the basic reproduction number of COVID-19 is greater than one.

Key words: Coronavirus; bacterial pneumonia; coinfection

AMS 2020 Classification: 34C60; 34D20; 92D30

1 Introduction

The virulent nature of Coronavirus Disease 2019 (COVID-19) has continued to be significant as a public health concern since the WHO declared it a global pandemic in the early part of 2020. Trend analysis has shown that one of the main causes of death resulting from Coronavirus has been attributed to secondary causes due to bacterial and viral infections. As the Coronavirus Disease continues to attract attention from various stakeholders in health and governance, who work relentlessly to unravel its dynamics and curtail its spread through pharmaceutical and non-pharmaceutical methods, studies have shown that Respiratory Tract Infections (RTIs) can predispose patients to coinfections [1, 2]. RTIs are infections of body parts involved in breathing, such as sinuses, throat, airways or lungs, which can be caused by several bacteria and viruses such as influenza [3]. The most significant of these RTIs, which affect the upper respiratory tract include tonsillitis, pharyngitis, sinusitis and certain types of influenza (such as H1N1) [4] with symptoms such as cough, sore throat, nasal congestion, headache, among others.

Historically, according to [5], a large part of the death toll recorded in the 1918 influenza pandemic was due to bacterial infection caused by *Streptococcus pneumoniae*. Evidence from the study in [6] revealed that poor outcomes in the influenza (H1N1) pandemic were associated with coinfections. Aside from H1N1, MERS and SARS-CoV have been identified as major respiratory tract infections in the last decade. These have so far been detected by highly sensitive techniques such as MALDI-TOF and Multiplex PCR. Therefore, the study of coinfections in a pandemic situation such as COVID-19 has become an essential need due to the clinical,

diagnostic and therapeutic challenges it raises [7]. To further buttress the aforesaid, Lansbury et al. [8] highlighted some important aspects of bacterial and viral infections in COVID-19 and antimicrobial prescription.

Despite the proven epidemiological significance of coinfections in the severity of respiratory diseases, they are largely understudied during a large outbreak of respiratory infections such as SARS-CoV-2 [9]. According to Zhou et al. [10], it was shown that 50% of the fatalities due to COVID-19 result from secondary bacterial infections. Also, Chen et al. [11] attribute these deaths to bacterial and fungal infections. Furthermore, in [9], clinical evidence has revealed the complexity in the diagnoses of coinfections when the causative virus is resident in the host before the viral infection or has been contacted nosocomially. The authors in [12] reported that patients presenting SARS-CoV-2 infection have a clinical phenotype that is very close to that of bacterial pneumonia.

Mathematical modelling of epidemics has become a crucial tool to forecast the future course of an outbreak, as well as to evaluate possible strategies to control the spread of diseases. The analysis of these models is useful to decide the best course of action to eradicate a disease since it is often less costly to perform numerical simulations than experimental studies. Also, it is easier to determine the different possible outcomes of an epidemic by studying the equilibrium states and the threshold dynamics of a model than to test it in real life. The history of epidemic modelling has developed in relatively recent times. Although an early model was created by Bernoulli in 1760 to evaluate the effectiveness of inoculating healthy people against the smallpox virus [13], deterministic epidemic models became increasingly popular in the early 20th century, starting with Ross's differential equation model on the control of malaria [14]. The susceptible-infectious-recovered model was inspired by the papers by Ross [15] in 1916 and Ross and Hudson [16, 17] in 1917, who studied *a priori* pathometry, followed by Kermack and McKendrick's integro-differential age-structured model [18] in 1927. In subsequent decades, a plethora of epidemic models was studied in the literature, many based on ordinary differential equations (ODEs). Recent works have employed a range of different methods, such as fractional order differential equations, partial differential equations, fuzzy logic, network-based and stochastic models, with the aim to describe the complexities of pathogen transmission. However, the complexity of these methods often precludes an intuitive understanding of the interactions between its variables and parameters [19], and simple models that can be adequately fitted to some epidemic data can be more useful than more complex models that also provide an adequate fit to the same data [20]. Deterministic ODE models have the advantage of having an extensive theory for their theoretical and numerical study [21], they have also been successfully fitted to real-world epidemic data and their prediction accuracy can be improved by methods such as segmentation of epidemic event sequences [22].

During the course of the COVID-19 pandemic, many different works have emerged to model mathematically the spread of SARS-CoV-2. Several recent papers have focused on analyzing the effects of vaccination campaigns [23, 24, 25, 26], as well as the relationship of COVID-19 with conditions such as diabetes [27] and heart attacks [28]. Some authors have incorporated the dynamics of new strains of SARS-CoV-2, such as the Omicron variant [28], while others have developed coinfection models. As a background to our present work, recent studies have established clinical evidence of coinfections of SARS-CoV-2 (COVID-19) with other diseases such as tuberculosis [7, 29, 30, 31, 32, 33], influenza A (H1N1) [34, 35, 36, 37, 38] and Middle East Respiratory Syndrome Coronavirus (MERS-CoV) [39], as well as bacterial coinfections [40]. In response to the foregoing, researchers have developed mathematical models to study the coinfection dynamics of COVID-19. Soni and Singh [41] used a systems biology approach to study a cellular-level model for SARS-CoV-2-influenza coinfection, they performed simulations with the Matlab SimBiology toolbox to suggest therapeutic intervention points. Tchoumi et al. [42] proposed a compartmental population model for coinfection with malaria. They determined conditions for the stability of equilibria, showed that the model may undergo a backward bifurcation and derived conditions for optimal control to mitigate the spread of both diseases. Tuberculosis-COVID-19 coinfection has been modelled by Bandedar and Ghosh [43], who considered a model with waning immunity and performed a bifurcation and stability analysis, as well as simulations using data from India. A different model for tuberculosis coinfection was studied by Rwezaura et al. [44], who investigated the effects of COVID-19 vaccination and treatment control and performed parameter fitting with data from Indonesia. Optimal control for a COVID-19-dengue model was studied by Omame et al. [45] using five controls; furthermore, the authors fitted their model to the cumulative COVID-19 cases and deaths in Brazil. In [46], Omame et al. analyzed a fractional coinfection model for diabetes and COVID-19 using the Atangana-Baleanu derivative. The authors studied the Hyers-Ulam stability and global asymptotic stability and fitted the model to COVID-19 data from Indonesia.

Despite the above-mentioned developments in the literature, no model has been proposed to study the coinfection dynamics of COVID-19 with bacterial pneumonia. Bacterial pneumonia is an inflammation of the lungs caused by infection with certain bacteria. Depending on the location where a person acquires the infection, it can be classified as either *community-acquired pneumonia* or *hospital-acquired pneumonia*. Community-acquired pneumonia is by far the most common type [47]. On the other hand, hospital-acquired pneumonia is usually more severe because the infecting organisms tend to be more aggressive, less likely to respond to antibiotics and harder to treat [48]. In this vein, we see from [49, 50, 51] that clinical studies have shown that critically ill COVID-19 patients admitted to the hospital suffer more frequent bacterial or fungal nosocomial infections, and patients with underlying risk factors such as advanced age, mechanical ventilation or prolonged hospital stay are more prone to these complications. Moreover, patients with mild COVID-19 infection are less likely to develop a more severe disease as a result of coinfection upon admission to medical facilities compared to those with high-risk factors due to bacterial and fungal infections.

In view of the above evidence, we think that there is a need to mathematically study the coinfection dynamics of COVID-19 with bacterial pneumonia. However, none of the models mentioned above has the structure necessary to be applied to this disease, considering that bacterial infections can be acquired both in the community and in the hospital. Hence, we aim to study here a new ODE model tailored specially to these needs. In contrast to the work by Giannella et al. [40], who developed a predictive model to stratify the risk of bacterial coinfection based on an observational study of hospitalised COVID-19 patients, we intend to use a theoretical approach of compartmental ODE models, which allows us to make simulations not only for the hospitalised subpopulation but in the community at large.

This paper is structured as follows: in Section 2, we introduce three models: a sub-model for COVID-19 infection, a sub-model for bacterial pneumonia, and a coinfection model that includes the dynamics of both diseases. In Section 3, we determine some basic properties for the two sub-models. In Section 4, we provide an analysis of the coinfection model. In Section 5, we perform some numerical simulations to illustrate the dynamics of the coinfection model. Finally, we provide a summary and discussion of our results in Section 6 and some concluding remarks in Section 7.

2 Description of the models

COVID-19 infection model

The COVID-19 infection model subdivides the human population into four compartments: susceptible (S), infected but not hospitalised (I), hospitalised (H), and recovered (R). This model can be described by the following system of equations:

$$\begin{aligned} S' &= \Lambda + \sigma R - \mu S - \alpha SI, \\ I' &= \alpha SI - (\gamma + \eta + \mu)I, \\ H' &= \eta I - (\theta + \delta + \mu)H, \\ R' &= \gamma I + \theta H - \mu R - \sigma R. \end{aligned} \quad (1)$$

The interpretation of parameters is as follows:

- Λ : recruitment rate of susceptible population.
- μ : natural death rate.
- α : transmission rate of COVID-19.
- γ : recovery rate of people infected with COVID-19 but not hospitalised.
- θ : recovery rate of hospitalised people.
- η : hospitalisation rate.
- δ : COVID-19-induced death rate of hospitalised people.
- σ : rate of loss of immunity against COVID-19 infection.

For model (1), we assume that COVID-19 is transmitted by contact between susceptible and infected (but not hospitalised) people at a bilinear rate αSI . A portion of the infected population is admitted to hospitals at a rate η . The average recovery time is $1/\gamma$ for non-hospitalised people and $1/\theta$ for hospitalised people. Further, we assume that only hospitalised patients may have a COVID-19-induced death. Lastly, people recovered from infection lose their natural immunity after an average time $1/\sigma$.

Bacterial pneumonia infection model

The model for bacterial pneumonia subdivides the human population into three compartments: susceptible (S), infected (I), and recovered (R). We also consider a compartment B representing the population of bacteria in the environment. The model is given by the following system:

$$\begin{aligned} S' &= \Lambda - \mu S - bSI - b_1SB, \\ I' &= bSI + b_1SB - \phi I - \mu I - \delta I, \\ R' &= \phi I - \mu R, \\ B' &= pI + rB \left(1 - \frac{B}{\kappa}\right) - mB. \end{aligned} \quad (2)$$

The parameters of this model can be interpreted as follows:

- Λ : recruitment rate of susceptible population.
- μ : natural death rate.
- b : transmission rate of community-acquired bacterial pneumonia.
- b_1 : transmission rate of hospital-acquired bacterial pneumonia.
- δ : disease-induced death rate of infected population.
- ϕ : recovery rate of people with bacterial infection.
- p : rate of excretion of bacteria in the environment by infected people.
- r : maximal per capita growth rate of bacteria in the environment.
- κ : carrying capacity of bacterial population.
- m : clearance rate of bacterial population.

For model (2), we assume that susceptible people get community-acquired pneumonia at a rate bSI and hospital-acquired pneumonia at a rate b_1SB . Infected people have a pneumonia-induced death rate δ and may recover at a rate ϕ . The population of bacteria in the environment follows a logistic growth rate and may additionally increase at a rate proportional to the number of infected people.

Coinfection model

Based on models (1) and (2), we propose a combined COVID-19–bacterial pneumonia coinfection model. We will consider three stages for COVID-19 infection and four for bacterial infection, which gives twelve mutually exclusive compartments: bacterial pneumonia susceptible and COVID-19 susceptible (X_{SS}); bacterial pneumonia susceptible and COVID-19 mildly infected (X_{SI}); bacterial pneumonia susceptible and COVID-19 hospitalised (X_{SH}); bacterial pneumonia susceptible and COVID-19 recovered (X_{SR}); bacterial pneumonia infected and COVID-19 susceptible (X_{IS}); bacterial pneumonia infected and COVID-19 mildly infected (X_{II}); bacterial pneumonia infected and COVID-19 hospitalised (X_{IH}); bacterial pneumonia infected and COVID-19 recovered (X_{IR}); bacterial pneumonia recovered and COVID-19 susceptible (X_{RS}); bacterial pneumonia recovered and COVID-19 mildly infected (X_{RI}); bacterial pneumonia recovered and COVID-19 hospitalised (X_{RH}); and bacterial pneumonia recovered and COVID-19 recovered (X_{RR}). Additionally, we consider a compartment B representing concentration of bacteria in the hospital environment. We make the following assumptions:

- i. COVID-19 is transmitted by contact with people in the X_{SI} , X_{II} and X_{RI} compartments.
- ii. The population susceptible to COVID-19 are infected by this disease at a rate α_1 if they have bacterial pneumonia, and at a rate α otherwise.
- iii. The hospitalisation rate for people coinfecting with COVID-19 and community-acquired pneumonia increases by an amount η_1 with respect to people with only COVID-19.
- iv. The COVID-19 recovery rate for hospitalised people is θ_1 if they are coinfecting, and θ otherwise.
- v. Non-hospitalised people get community-acquired pneumonia by contact with people in the X_{IS} , X_{II} and X_{IR} compartments.
- vi. Non-hospitalised people are infected with pneumonia at a rate b_1 if they have COVID-19, and at a rate b otherwise.
- vii. People hospitalised due to COVID-19 get hospital-acquired pneumonia at a rate proportional to the concentration of bacteria in the environment.
- viii. The disease-induced death rate for coinfecting hospitalised patients is increased by an amount δ_2 with respect to those with only COVID-19.
- ix. The pneumonia-induced death rate for non-hospitalised people is δ_0 if they have COVID-19, and δ otherwise.
- x. The pneumonia recovery rate is ϕ_1 for people in the X_{II} compartment, ϕ_2 for the X_{IH} compartment, and ϕ for the X_{IS} and X_{IR} compartments.

The schematic diagram of model (3) can be seen in Figure 1. All parameters are assumed to be positive.

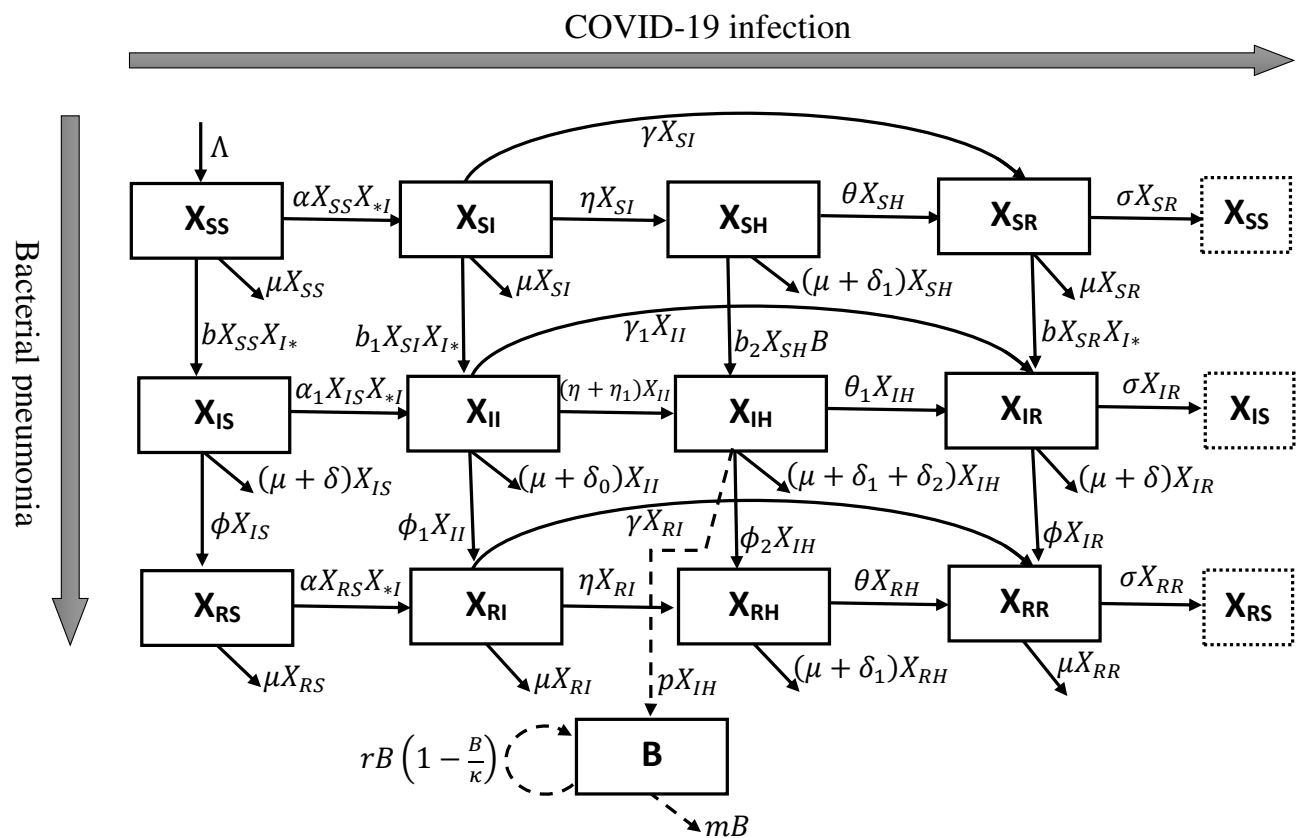


Figure 1. Schematic diagram of the coinfection model. Solid lines represent the transition between compartments. Dashed lines represent the proliferation of bacteria. X_{*I} denotes $X_{SI} + X_{II} + X_{RI}$ and X_{I*} denotes $X_{IS} + X_{II} + X_{IR}$.

The above assumptions yield a coinfection model given by the following system of 13 differential equations:

$$\begin{aligned}
 X'_{SS} &= \Lambda + \sigma X_{SR} - \mu X_{SS} - \alpha X_{SS} (X_{SI} + X_{II} + X_{RI}) - b X_{SS} (X_{IS} + X_{II} + X_{IR}), \\
 X'_{SI} &= \alpha X_{SS} (X_{SI} + X_{II} + X_{RI}) - (\gamma + \eta + \mu) X_{SI} - b_1 X_{SI} (X_{IS} + X_{II} + X_{IR}), \\
 X'_{SH} &= \eta X_{SI} - \theta X_{SH} - (\mu + \delta_1) X_{SH} - b_2 X_{SH} B, \\
 X'_{SR} &= \gamma X_{SI} + \theta X_{SH} - \mu X_{SR} - \sigma X_{SR} - b X_{SR} (X_{IS} + X_{II} + X_{IR}), \\
 X'_{IS} &= \sigma X_{IR} + b X_{SS} (X_{IS} + X_{II} + X_{IR}) - \alpha_1 X_{IS} (X_{SI} + X_{II} + X_{RI}) - (\mu + \delta) X_{IS} - \phi X_{IS}, \\
 X'_{II} &= b_1 X_{SI} (X_{IS} + X_{II} + X_{IR}) + \alpha_1 X_{IS} (X_{SI} + X_{II} + X_{RI}) - (\gamma_1 + \eta + \eta_1 + \mu + \delta_0 + \phi_1) X_{II}, \\
 X'_{IH} &= (\eta + \eta_1) X_{II} + b_2 X_{SH} B - \theta_1 X_{IH} - (\mu + \delta_1 + \delta_2) X_{IH} - \phi_2 X_{IH}, \\
 X'_{IR} &= b X_{SR} (X_{IS} + X_{II} + X_{IR}) + \gamma_1 X_{II} + \theta_1 X_{IH} - (\mu + \delta) X_{IR} - \phi X_{IR} - \sigma X_{IR}, \\
 X'_{RS} &= \sigma X_{RR} + \phi X_{IS} - \mu X_{RS} - \alpha X_{RS} (X_{SI} + X_{II} + X_{RI}), \\
 X'_{RI} &= \phi_1 X_{II} + \alpha X_{RS} (X_{SI} + X_{II} + X_{RI}) - (\gamma + \eta + \mu) X_{RI}, \\
 X'_{RH} &= \eta X_{RI} + \phi_2 X_{IH} - \theta X_{RH} - (\mu + \delta_1) X_{RH}, \\
 X'_{RR} &= \phi X_{IR} + \gamma X_{RI} + \theta X_{RH} - \mu X_{RR} - \sigma X_{RR}, \\
 B' &= p X_{IH} + r B \left(1 - \frac{B}{\kappa}\right) - m B.
 \end{aligned} \tag{3}$$

3 Analysis of sub-models

Before studying the dynamics of the coinfection model (3), we will analyze the two sub-models (COVID-19 only and bacterial pneumonia only).

Analysis of the COVID-19 infection model

The COVID-19-only model (1) has a disease-free equilibrium (DFE) given by

$$\mathcal{E}_{C0} = (S, I, H, R) = \left(\frac{\Lambda}{\mu}, 0, 0, 0\right).$$

The stability of \mathcal{E}_{C0} depends on the basic reproduction number of model (1).

Theorem 1 *Let*

$$\mathcal{R}_C = \frac{\alpha \Lambda}{\mu(\gamma + \eta + \mu)}. \tag{4}$$

Then, the disease-free equilibrium \mathcal{E}_{C0} of model (1) is locally asymptotically stable if $\mathcal{R}_C < 1$, but unstable if $\mathcal{R}_C > 1$.

Proof 1 *Using the notation in [52], we define the matrix of new infections \mathcal{F} and the transition matrix $\nu = \nu^- - \nu^+$ by*

$$\mathcal{F} = \begin{bmatrix} \alpha SI \\ 0 \end{bmatrix}, \quad \nu^- = \begin{bmatrix} (\gamma + \eta + \mu)I \\ (\theta + \delta + \mu)H \end{bmatrix}, \quad \nu^+ = \begin{bmatrix} 0 \\ \eta I \end{bmatrix}.$$

Then, we compute the matrices $F = D\mathcal{F}(\mathcal{E}_{C0})$ and $V = D\nu(\mathcal{E}_{C0})$, as follows:

$$F = \begin{bmatrix} \frac{\alpha \Lambda}{\mu} & 0 \\ 0 & 0 \end{bmatrix}, \quad V = \begin{bmatrix} \gamma + \eta + \mu & 0 \\ -\eta & \theta + \delta + \mu \end{bmatrix}.$$

The basic reproduction number \mathcal{R}_C of the COVID-19-only model is given by the spectral radius of FV^{-1} . From this, we obtain that \mathcal{R}_C is given by (4).

By an application of [52, Theorem 2], we conclude that \mathcal{E}_{C0} is locally asymptotically stable if $\mathcal{R}_C < 1$ and unstable if $\mathcal{R}_C > 1$.

Analysis of the bacterial pneumonia infection model

The bacterial pneumonia model (2) has a DFE given by

$$\mathcal{E}_{P0} = (S, I, R, B) = \left(\frac{\Lambda}{\mu}, 0, 0, 0\right).$$

The stability of \mathcal{E}_{P0} will depend on a parameter \mathcal{R}_P , as detailed in the following result.

Theorem 2 *Let*

$$\mathcal{R}_P = \frac{b \Lambda}{\mu(\phi + \mu + \delta)}. \tag{5}$$

Then, the disease-free equilibrium ε_{P0} of model (2) is locally asymptotically stable if $\mathcal{R}_P < 1$, but unstable if $\mathcal{R}_P > 1$.

Proof 2 Using the notation in [52], we define the matrix of new infections \mathcal{F} and the transition matrix $\nu = \nu^- - \nu^+$ by

$$\mathcal{F} = [bSI + b_1SB], \quad \nu^- = [(\phi + \mu + \delta)I], \quad \nu^+ = [0].$$

To apply the next-generation matrix method, we compute $F = D\mathcal{F}(\varepsilon_{C0})$ and $V = D\nu(\varepsilon_{C0})$, which are given by

$$F = \left[\frac{b\Lambda}{\mu} \right], \quad V = [\phi + \mu + \delta].$$

Using the same method as before, we obtain the basic reproduction number \mathcal{R}_P of the bacterial pneumonia-only model as the spectral radius of FV^{-1} , which gives the expression (5).

Finally, by [52, Theorem 2], we conclude that ε_{P0} is locally asymptotically stable if $\mathcal{R}_P < 1$ and unstable if $\mathcal{R}_P > 1$.

4 Analysis of the COVID-19–bacterial pneumonia coinfection model

Next, we consider the dynamics of the coinfection model (3). The existence and stability of equilibria for model (3) will depend on three parameters, which are defined as follows:

$$\mathcal{R}_C := \frac{\alpha\Lambda}{\mu(\gamma + \eta + \mu)}, \quad \mathcal{R}_P := \frac{b\Lambda}{\mu(\phi + \mu + \delta)}, \quad \mathcal{R}_B := \frac{r}{m}.$$

As we saw in the previous section, the parameters \mathcal{R}_C and \mathcal{R}_P represent the basic reproduction numbers of COVID-19 and bacterial pneumonia, respectively. On the other hand, \mathcal{R}_B can be interpreted as the reproduction number of bacterial population in the hospital.

Equilibria of the model

By direct computation, we obtain the following result about the equilibria of model (3).

Theorem 3 The coinfection model (3) has the following steady states:

- i. The disease-free, bacterial population-free equilibrium:

$$\varepsilon_0 = (X_{SS}^{(0)}, 0, 0, 0, 0, 0, 0, 0, 0, 0, 0, 0, 0, 0),$$

where

$$X_{SS}^{(0)} = \frac{\Lambda}{\mu}.$$

- ii. The disease-free, bacterial population-present equilibrium:

$$\varepsilon_1 = (X_{SS}^{(1)}, 0, 0, 0, 0, 0, 0, 0, 0, 0, 0, 0, 0, B^{(1)}),$$

where

$$X_{SS}^{(1)} = \frac{\Lambda}{\mu}, \quad B^{(1)} = \frac{\kappa}{r}(r - m).$$

This equilibrium exists if and only if $\mathcal{R}_B > 1$.

- iii. The COVID-19-free, pneumonia-present, bacterial population-free equilibrium:

$$\varepsilon_2 = (X_{SS}^{(2)}, 0, 0, 0, X_{IS}^{(2)}, 0, 0, 0, X_{RS}^{(2)}, 0, 0, 0, 0, 0),$$

where

$$X_{SS}^{(2)} = \frac{\mu + \delta + \phi}{b}, \quad X_{IS}^{(2)} = \frac{\Lambda}{\mu + \delta + \phi} - \frac{\mu}{b}, \quad X_{RS}^{(2)} = \frac{\phi}{\mu} X_{IS}^{(2)}.$$

This equilibrium exists if and only if $\mathcal{R}_P > 1$.

- iv. The COVID-19-free, pneumonia-present, bacterial population-present equilibrium:

$$\varepsilon_3 = (X_{SS}^{(3)}, 0, 0, 0, X_{IS}^{(3)}, 0, 0, 0, X_{RS}^{(3)}, 0, 0, 0, B^{(3)}),$$

where

$$X_{SS}^{(3)} = \frac{\mu + \delta + \phi}{b}, \quad X_{IS}^{(3)} = \frac{\Lambda}{\mu + \delta + \phi} - \frac{\mu}{b}, \quad X_{RS}^{(3)} = \frac{\phi}{\mu} X_{IS}^{(3)},$$

$$B^{(3)} = \frac{\kappa}{r}(r - m).$$

This equilibrium exists if and only if

$$\mathcal{R}_B > 1 \quad \text{and} \quad \mathcal{R}_p > 1.$$

v. The COVID-19-present, pneumonia-free, bacterial population-free equilibrium:

$$\varepsilon_4 = (X_{SS}^{(4)}, X_{SI}^{(4)}, X_{SH}^{(4)}, X_{SR}^{(4)}, 0, 0, 0, 0, 0, 0, 0, 0, 0, 0),$$

where

$$X_{SS}^{(4)} = \frac{\gamma + \eta + \mu}{\alpha}, \quad X_{SI}^{(4)} = \frac{(\mu + \sigma)(\theta + \mu + \delta_1)[\alpha\Lambda - \mu(\gamma + \eta + \mu)]}{\alpha[\mu(\theta + \mu + \delta_1)(\gamma + \eta + \mu + \sigma) + \eta\sigma(\mu + \delta_1)]},$$

$$X_{SH}^{(4)} = \frac{\eta}{\theta + \mu + \delta_1} X_{SI}^{(4)}, \quad X_{SR}^{(4)} = \left(\frac{\gamma}{\mu + \sigma} + \frac{\eta\theta}{(\mu + \sigma)(\theta + \mu + \delta_1)} \right) X_{SI}^{(4)}.$$

This equilibrium exists if and only if

$$\mathcal{R}_C > 1.$$

Proof 3 Equilibria $\varepsilon_0, \varepsilon_1, \varepsilon_2$ and ε_3 are obtained by assuming that $X_{SI} = 0$ in the system at equilibrium and solving the resulting algebraic equations. This yields four different cases: one for each equilibrium.

On the other hand, assuming $X_{SI} > 0$ and $X_{IS} = 0$ results in only one case, corresponding to the equilibrium ε_4 .

The case when $X_{SI} > 0$ and $X_{IS} > 0$ will be discussed below.

Theorem 3 shows that, under certain conditions, the coinfection model has five different steady states. Moreover, we conjecture that a sixth equilibrium, with positive values for all variables, may exist. We will denote this interior equilibrium by ε_5 . Since the theoretical analysis becomes too cumbersome in this case, we will resort to numerical simulations to investigate the dynamics of equilibrium ε_5 (see Section 5).

Stability analysis

We will now analyze the local stability for the equilibria of system (3) by means of the linearisation method and the Hartman-Grobman theorem. Our results will focus only on the disease-free equilibria ε_0 and ε_1 .

Theorem 4

(i) The disease-free, bacterial population-free equilibrium ε_0 is locally asymptotically stable if

$$\mathcal{R}_C < 1, \quad \mathcal{R}_p < 1 \quad \text{and} \quad \mathcal{R}_B < 1, \tag{6}$$

and it is unstable if one of $\mathcal{R}_C > 1, \mathcal{R}_p > 1$ or $\mathcal{R}_B > 1$ holds.

(ii) The disease-free, bacterial population-present equilibrium ε_1 is locally asymptotically stable if

$$\mathcal{R}_C < 1, \quad \mathcal{R}_p < 1 \quad \text{and} \quad \mathcal{R}_B > 1, \tag{7}$$

and it is unstable if one of $\mathcal{R}_C > 1, \mathcal{R}_p > 1$ or $\mathcal{R}_B < 1$ holds.

Proof 4 The Jacobian of system (3) evaluated at ε_0 is given by

$$J_0 = \begin{pmatrix} -\mu & -\frac{\alpha\Lambda}{\mu} & 0 & \sigma & -\frac{b\Lambda}{\mu} & -\frac{(\alpha+b)\Lambda}{\mu} & 0 & -\frac{b\Lambda}{\mu} & 0 & -\frac{\alpha\Lambda}{\mu} & 0 & 0 & 0 \\ 0 & \frac{\alpha\Lambda}{\mu} - k_1 & 0 & 0 & 0 & \frac{\alpha\Lambda}{\mu} & 0 & 0 & 0 & \frac{\alpha\Lambda}{\mu} & 0 & 0 & 0 \\ 0 & \eta & -k_2 & 0 & 0 & 0 & 0 & 0 & 0 & 0 & 0 & 0 & 0 \\ 0 & \gamma & \theta & -k_3 & 0 & 0 & 0 & 0 & 0 & 0 & 0 & 0 & 0 \\ 0 & 0 & 0 & 0 & \frac{b\Lambda}{\mu} - k_4 & \frac{b\Lambda}{\mu} & 0 & \frac{b\Lambda}{\mu} + \sigma & 0 & 0 & 0 & 0 & 0 \\ 0 & 0 & 0 & 0 & 0 & -k_5 & 0 & 0 & 0 & 0 & 0 & 0 & 0 \\ 0 & 0 & 0 & 0 & 0 & \eta + \eta_1 & -\theta_1 - k_6 & 0 & 0 & 0 & 0 & 0 & 0 \\ 0 & 0 & 0 & 0 & 0 & \gamma_1 & \theta_1 & -k_7 & 0 & 0 & 0 & 0 & 0 \\ 0 & 0 & 0 & 0 & \phi & 0 & 0 & 0 & -\mu & 0 & 0 & \sigma & 0 \\ 0 & 0 & 0 & 0 & 0 & \phi_1 & 0 & 0 & 0 & -k_1 & 0 & 0 & 0 \\ 0 & 0 & 0 & 0 & 0 & 0 & \phi_2 & 0 & 0 & \eta & -k_2 & 0 & 0 \\ 0 & 0 & 0 & 0 & 0 & 0 & 0 & \phi & 0 & \gamma & \theta & -k_3 & 0 \\ 0 & 0 & 0 & 0 & 0 & 0 & p & 0 & 0 & 0 & 0 & 0 & r - m \end{pmatrix},$$

where

$$k_1 = \gamma + \eta + \mu, \quad k_2 = \theta + \mu + \delta_1, \quad k_3 = \mu + \sigma, \quad k_4 = \mu + \delta + \phi,$$

$$k_5 = \gamma_1 + \eta + \eta_1 + \mu + \delta_0 + \phi_1, \quad k_6 = \mu + \delta_1 + \delta_2 + \phi_2, \quad k_7 = \mu + \delta + \phi + \sigma.$$

From this, we obtain the characteristic polynomial

$$(\lambda + \mu)^2 (\lambda + k_1) (\lambda + k_2)^2 (\lambda + k_3)^2 (\lambda + k_5) (\lambda + \theta_1 + k_6) (\lambda + k_7)$$

$$\times \left(\lambda + k_1 - \frac{\alpha\Lambda}{\mu} \right) \left(\lambda + k_4 - \frac{b\Lambda}{\mu} \right) (\lambda + m - r) = 0.$$

By the Hartman–Grobman theorem [53, p. 311], we know that the solutions of (3) and its linearisation are qualitatively equivalent near ε_0 provided that ε_0 is a hyperbolic equilibrium. Due to positivity of parameters, it is clear that all eigenvalues have negative real part if and only if

$$\gamma + \eta + \mu - \frac{\alpha\Lambda}{\mu} > 0, \quad \mu + \delta + \phi - \frac{b\Lambda}{\mu} > 0 \quad \text{and} \quad m - r > 0,$$

which is equivalent to the condition (6). On the other hand, the opposite inequalities guarantee that there is at least one eigenvalue with positive real part and no eigenvalues with zero real part. Hence, we can conclude part (i) of the theorem.

Next, we compute the Jacobian at ε_1 , which is given by

$$J_1 = \begin{bmatrix} -\mu & -\frac{\alpha\Lambda}{\mu} & 0 & \sigma & -\frac{b\Lambda}{\mu} & -\frac{(\alpha+b)\Lambda}{\mu} & 0 & -\frac{b\Lambda}{\mu} & 0 & -\frac{\alpha\Lambda}{\mu} & 0 & 0 & 0 \\ 0 & \frac{\alpha\Lambda}{\mu} - k_1 & 0 & 0 & 0 & \frac{\alpha\Lambda}{\mu} & 0 & 0 & 0 & \frac{\alpha\Lambda}{\mu} & 0 & 0 & 0 \\ 0 & \eta & -k_0 - k_2 & 0 & 0 & 0 & 0 & 0 & 0 & 0 & 0 & 0 & 0 \\ 0 & \gamma & \theta & -k_3 & 0 & 0 & 0 & 0 & 0 & 0 & 0 & 0 & 0 \\ 0 & 0 & 0 & 0 & \frac{b\Lambda}{\mu} - k_4 & \frac{b\Lambda}{\mu} & 0 & \frac{b\Lambda}{\mu} + \sigma & 0 & 0 & 0 & 0 & 0 \\ 0 & 0 & 0 & 0 & 0 & -k_5 & 0 & 0 & 0 & 0 & 0 & 0 & 0 \\ 0 & 0 & k_0 & 0 & 0 & \eta + \eta_1 & -\theta_1 - k_6 & 0 & 0 & 0 & 0 & 0 & 0 \\ 0 & 0 & 0 & 0 & 0 & \gamma_1 & \theta_1 & -k_7 & 0 & 0 & 0 & 0 & 0 \\ 0 & 0 & 0 & 0 & 0 & \phi & 0 & 0 & -\mu & 0 & 0 & \sigma & 0 \\ 0 & 0 & 0 & 0 & 0 & \phi_1 & 0 & 0 & 0 & -k_1 & 0 & 0 & 0 \\ 0 & 0 & 0 & 0 & 0 & 0 & \phi_2 & 0 & 0 & \eta & -k_2 & 0 & 0 \\ 0 & 0 & 0 & 0 & 0 & 0 & 0 & \phi & 0 & \gamma & \theta & -k_3 & 0 \\ 0 & 0 & 0 & 0 & 0 & 0 & p & 0 & 0 & 0 & 0 & 0 & m - r \end{bmatrix},$$

where $k_0 = b_2 \kappa (1 - \frac{m}{r})$, and k_1, \dots, k_7 are as defined above. Notice that $k_0 > 0$ if and only if $\mathcal{R}_B > 1$.

The characteristic polynomial at ε_1 is

$$(\lambda + \mu)^2 (\lambda + k_1) (\lambda + k_2) (\lambda + k_3)^2 (\lambda + k_5) (\lambda + \theta_1 + k_6) (\lambda + k_7)$$

$$\times (\lambda + k_0 + k_2) \left(\lambda + k_1 - \frac{\alpha\Lambda}{\mu} \right) \left(\lambda + k_4 - \frac{b\Lambda}{\mu} \right) (\lambda + r - m) = 0.$$

It follows that all eigenvalues have negative real part if and only if

$$k_0 + k_2 > 0, \quad \gamma + \eta + \mu - \frac{\alpha\Lambda}{\mu} > 0, \quad \mu + \delta + \phi - \frac{b\Lambda}{\mu} > 0 \quad \text{and} \quad r - m > 0.$$

The first of these inequalities holds automatically when $\mathcal{R}_B > 1$. Hence, we can see that all eigenvalues have negative real part if and only if the last three inequalities hold, and this is equivalent to condition (7). Otherwise, if $\mathcal{R}_C > 1$, $\mathcal{R}_p > 1$ or $\mathcal{R}_B < 1$, there will be at least one eigenvalue with positive real part and no eigenvalues with zero real part. Applying the Hartman–Grobman theorem as before, the proof of (ii) is complete.

5 Numerical analysis

In this section, we perform some simulations for system (3) to illustrate the dynamics of the coinfection model in some cases that are not covered by the analysis in Section 4. We will consider the initial conditions

$$X_{SS}(0) = 8.33 \times 10^7, \quad X_{SI}(0) = 10^5, \quad X_{SH}(0) = 10^3, \quad X_{SR}(0) = 10^5, \quad X_{IS}(0) = 10^3,$$

$$B(0) = 0.8, \quad X_{II}(0) = X_{IH}(0) = X_{IR}(0) = X_{RS}(0) = X_{RI}(0) = X_{RH}(0) = X_{RR}(0) = 0,$$

which represent a case when a fraction of the population is infected with either COVID-19 or bacterial pneumonia, but there are initially no people coinfecting with both diseases.

Throughout this section, we will use the parameter values shown in Table 1. The parameters related to demography (Λ and μ) and COVID-19 dynamics (σ , α and α_1) are based on the values used in [54]. Since the literature regarding the modelling of bacterial pneumonia dynamics is scarce, the rest of the parameter values are not based on specific models or real data sets. Instead, we use generic values to show the different dynamics of our model.

Thus, we obtain a fixed value for \mathcal{R}_C , which is greater than one ($\mathcal{R}_C = 1.2294$), while \mathcal{R}_p and \mathcal{R}_B will vary as the parameters b and r take different values.

Table 1. Parameter values used for the coinfection model.

Parameter	Value	Unit
Λ	2000	people/day
μ	2.4×10^{-5}	(people · day) ⁻¹
σ	1/100	day ⁻¹
γ	1/12	day ⁻¹
γ_1	1/20	day ⁻¹
θ	1/14	day ⁻¹
θ_1	1/24	day ⁻¹
b_1	2×10^{-9}	(people · day) ⁻¹
b_2	0.1	day ⁻¹
δ	0.001	day ⁻¹
δ_0	0.005	day ⁻¹
δ_1	0.01	day ⁻¹
δ_2	0.2	day ⁻¹
η	0.12	day ⁻¹
η_1	0.1	day ⁻¹
ϕ	1/14	day ⁻¹
ϕ_1	1/30	day ⁻¹
ϕ_2	1/40	day ⁻¹
p	10^{-5}	(people · day) ⁻¹
κ	1	
m	0.01	day ⁻¹
α	3×10^{-9}	(people · day) ⁻¹
α_1	10^{-8}	(people · day) ⁻¹
b	variable	(people · day) ⁻¹
r	variable	day ⁻¹

Case 1. When $b = 10^{-10}$ and $r = 0.004$, we have $\mathcal{R}_p = 0.1150 < 1$ and $\mathcal{R}_B = 0.4 < 1$. The time plots of the solutions for this case are shown in Figure 2. The solutions converge to a positive equilibrium

$$\varepsilon_5 \approx (6.3418 \times 10^7, 5684, 3153, 69716, 191.8, 0.0735, 1537, 776.8, 4.368 \times 10^6, 391.5, 1048, 16263, 1.3487).$$

As we can see in Figure 2, the population infected with pneumonia presents a peak during the first 200 days, after which it oscillates until settling down to the equilibrium value. The majority of the coinfecting population consists of hospitalised individuals (X_{IH}), which reach a peak of 760 000, while the coinfecting non-hospitalised population (X_{II}) grows to less than 10 000 individuals. For people recovered from bacterial pneumonia, a similar relationship is seen: there are more hospitalised than non-hospitalised individuals; however, for individuals susceptible to pneumonia, the opposite occurs.

Case 2. When $b = 9 \times 10^{-10}$ and $r = 0.004$, we have $\mathcal{R}_p = 1.0352 > 1$ and $\mathcal{R}_B = 0.4 < 1$. The time plots of the solutions are depicted in Figure 3; we can see that they converge to a positive equilibrium

$$\varepsilon_5 \approx (5.711 \times 10^7, 5602, 3130, 6.89 \times 10^4, 2229, 0.59, 1509, 765, 1.066 \times 10^7, 1046, 2005, 2.85 \times 10^4, 1.33).$$

As seen in Figure 3, the dynamics, in this case, are mostly similar to those of Case 1. The largest difference is the increase in the population infected with pneumonia only (X_{IS}), which reaches a peak about 10 times larger than in Case 1. Also notable is the increase in the population recovered from pneumonia and infected by COVID-19 (X_{RI}), whose peak and equilibrium values are about 3 times larger than in Case 1.

Case 3. When $b = 10^{-10}$ and $r = 0.08$, we have $\mathcal{R}_p = 0.1150 < 1$ and $\mathcal{R}_B = 8 > 1$. The time plots of the solutions are depicted in Figure 4. We can see that they converge to the positive equilibrium

$$\varepsilon_5 \approx (6.353 \times 10^7, 6206, 3984, 8.0 \times 10^4, 189.8, 0.0793, 1519, 768, 4.251 \times 10^6, 415.3, 1078, 16605, 1.055).$$

If we compare these simulations with the case when both \mathcal{R}_p and \mathcal{R}_B are less than one, we can see that there is a slight increment in all the pneumonia-susceptible compartments and a slight decrease in the pneumonia-infected compartments. The concentration of bacteria also reaches a lower value at the peak and at equilibrium.

Case 4. When $b = 9 \times 10^{-10}$ and $r = 0.08$, we have $\mathcal{R}_p = 1.0352 > 1$ and $\mathcal{R}_B = 8 > 1$. The time plots of the solutions are shown in Figure 5. We can see that the solutions converge to the positive equilibrium

$$\varepsilon_5 \approx (5.728 \times 10^7, 6007, 3867, 7.747 \times 10^4, 2186, 0.618, 1467, 744.4, 1.050 \times 10^7, 1102, 2074, 2.92 \times 10^4, 1.0497).$$

In this case, the number of hospitalised coinfecting people becomes lower than in all other cases, while the non-hospitalised coinfecting population reaches its highest value (although it still remains less than one individual at equilibrium). The concentration of bacteria in environment approaches a lower value at equilibrium in comparison to Cases 1–3.

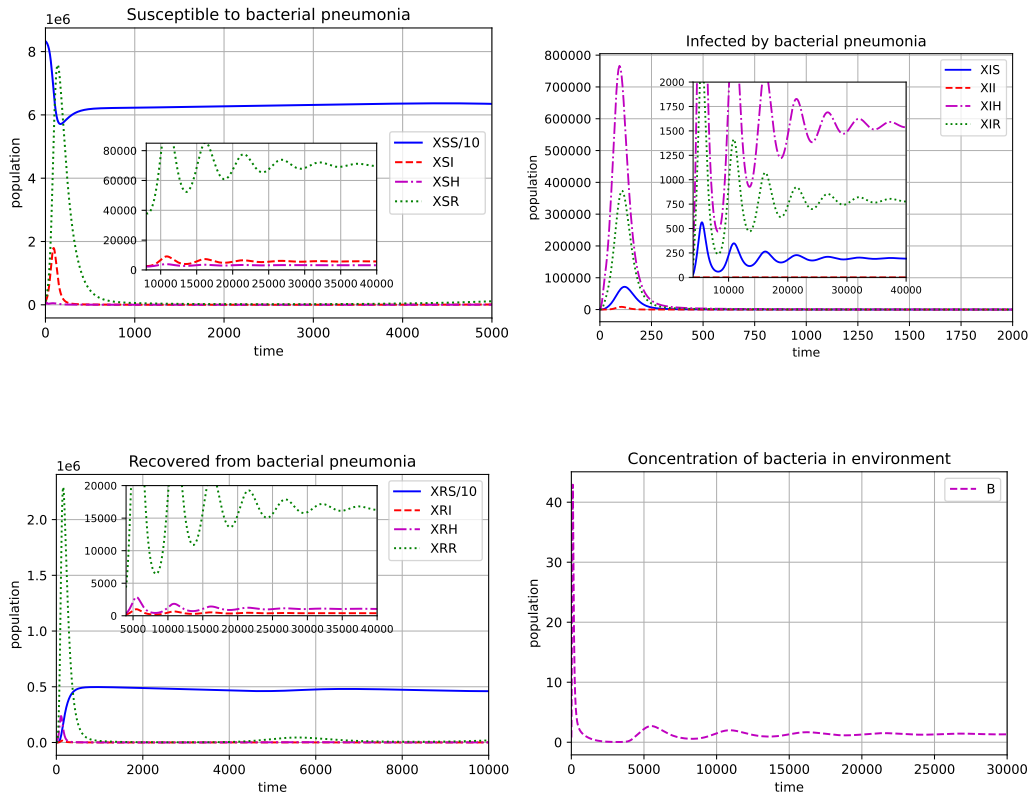


Figure 2. Dynamics of the coinfection model when $\mathcal{R}_C > 1$, $\mathcal{R}_P < 1$ and $\mathcal{R}_B < 1$.

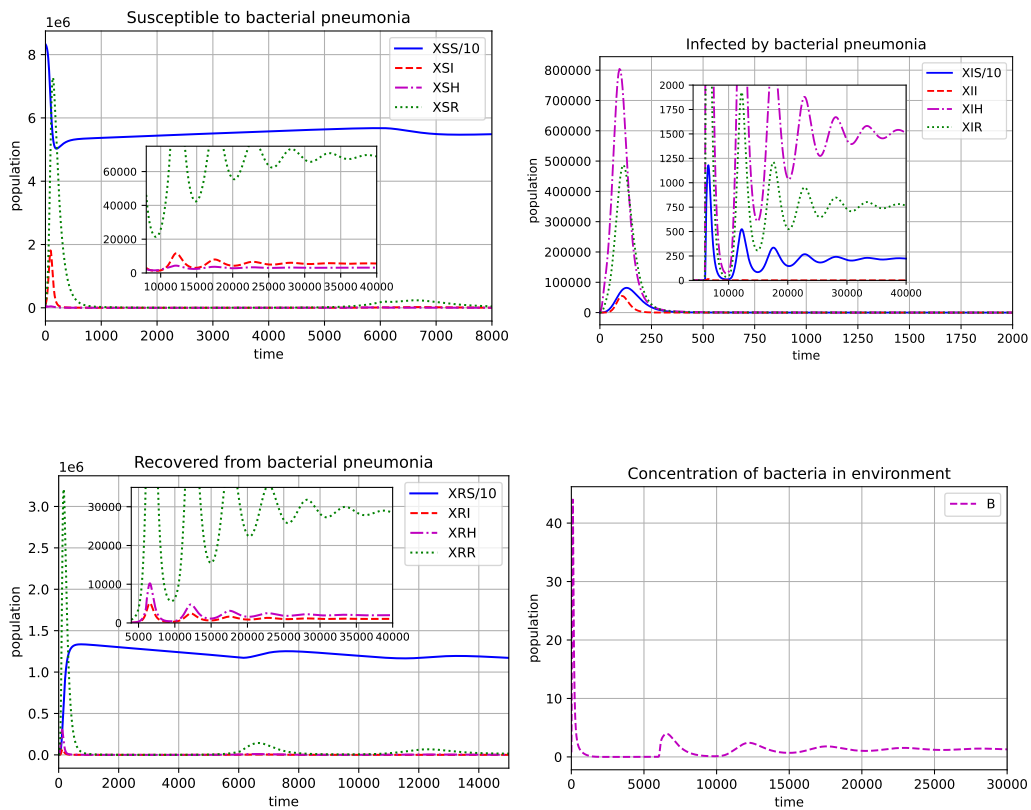


Figure 3. Dynamics of the coinfection model when $\mathcal{R}_C > 1$, $\mathcal{R}_P > 1$ and $\mathcal{R}_B < 1$.

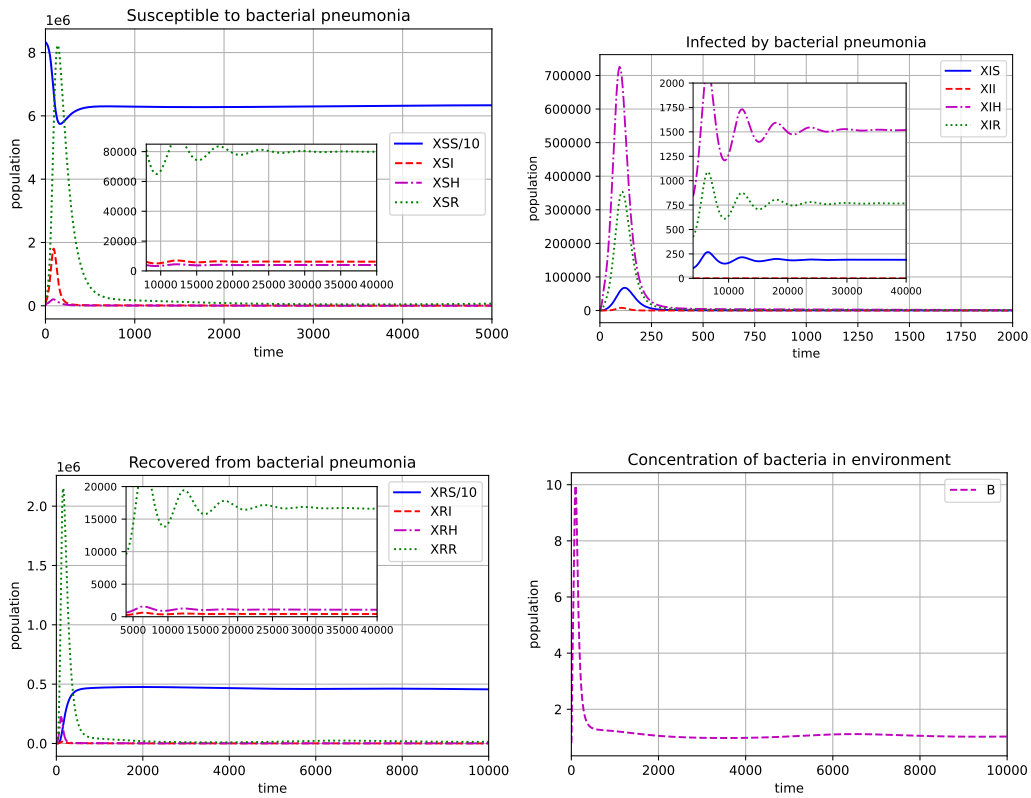


Figure 4. Dynamics of the coinfection model when $\mathcal{R}_C > 1$, $\mathcal{R}_P < 1$ and $\mathcal{R}_B > 1$.

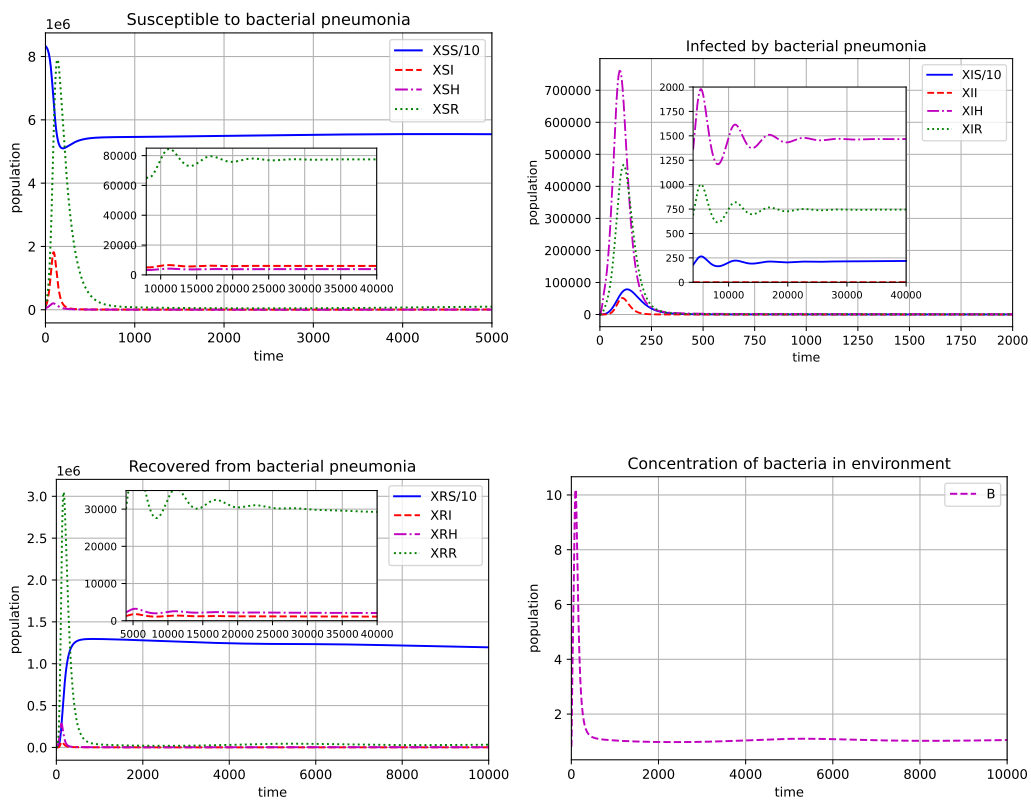


Figure 5. Dynamics of the coinfection model when $\mathcal{R}_C > 1$, $\mathcal{R}_P > 1$ and $\mathcal{R}_B > 1$.

6 Results and discussion

In this work, we proposed a novel mathematical model to study the coinfection dynamics of COVID-19 and bacterial pneumonia. We established some basic properties of the sub-models (COVID-19 only and bacterial pneumonia only) and computed their basic reproduction numbers. We obtained some analytical results for the coinfection model and showed that its dynamics depend on three parameters: \mathcal{R}_C , \mathcal{R}_P and \mathcal{R}_B .

We established in Theorem 4 that a necessary and sufficient condition to ensure that both diseases are eradicated from the population is to decrease \mathcal{R}_C and \mathcal{R}_P below unity. Biologically, this can be achieved by encouraging social distancing and wearing face masks. Moreover, part (ii) of Theorem 4 shows that a high reproduction number for the bacterial population in hospitals (\mathcal{R}_B) is not enough for bacterial pneumonia to persist in the population.

Furthermore, we determined the conditions for the existence of five equilibrium points. By means of numerical simulations, we showed that a sixth equilibrium may exist. Based on the simulations in Section 5, we conjecture that the COVID-19-present, pneumonia-present, bacterial population-present equilibrium ε_5 exists and is locally stable whenever $\mathcal{R}_C > 1$. This implies that both diseases can coexist in the population even if reproduction numbers of bacterial pneumonia (\mathcal{R}_P) and bacterial population (\mathcal{R}_B) are reduced below unity. Hence, epidemic policies should focus on reducing the basic reproduction number of COVID-19 in order to control the pandemic.

The simulations obtained in Section 5 show qualitatively similar dynamics for all four cases depicted in Figures 2–5: all subpopulations converge to a positive value. However, we must remark that the number of coinfecting, non-hospitalised individuals (X_{II}) remains very low (less than one individual at equilibrium) in all cases; in contrast, most of the coinfection cases occur in the hospitalised compartment (X_{IH}). This is in line with the increased susceptibility of hospitalised COVID-19 patients to bacterial or fungal infections that has been observed in clinical trials [49, 50, 51].

Although many models have been proposed recently to study the coinfection dynamics of COVID-19 and other diseases [41, 42, 43, 44, 45, 46], our work is the first that takes into account the distinctive features of bacterial pneumonia, in particular, the inclusion of two infection ways (community and hospital transmission).

7 Conclusions

We proposed and analyzed an ODE model which, to the best of our knowledge, is the first epidemic model used to describe the coinfection of bacterial pneumonia and COVID-19. The highlights of our work include determining the stability conditions for the disease-free equilibria, as well as the existence conditions for five different equilibria. Due to the complexity of our model, we did not include a stability analysis for all equilibrium points. This is an area of research that could be elaborated on in future works. Other approaches that could be tackled in further research include expanding our coinfection model using vaccination against COVID-19 or multiple SARS-CoV-2 variants, as well as performing parameter fitting using real data.

Declarations

Code availability

The code used in this paper was written in Python and can be downloaded from <https://github.com/agcp26/COVID19-pneumonia>.

Consent for publication

Not applicable.

Conflicts of interest

The authors declare that they have no conflict of interests.

Funding

Not applicable.

Author's contributions

A.G.C.P.: Conceptualization, Methodology, Software, Formal Analysis, Writing – Original Draft, Writing – Review & Editing. D.A.O.: Conceptualization, Validation, Formal Analysis, Writing – Original Draft. All authors discussed the results and contributed to the final manuscript.

Acknowledgements

Not applicable.

References

- [1] Nasir, N., Rehman, F., & Omair, S.F. Risk factors for bacterial infections in patients with moderate to severe COVID-19: A case-control study. *Journal of medical virology*, 93(7), 4564–4569, (2021). [CrossRef]
- [2] Mirzaei, R., Goodarzi, P., Asadi, M., Soltani, A., Aljanabi, H.A.A., Jeda, A.S., ... & Karampoor, S. Bacterial co-infections with SARS-CoV-2. *IUBMB life*, 72(10), 2097–2111, (2020). [CrossRef]
- [3] National Health Service, Respiratory tract infections (RTIs), <https://www.nhs.uk/conditions/respiratory-tract-infection/> Access date: 19 November 2022.
- [4] Hegazy, N.N., Mahrous, O.A., & Salah, M.A. An overview of respiratory tract infections in preschool children in primary healthcare. *Menoufia Medical Journal*, 31(3), 862, (2018). [CrossRef]
- [5] Morens, D.M., Taubenberger, J.K., & Fauci, A.S. Predominant role of bacterial pneumonia as a cause of death in pandemic influenza: implications for pandemic influenza preparedness. *The Journal of infectious diseases*, 198(7), 962–970, (2008). [Cross-Ref]
- [6] MacIntyre, C.R., Chughtai, A.A., Barnes, M., Ridda, I., Seale, H., Toms, R., & Heywood, A. The role of pneumonia and secondary bacterial infection in fatal and serious outcomes of pandemic influenza a (H1N1) pdm09. *BMC infectious diseases*, 18(1), 1–20, (2018). [CrossRef]
- [7] Kumar, R., Bhattacharya, B., Meena, V., Soneja, M., & Wig, N. COVID-19 and TB co-infection- 'Finishing touch' in perfect recipe to 'severity' or 'death'. *Journal of Infection*, 81(3), e39–e40, (2020). [CrossRef]
- [8] Lansbury, L., Lim, B., Baskaran, V., & Lim, W.S. Co-infections in people with COVID-19: a systematic review and meta-analysis. *Journal of Infection*, 81(2), 266–275, (2020). [CrossRef]
- [9] Cox, M.J., Loman, N., Bogaert, D., & O'Grady, J. Co-infections: potentially lethal and unexplored in COVID-19. *The Lancet Microbe*, 1(1), e11, (2020). [CrossRef]
- [10] Zhou, F., Yu, T., Du, R., Fan, G., Liu, Y., Liu, Z., ... & Cao, B. Clinical course and risk factors for mortality of adult inpatients with COVID-19 in Wuhan, China: a retrospective cohort study. *The lancet*, 395(10229), 1054–1062, (2020). [CrossRef]
- [11] Chen, N., Zhou, M., Dong, X., Qu, J., Gong, F., Han, Y., ... & Zhang, L. Epidemiological and clinical characteristics of 99 cases of 2019 novel coronavirus pneumonia in Wuhan, China: a descriptive study. *The lancet*, 395(10223), 507–513, (2020). [CrossRef]
- [12] Rawson, T.M., Moore, L.S., Zhu, N., Ranganathan, N., Skolimowska, K., Gilchrist, M., ... & Holmes, A. Bacterial and fungal coinfection in individuals with coronavirus: a rapid review to support COVID-19 antimicrobial prescribing. *Clinical infectious diseases*, 71(9), 2459–2468, (2020). [CrossRef]
- [13] Bernoulli, D. Essai d'une nouvelle analyse de la mortalité causée par la petite vérole, et des avantages de l'inoculation pour la prévenir. *Histoire de l'Acad., Roy. Sci.(Paris) avec Mem*, 1–45, (1760).
- [14] Ross, R. The prevention of malaria. *John Murray*, (1911).
- [15] Ross, R. An application of the theory of probabilities to the study of a priori pathometry.—Part I. *Proceedings of the Royal Society of London. Series A, Containing papers of a mathematical and physical character*, 92(638), 204–230, (1916). [CrossRef]
- [16] Ross, R., & Hudson, H.P. An application of the theory of probabilities to the study of a priori pathometry.—Part II. *Proceedings of the Royal Society of London. Series A, Containing papers of a mathematical and physical character*, 93(650), 212–225, (1917).
- [17] Ross, R., & Hudson, H.P. An application of the theory of probabilities to the study of a priori pathometry.—Part III. *Proceedings of the Royal Society of London. Series A, Containing papers of a mathematical and physical character*, 93(650), 225–240, (1917). [CrossRef]
- [18] Kermack, W.O., & McKendrick, A. G. A contribution to the mathematical theory of epidemics. *Proceedings of the royal society of London. Series A, Containing papers of a mathematical and physical character*, 115(772), 700–721, (1927). [CrossRef]
- [19] House, T., & Keeling, M.J. Deterministic epidemic models with explicit household structure. *Mathematical biosciences*, 213(1), 29–39, (2008). [CrossRef]
- [20] Becker, N. The uses of epidemic models. *Biometrics*, 35(1), 295–305, (1979). [CrossRef]
- [21] Hethcote, H.W. The mathematics of infectious diseases. *SIAM review*, 42(4), 599–653, (2000). [CrossRef]
- [22] Lee, G., Yoon, S.E., & Shin, K. Simple epidemic models with segmentation can be better than complex ones. *Plos one*, 17(1), e0262244, (2022). [CrossRef]
- [23] Allegrretti, S., Bulai, I.M., Marino, R., Menandro, M.A., & Parisi, K. Vaccination effect conjoint to fraction of avoided contacts for a Sars-Cov-2 mathematical model. *Mathematical Modelling and Numerical Simulation with Applications*, 1(2), 56–66, (2021). [CrossRef]
- [24] Ikram, R., Khan, A., Zahri, M., Saeed, A., Yavuz, M., & Kumam, P. Extinction and stationary distribution of a stochastic COVID-19 epidemic model with time-delay. *Computers in Biology and Medicine*, 141, 105115, (2022). [CrossRef]
- [25] Sinan, M., Leng, J., Anjum, M., & Fiaz, M. Asymptotic behavior and semi-analytic solution of a novel compartmental biological model. *Mathematical Modelling and Numerical Simulation with Applications*, 2(2), 88–107, (2022). [CrossRef]
- [26] Yavuz, M., Coşar, F.Ö., Günay, F., & Özdemir, F.N. A new mathematical modeling of the COVID-19 pandemic including the vaccination campaign. *Open Journal of Modelling and Simulation*, 9(3), 299–321, (2021). [CrossRef]
- [27] Özköse, F., & Yavuz, M. Investigation of interactions between COVID-19 and diabetes with hereditary traits using real data: A case study in Turkey. *Computers in biology and medicine*, 141, 105044, (2022). [CrossRef]
- [28] Özköse, F., Yavuz, M., Şenel, M.T., & Habbireeh, R. Fractional order modelling of omicron SARS-CoV-2 variant containing heart attack effect using real data from the United Kingdom. *Chaos, Solitons & Fractals*, 157, 111954, (2022). [CrossRef]
- [29] Orozco, J.A.M., Tinajero, Á.S., Vargas, E.B., Cueva, A.I.D., Escobar, H.R., Alcocer, E.V., ... & Santillán, D.P.R. COVID-19 and tuberculosis coinfection in a 51-year-old taxi driver in Mexico city. *The American journal of case reports*, 21, e927628–1, (2020). [CrossRef]
- [30] Tadolini, M., Codecasa, L.R., García-García, J.M., Blanc, F.X., Borisov, S., Alffenaar, J.W., ... & Migliori, G.B. Active tuberculosis, sequelae and COVID-19 co-infection: first cohort of 49 cases. *European Respiratory Journal*, 56(1), (2020). [CrossRef]
- [31] Yadav, S., & Rawal, G. The case of pulmonary tuberculosis with COVID-19 in an Indian male—a first of its type case ever reported from South Asia. *Pan African Medical Journal*, 36(1), (2020). [CrossRef]

- [32] Khurana, A.K., & Aggarwal, D. The (in) significance of TB and COVID-19 co-infection. *European Respiratory Journal*, 56(2), (2020). [[CrossRef](#)]
- [33] Petrone, L., Petruccioli, E., Vanini, V., Cuzzi, G., Gualano, G., Vittozzi, P., ... & Goletti, D. Coinfection of tuberculosis and COVID-19 limits the ability to in vitro respond to SARS-CoV-2. *International Journal of Infectious Diseases*, 113, S82–S87, (2021). [[CrossRef](#)]
- [34] Lew, S., Manes, P., & Smith, B. Coinfection with SARS-CoV-2 and influenza A virus in a 32-year-old man. *The American Journal of Case Reports*, 21, e926092–1, (2020). [[CrossRef](#)]
- [35] Jing, R., Vunnam, R.R., Schnaubelt, E., Vokoun, C., Cushman-Vokoun, A., Goldner, D., & Vunnam, S.R. Co-infection of COVID-19 and influenza A in a hemodialysis patient: a case report. *BMC Infectious Diseases*, 21(1), 1–6, (2021). [[CrossRef](#)]
- [36] Fahim, M., Ghonim, H.A.E.S., Roshdy, W.H., Naguib, A., Elguindy, N., AbdelFatah, M., ... & Eid, A. Coinfection with SARS-CoV-2 and influenza A (H1N1) in a patient seen at an influenza-like illness surveillance site in Egypt: case report. *JMIR public health and surveillance*, 7(4), e27433, (2021). [[CrossRef](#)]
- [37] Xiang, X., Wang, Z.H., Ye, L.L., He, X.L., Wei, X.S., Ma, Y.L., ... & Zhou, Q. Co-infection of SARS-CoV-2 and influenza A virus: a case series and fast review. *Current Medical Science*, 41(1), 51–57, (2021). [[CrossRef](#)]
- [38] Ata, F., Yousaf, Q., Parambil, J.V., Parengal, J., Mohamedali, M.G., & Yousaf, Z. A 28-year-old man from India with SARS-CoV-2 and pulmonary tuberculosis co-infection with central nervous system involvement. *The American journal of case reports*, 21, e926034–1, (2020). [[CrossRef](#)]
- [39] Elhazmi, A., Al-Tawfiq, J.A., Sallam, H., Al-Omari, A., Alhumaid, S., Mady, A., & Al Mutair, A. Severe acute respiratory syndrome coronavirus 2 (SARS-CoV-2) and Middle East Respiratory Syndrome Coronavirus (MERS-CoV) coinfection: A unique case series. *Travel Medicine and Infectious Disease*, 41, 102026, (2021). [[CrossRef](#)]
- [40] Giannella, M., Rinaldi, M., Tesini, G., Gallo, M., Cipriani, V., Vatamanu, O., ... & Curti, S. Predictive model for bacterial co-infection in patients hospitalized for COVID-19: A multicenter observational cohort study. *Infection*, 50, 1243–1253, (2022). [[CrossRef](#)]
- [41] Soni, B., & Singh, S. COVID-19 co-infection mathematical model as guided through signaling structural framework. *Computational and Structural Biotechnology Journal*, 19, 1672–1683, (2021). [[CrossRef](#)]
- [42] Tchoumi, S.Y., Diagne, M.L., Rwezaura, H., & Tchuenche, J.M. Malaria and COVID-19 co-dynamics: A mathematical model and optimal control. *Applied mathematical modelling*, 99, 294–327, (2021). [[CrossRef](#)]
- [43] Bandekar, S.R., & Ghosh, M. A co-infection model on TB–COVID-19 with optimal control and sensitivity analysis. *Mathematics and Computers in Simulation*, 200, 1–31, (2022). [[CrossRef](#)]
- [44] Rwezaura, H., Diagne, M.L., Omame, A., de Espindola, A.L., & Tchuenche, J.M. Mathematical modeling and optimal control of SARS-CoV-2 and tuberculosis co-infection: a case study of Indonesia. *Modeling Earth Systems and Environment*, 8(4), 5493–5520, (2022). [[CrossRef](#)]
- [45] Omame, A., Rwezaura, H., Diagne, M.L., Inyama, S.C., & Tchuenche, J.M. COVID-19 and dengue co-infection in Brazil: optimal control and cost-effectiveness analysis. *The European Physical Journal Plus*, 136(10), 1–33, (2021). [[CrossRef](#)]
- [46] Omame, A., Nwajeri, U.K., Abbas, M., & Onyenegecha, C.P. A fractional order control model for Diabetes and COVID-19 co-dynamics with Mittag-Leffler function. *Alexandria Engineering Journal*, 61(10), 7619–7635, (2022). [[CrossRef](#)]
- [47] Sampson, S. and De Pietro, M. What to know about bacterial pneumonia, <https://www.medicalnewstoday.com/articles/312565>, Access date: 31 August 2022.
- [48] Sethi, S. Hospital-acquired pneumonia, <https://www.msmanuals.com/home/lung-and-airway-disorders/pneumonia/hospital-acquired-pneumonia>, Access date: 31 August 2022.
- [49] Ansari, S., Hays, J.P., Kemp, A., Okechukwu, R., Murugaiyan, J., Ekwanzala, M.D., ... & van Dongen, M.B. The potential impact of the COVID-19 pandemic on global antimicrobial and biocide resistance: an AMR Insights global perspective. *JAC-Antimicrobial Resistance*, 3(2), dlab038, (2021). [[CrossRef](#)]
- [50] Huang, C., Wang, Y., Li, X., Ren, L., Zhao, J., Hu, Y., ... & Cao, B. Clinical features of patients infected with 2019 novel coronavirus in Wuhan, China. *The lancet*, 395(10223), 497–506, (2020). [[CrossRef](#)]
- [51] Wang, D., Hu, B., Hu, C., Zhu, F., Liu, X., Zhang, J., ... & Peng, Z. Clinical characteristics of 138 hospitalized patients with 2019 novel coronavirus-infected pneumonia in Wuhan, China. *Jama*, 323(11), 1061–1069, (2020). [[CrossRef](#)]
- [52] Van den Driessche, P., & Watmough, J. Reproduction numbers and sub-threshold endemic equilibria for compartmental models of disease transmission. *Mathematical biosciences*, 180(1–2), 29–48, (2002). [[CrossRef](#)]
- [53] Chicone, C. *Types of Differential Equations. Ordinary Differential Equations with Applications* (Vol. 34). Springer: New York, (1999).
- [54] Oluyori, D.A., Adebayo, H.O., & Pérez, Á.G. Global analysis of an SEIRS model for COVID-19 capturing saturated incidence with treatment response. *Applications and Applied Mathematics: An International Journal (AAM)*, 16(2), 9, (2021). [[CrossRef](#)]

Mathematical Modelling and Numerical Simulation with Applications (MMNSA) (<https://www.mmnsa.org>)



Copyright: © 2022 by the authors. This work is licensed under a Creative Commons Attribution 4.0 (CC BY) International License. The authors retain ownership of the copyright for their article, but they allow anyone to download, reuse, reprint, modify, distribute, and/or copy articles in MMNSA, so long as the original authors and source are credited. To see the complete license contents, please visit (<http://creativecommons.org/licenses/by/4.0/>).



RESEARCH PAPER

A new analytical approach to the (1+1)-dimensional conformable Fisher equation

Gülnür Yel^{1,*}, Miraç Kayhan^{2,†} and Armando Ciancio^{3,†}

¹Faculty of Education, Final International University, Kyrenia, 10 Mersin, Türkiye, ²Department of Mathematics, University of Inonu, 44280 Malatya, Türkiye, ³ Department of Biomedical and Dental Sciences and Morphofunctional Imaging, University of Messina, 98125 Messina, Italy

*Corresponding Author

†gulnur.yel@final.edu.tr (Gülnür Yel); mirackayhan@yandex.com (Miraç Kayhan); aciancio@unime.it (Armando Ciancio)

Abstract

In this paper, we use an effective method which is the rational sine-Gordon expansion method to present new wave simulations of a governing model. We consider the (1+1)-dimensional conformable Fisher equation which is used to describe the interactive relation between diffusion and reaction. Various types of solutions such as multi-soliton, kink, and anti-kink wave soliton solutions are obtained. Finally, the physical behaviours of the obtained solutions are shown by 3D, 2D, and contour surfaces.

Key words: Rational sine-Gordon expansion method; (1+1)-dimensional Fisher equation; conformable derivative; traveling wave solutions

AMS 2020 Classification: 35A25; 35C07; 35R11

1 Introduction

Mathematical modelling of physical systems leads to linear and nonlinear differential equations in physics, engineering, and other fields. Understanding physical processes described by nonlinear equations necessitates finding exact solutions. Aside from that, exact solutions can be used to calculate specific critical physical quantities analytically and for simulation [1]. There are some methods to calculate analytically including the Hirota's direct method [2], the tanh method [3], the extended tanh-function method [4], the multiple exp-function method [5], the transformed rational function method [6], the first integral method [7], the modified simplest equation method [8], the improved Bernoulli sub-ODE method [9], the Sine-Gordon expansion method [10, 11, 12], the modified exponential method [13]. Besides these analytical methods, there are many efficient numerical techniques have been submitted to the literature by mathematicians. For example, the q-homotopy analysis transform technique [14], the trapezoidal base homotopy perturbation method [15], and others [16, 17, 18]. The paper aims to find exact soliton solutions of the conformable (1+1)-dimensional Fisher equation [19] by using the rational sine-Gordon expansion method. The (1+1)-dimensional Fisher equation

$$u_t = \alpha^2 u_{xx} + pu - \beta u^3, \quad (1)$$

describes the process of diffusion and reaction interacting. Fisher presented this equation as a model for mutant gene propagation, with $u(x, t)$ denoting the density of favourable mutations, α^2 as diffusion factor [20]. This equation is used in chemical kinetics and population dynamics and is also used to solve problems like the nonlinear evolution of a population in one-dimensional habitat space or the neutron population in a nuclear reaction [21]. Zhou et al. have applied the improved $\tan(\varphi(\xi)/2)$ -expansion

method, the generalized Kudryashov method and the extended (G'/G)-expansion method, and gained the bright-like, dark-like and singular-like solitary wave solutions [19]. Triki and Wazwaz have used the trial equation method to a generalized Fisher equation, and gained some new wave solutions [22]. As a different approach, Matinfar et al. [23] focused on the numerical solution. In this context, they obtained solutions compatible with the exact solution by applying the generalized two-dimensional differential transform method. In this article, we will apply the rational sine-Gordon expansion method to the (1+1)-dimensional Fisher equation with conformable derivative to construct wave solutions. The conformable derivative operator overcomes some limitations of other fractional operators (Caputo, Riemann-Liouville, Caputo-Fabrizio and etc.) and provides basic properties of classical calculus such as the quotient rule, the chain rule, the product of two functions, Rolle's and mean value theorems. The application of the conformable derivative is simpler and very effective.

The rest of the paper is organized as follows: In Section 2, we describe the conformable derivative and its fundamental properties. In Section 3, the basic steps of the rational sine-Gordon expansion method, which is the novelty of the paper are presented. In Section 4, we apply the proposed method to the (1+1)-dimensional Fisher equation. Several conclusions are given in the last section.

2 Preliminary remarks on the conformable derivative

Definition 1 Given a function $h : [0, \infty) \rightarrow \mathbb{R}$. Then the conformable derivative of h order γ is defined by

$$L_\gamma(h)(t) = \lim_{\varepsilon \rightarrow 0} \frac{h(t + \varepsilon t^{1-\gamma}) - h(t)}{\varepsilon},$$

for all $t > 0, \gamma \in (0, 1]$ [24].

Theorem 1 Let L_γ be the derivative operator with order $\gamma \in (0, 1]$ and h, k be γ -differentiable at a point $t > 0$. Then we have the following properties [24, 25]:

- i. $L_\gamma(ah + bk) = aL_\gamma(h) + bL_\gamma(k), \forall a, b \in \mathbb{R}$.
- ii. $L_\gamma(t^p) = pt^{p-\gamma}, \forall p \in \mathbb{R}$.
- iii. $L_\gamma(hk) = hL_\gamma(k) + kL_\gamma(h)$.
- iv. $L_\gamma\left(\frac{h}{k}\right) = \frac{kL_\gamma(h) - hL_\gamma(k)}{k^2}$.
- v. $L_\gamma(\lambda) = 0$, for all constant functions $h(t) = \lambda$.
- vi. If h is differentiable, then $L_\gamma(h)(t) = t^{1-\gamma} \frac{dh}{dt}(t)$.

■

3 Fundamental structure of the RSGEM

Before giving the rational sine-Gordon expansion method (RSGEM) [26, 27, 28], we will explain the sine-Gordon expansion method (SGEM). Let us suppose the sine-Gordon equation

$$\varphi_{xx} - \varphi_{tt} = m^2 \sin(\varphi), \quad (2)$$

where $\varphi = \varphi(x, t)$, m is a real constant. Considering the wave transform $\varphi = \varphi(x, t) = \Phi(\xi)$, $\xi = \mu(x - ct)$ into Eq. (2), gives the nonlinear ordinary differential equation (NODE) as,

$$\Phi'' = \frac{m^2}{\mu^2(1-c^2)} \sin(\Phi), \quad (3)$$

where $\Phi = \Phi(\xi)$, μ is the amplitude and c is the velocity of the travelling wave, respectively. We find as follows after full simplification of Eq. (3);

$$\left[\left(\frac{\Phi}{2}\right)'\right]^2 = \frac{m^2}{\mu^2(1-c^2)} \sin^2\left(\frac{\Phi}{2}\right) + C, \quad (4)$$

where C is the constant of integration. Replacing $C = 0$, $\omega(\xi) = \frac{\Phi}{2}$ and $A^2 = \frac{m^2}{\mu^2(1-c^2)}$ in Eq. (4), gives;

$$\omega' = A \sin(\omega). \quad (5)$$

Setting $A = 1$ in Eq. (5), gives

$$\omega' = \sin(\omega). \quad (6)$$

Solving Eq. (6) by variables separable, we get the two significant properties of trigonometric functions as follows;

$$\sin(w) = \sin[w(\xi)] = \frac{2pe^\xi}{p^2e^{2\xi} + 1} \Big|_{p=1} = \operatorname{sech}(\xi), \tag{7}$$

$$\cos(w) = \cos[w(\xi)] = \frac{p^2e^{2\xi} - 1}{p^2e^{2\xi} + 1} \Big|_{p=1} = \operatorname{tanh}(\xi), \tag{8}$$

where $p \neq 0$ is the integration constant. Let's consider the nonlinear partial differential equation (NPDE) of the form below, for which the solution is searched;

$$P(\varphi, \varphi_x, \varphi_t, \varphi_{xx}, \varphi_{tt}, \varphi_{xt}, \varphi_{xxx}, \varphi_{xxt}, \varphi^2, \dots) = 0. \tag{9}$$

We apply the wave transformation, $\varphi = \varphi(x, t) = \Phi(\xi)$, $\xi = kx + w\frac{t^\gamma}{\gamma}$ into Eq. (9), it gives the following equation,

$$N\left(\Phi, \frac{d\Phi}{d\xi}, \frac{d^2\Phi}{d\xi^2}, \dots\right) = 0, \tag{10}$$

where N is a nonlinear ordinary equation (NODE) that has partial derivatives of Φ depending on ξ . The SGEM, the solution of Eq. (9) is considered in the following form

$$\Phi(\xi) = \sum_{i=1}^n \operatorname{tanh}^{i-1}(\xi) [b_i \operatorname{sech}(\xi) + a_i \operatorname{tanh}(\xi)] + a_0. \tag{11}$$

Eq. (11) can be rearranged considering Eqs. (7) and (8) as follows;

$$\Phi(\omega) = \sum_{i=1}^n \cos^{i-1}(\omega) [b_i \sin(\omega) + a_i \cos(\omega)] + a_0. \tag{12}$$

As we know, rational functions are more general functions than polynomial functions. We can obtain significantly general forms of wave solutions which are including polynomial function solutions by this way. The different point of the method is the solution functions have two auxiliary functions, viz. $\operatorname{sech}(\xi)$, $\operatorname{tanh}(\xi)$ We consider the following solution form

$$\Phi(\xi) = \frac{\sum_{i=1}^M \operatorname{tanh}^{i-1}(\xi) [a_i \operatorname{sech}(\xi) + c_i \operatorname{tanh}(\xi)] + a_0}{\sum_{i=1}^M \operatorname{tanh}^{i-1}(\xi) [b_i \operatorname{sech}(\xi) + d_i \operatorname{tanh}(\xi)] + b_0}, \tag{13}$$

which is also written as

$$\Phi(\omega) = \frac{\sum_{i=1}^M \cos^{i-1}(\omega) [a_i \sin(\omega) + c_i \cos(\omega)] + a_0}{\sum_{i=1}^M \cos^{i-1}(\omega) [b_i \sin(\omega) + d_i \cos(\omega)] + b_0}, \tag{14}$$

where $a_i, b_i, c_i, d_i, a_0, b_0$ are constants that will be determined later. a_i, b_i, c_i, d_i values are not all zero at the same time. The value of M is determined using the balance principle between the highest power nonlinear term and the highest derivative in NODE. After equating the coefficients of $\sin^i(\omega) \cos^j(\omega)$ to zero, we find a set of algebraic equations. $a_i, b_i, c_i, d_i, a_0, b_0$ values are found in solving the set of algebraic equations by Wolfram Mathematica 12. At the end, we substitute these values into Eq. (13) and get the new travelling wave solutions of Eq. (9).

4 Application of RSGEM

The (1+1)-dimensional conformable Fisher equation is given as

$$u_t^\gamma = \alpha^2 u_{xx} + pu - \beta u^3, \tag{15}$$

where γ is the order of the conformable derivative between $0 < \gamma \leq 1$.

We use the wave transformation as given below,

$$u(x, t) = U(\xi), \xi = kx + w\frac{t^\gamma}{\gamma}, \tag{16}$$

where k, w are constants that will be determined. Getting partial derivatives of $U(\xi)$ the function with respect to x, t , we find a non-linear ordinary differential equation as

$$wU' - \alpha^2 k^2 U'' - pU + \beta U^3 = 0. \tag{17}$$

According to the homogeneous balance principle, we obtain a relationship between U'' and U^3 in Eq. (17), $M = 1$. For $M = 1$, Eq. (13) turns to the below form.

$$U(\xi) = \frac{a_0 + a_1 \operatorname{sech}(\xi) + c_1 \tanh(\xi)}{b_0 + b_1 \operatorname{sech}(\xi) + d_1 \tanh(\xi)}. \tag{18}$$

We put Eq. (18) and its first and second-order derivatives into Eq. (17) and can obtain a system of algebraic equations. By using Wolfram Mathematica 12, $a_0, a_1, b_0, b_1, c_1, d_1$ and the other parameters can be found. Finally, we put these coefficients into Eq. (13) and obtain new travelling wave solutions of Eq. (1).

Case-1

$$a_1 = \frac{ib_1\sqrt{w\beta} - \sqrt{\beta(6\beta a_0^2 - wb_1^2)}}{\beta\sqrt{6}}, d_1 = \frac{ia_0\sqrt{6\beta}}{\sqrt{w}}, c_1 = -a_0, p = -\frac{2w}{3}, k = \frac{i\sqrt{w}}{\alpha\sqrt{3}}, b_0 = 0.$$

Putting the above coefficients into Eq. (13), yields

$$u_1(x, t) = - \left\{ \frac{\operatorname{Sec} \left[\frac{\sqrt{wx}}{\sqrt{3}\alpha} - \frac{it^\gamma w}{\gamma} \right] \left(-i\sqrt{w\beta}b_1 + \sqrt{\beta(6\beta a_0^2 - wb_1^2)} \right)}{\sqrt{6}\beta} - a_0 \left(-1 + i \operatorname{Tan} \left[\frac{\sqrt{wx}}{\sqrt{3}\alpha} - \frac{it^\gamma w}{\gamma} \right] \right) \right\} / \operatorname{Sec} \left[\frac{\sqrt{wx}}{\sqrt{3}\alpha} - \frac{it^\gamma w}{\gamma} \right] b_1 - \sqrt{\frac{6\beta}{w}} a_0 \operatorname{Tan} \left[\frac{\sqrt{wx}}{\sqrt{3}\alpha} - \frac{it^\gamma w}{\gamma} \right]. \tag{19}$$

where $i^2 = \sqrt{-1}$. Considering the suitable values of parameters, we can find wave simulations for Eq. (19) as following Figures 1 and 2:

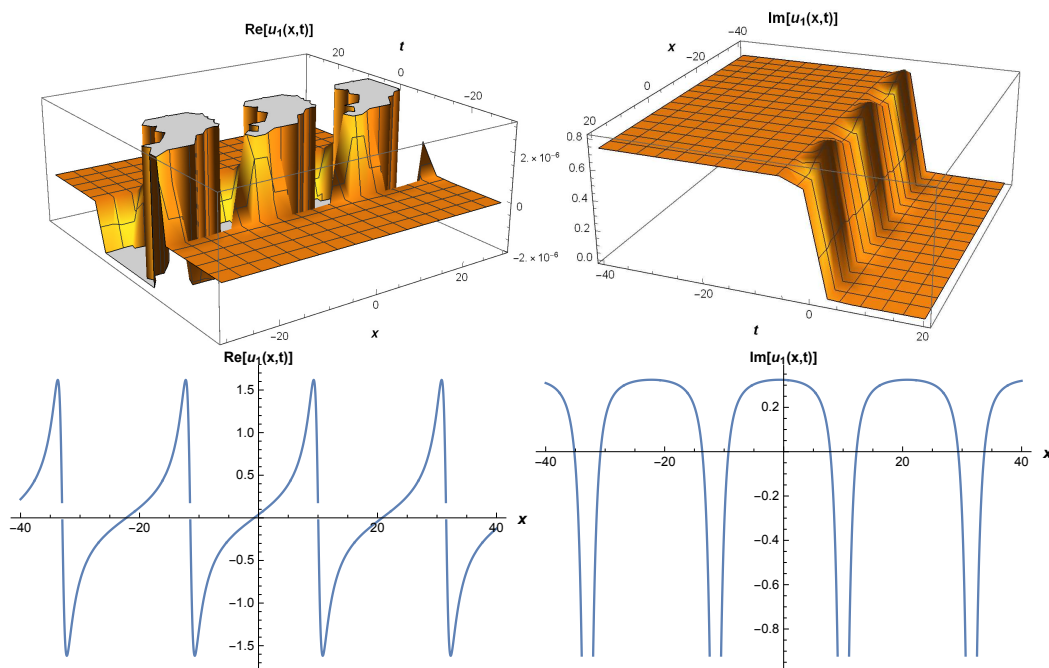


Figure 1. The 3D and 2D surfaces of the wave solution (19) by considering the values $\gamma = 0.9, a_0 = 2.1, b_1 = 1.2, \alpha = 2.5, w = 1.6, \beta = 2, t = 0.1$.

Case-2

$$a_1 = \frac{a_0 b_1}{b_0} - \sqrt{a_0^2 \left(-1 + \frac{b_1^2}{b_0^2} \right)}, c_1 = -a_0, w = -\frac{6\beta a_0^2}{b_0^2}, \alpha = \frac{\sqrt{2\beta} a_0}{k b_0}, p = \frac{4\beta a_0^2}{b_0^2}, d_1 = 0.$$

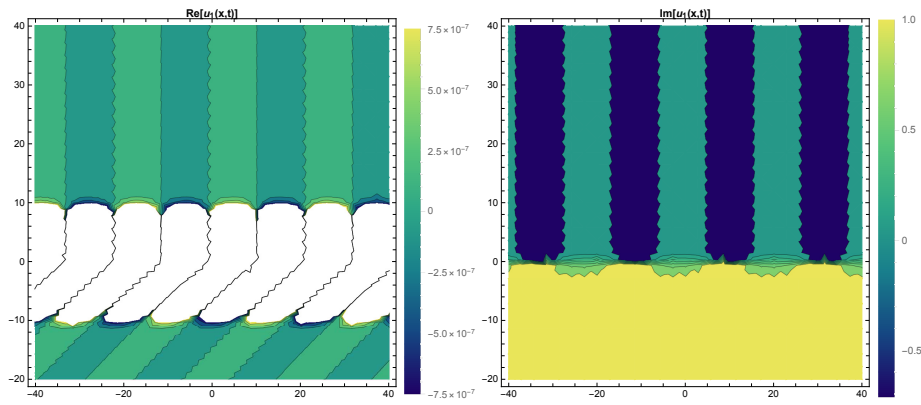


Figure 2. The contour plot surfaces of the wave solution Eq. (19) by considering the values $\gamma = 0.9, a_0 = 2.1, b_1 = 1.2, \alpha = 2.5, w = 1.6, \beta = 2, t = 0.1$.

Putting the above coefficients into Eq. (13), yields

$$u_2(x, t) = \frac{-\operatorname{Sech}\left[kx - \frac{6t\gamma\beta a_0^2}{\gamma b_0^2}\right] \sqrt{a_0^2\left(-1 + \frac{b_1^2}{b_0^2}\right)} + a_0 \left(1 + \frac{\operatorname{Sech}\left[kx - \frac{6t\gamma\beta a_0^2}{\gamma b_0^2}\right] b_1}{b_0} - \operatorname{Tanh}\left[kx - \frac{6t\gamma\beta a_0^2}{\gamma b_0^2}\right]\right)}{b_0 + \operatorname{Sech}\left[kx - \frac{6t\gamma\beta a_0^2}{\gamma b_0^2}\right] b_1} \quad (20)$$

When we consider the suitable values of parameters, we can find wave simulations for Eq. (20) as following figures:

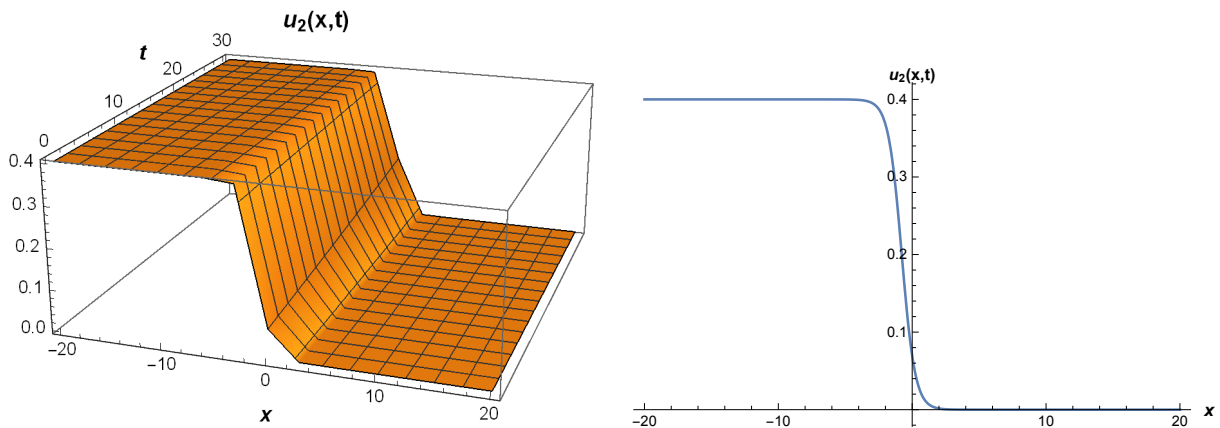


Figure 3. The 3D and 2D surfaces of the wave solution Eq. (20) by considering the values $\gamma = 0.9, a_0 = 0.2, b_1 = 2.5, b_0 = 1, k = 2, \beta = 0.2, t = 0.1$.

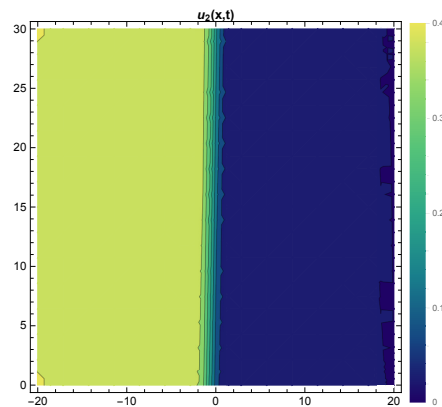


Figure 4. The contour plot surfaces of the wave solution (20) by considering the values $\gamma = 0.9, a_0 = 0.2, b_1 = 2.5, b_0 = 1, k = 2, \beta = 0.2, t = 0.1$.

Case-3

$$a_1 = -\sqrt{\frac{\beta a_0^2 + k^2 \alpha^2 b_1^2 - \sqrt{2k^2 \alpha^2 \beta a_0^2 b_1^2 + k^4 \alpha^4 b_1^4}}{\beta}}, d_1 = -\frac{\sqrt{2\beta} a_0}{k\alpha}, b_0 = 0, c_1 = -\frac{a_1 \left(k^2 \alpha^2 b_1^2 + \sqrt{2k^2 \alpha^2 \beta a_0^2 b_1^2 + k^4 \alpha^4 b_1^4} \right)}{\sqrt{2\beta} k \alpha a_0 b_1},$$

$$p = 2k^2 \alpha^2, \quad w = \frac{3c_1}{a_0}.$$

Putting these coefficients into Eq. (13), yields

$$u_3(x, t) = \frac{k\alpha \left(a_0 + a_1 \operatorname{Sech} \left[kx + \frac{3c_1 t \gamma}{a_0 \gamma} \right] + c_1 \operatorname{Tanh} \left[kx + \frac{3c_1 t \gamma}{a_0 \gamma} \right] \right)}{k\alpha b_1 \operatorname{Sech} \left[kx + \frac{3c_1 t \gamma}{a_0 \gamma} \right] - \sqrt{2\beta} a_0 \operatorname{Tanh} \left[kx + \frac{3c_1 t \gamma}{a_0 \gamma} \right]}. \tag{21}$$

When we consider the suitable values of parameters, we can find wave simulations for Eq. (21) as following figures:

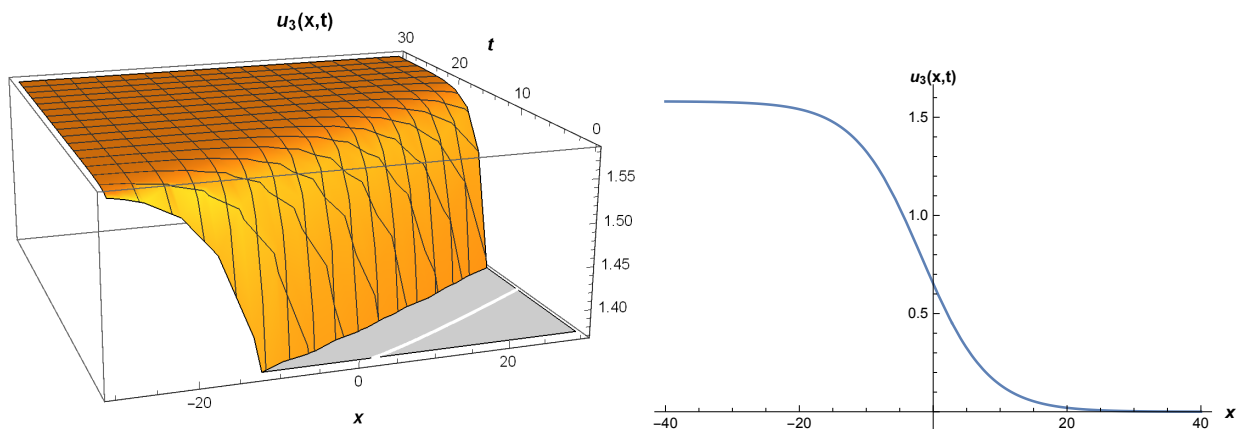


Figure 5. The 3D and 2D surfaces of the wave solution (21) by considering the values $\gamma = 0.9, a_0 = 2.5, b_1 = 1.5, \alpha = 2.5, k = 0.2, \beta = 0.2, t = 0.1$

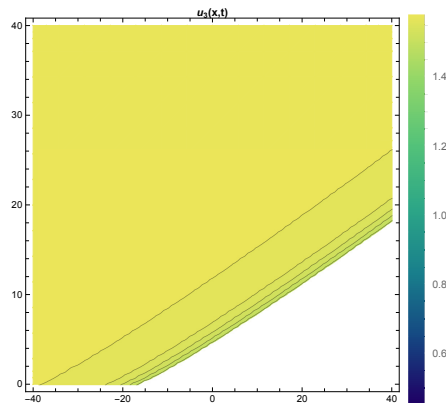


Figure 6. The contour plot surfaces of the wave solution (21) by considering the values $\gamma = 0.9, a_0 = 2.5, b_1 = 1.5, \alpha = 2.5, k = 0.2, \beta = 0.2, t = 0.1$.

Case-4

$$a_1 = -\frac{a_0 b_1 + \sqrt{a_0^2 (b_1^2 + d_1^2)}}{d_1}, c_1 = -a_0, \alpha = -\frac{\sqrt{p}}{\sqrt{2k}}, \beta = \frac{p d_1^2}{4 a_0^2}, w = -\frac{3p}{2}, b_0 = 0,$$

Putting these values into Eq. (13), yields

$$u_4(x, t) = -\frac{a_0 \left(b_1 - e^{-kx + \frac{3pt\gamma}{2\gamma}} d_1 \right) + \sqrt{a_0^2 (b_1^2 + d_1^2)}}{d_1 \left(b_1 + \text{Sinh} \left[kx - \frac{3pt\gamma}{2\gamma} \right] d_1 \right)}. \tag{22}$$

When we consider the suitable values of parameters, we can find wave simulations for Eq. (22) as following figures:

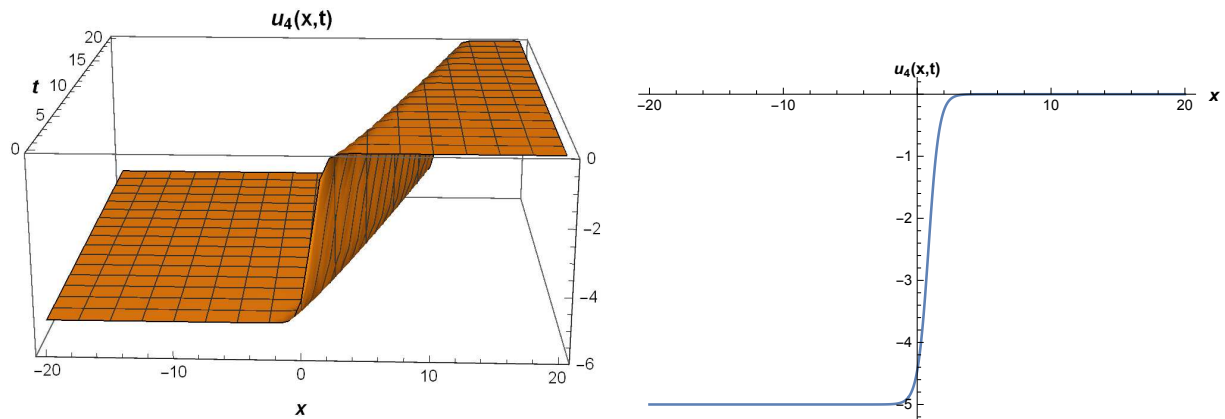


Figure 7. The 3D and 2D surfaces of the wave solution (22) by considering the values $\gamma = 0.9, a_0 = 2.5, b_1 = 3.1, d_1 = 1, p = 1.2, k = 2.5, t = 0.1$.

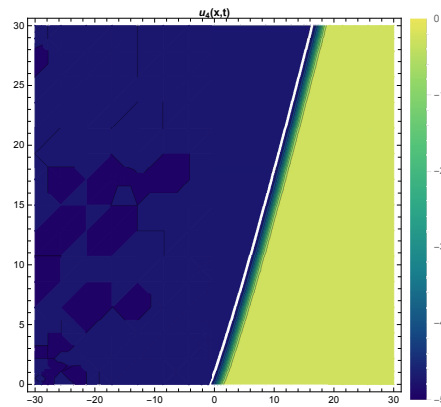


Figure 8. The contour plot surfaces of the wave solution (22) by considering the values $\gamma = 0.9, a_0 = 2.5, b_1 = 3.1, d_1 = 1, p = 1.2, k = 2.5, t = 0.1$.

Case-5

$$c_1 = \frac{-a_1 b_1 + \sqrt{a_1^2 (-b_0^2 + b_1^2)}}{b_0}, a_0 = \frac{a_1 b_1 - \sqrt{a_1^2 (-b_0^2 + b_1^2)}}{b_0}, w = -3k^2 \alpha^2, \beta = \frac{k^2 \alpha^2 \left(-a_1 (b_0^2 - 2b_1^2) + 2b_1 \sqrt{a_1^2 (-b_0^2 + b_1^2)} \right)}{2a_1^3},$$

$$p = 2k^2 \alpha^2, d_1 = 0.$$

Putting these values into Eq. (13), yields

$$u_5(x, t) = \frac{2 \left(a_1 \left(e^{kx - \frac{3k^2 \alpha^2 t \gamma}{\gamma}} b_0 + b_1 \right) - \sqrt{a_1^2 (-b_0^2 + b_1^2)} \right)}{\left(1 + e^{2 \left(kx - \frac{3k^2 \alpha^2 t \gamma}{\gamma} \right)} \right) b_0 \left(b_0 + \operatorname{Sech} \left[kx - \frac{3k^2 \alpha^2 t \gamma}{\gamma} \right] b_1 \right)} \tag{23}$$

When we consider the suitable values of parameters, we can find wave simulations for Eq. (23) as following figures:

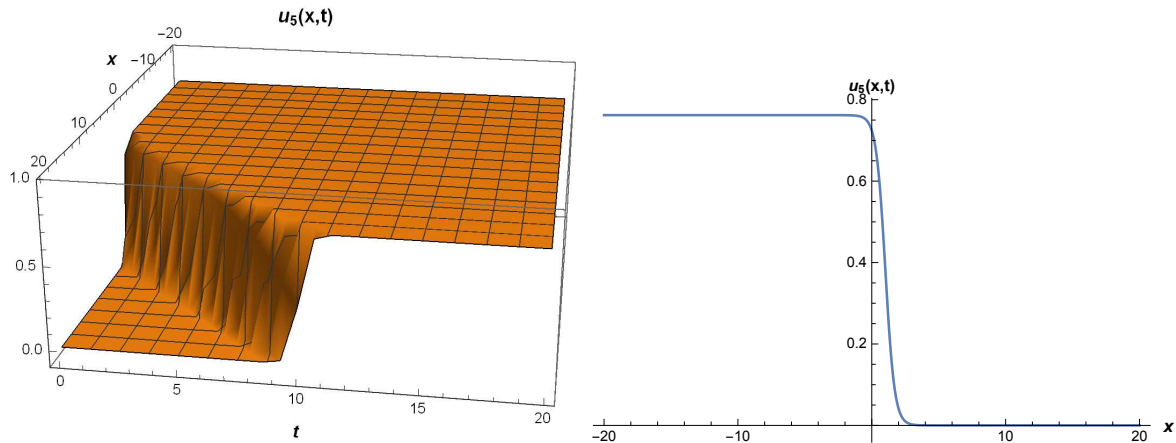


Figure 9. The 3D and 2D surfaces of the wave solution (23) by considering the values $\theta = 0.9, a_1 = 1.5, b_1 = 2, b_0 = 0.5, \alpha = 0.5, k = 2.9, t = 0.1$.

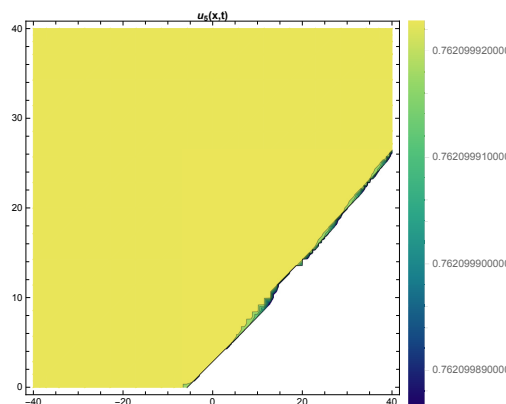


Figure 10. The contour plot surfaces of the wave solution (23) by considering the values $\theta = 0.9, a_1 = 1.5, b_1 = 2, b_0 = 0.5, \alpha = 0.5, k = 2.9, t = 0.1$.

5 Conclusion

In this paper, the rational sine-Gordon expansion method has been applied to the (1+1)-dimensional conformable Fisher equation. We have obtained some new wave solutions including hyperbolic and trigonometric functions. Figure 1 shows multi-soliton solution surfaces both imaginary and real parts of Eq. (19). Figure 3, Figure 5, and Figure 9 show the anti-kink soliton surfaces for Eq. (20), Eq. (21) and Eq. (23), respectively. Figure 7 shows the kink soliton surface for Eq. (22). Kink-type solitons are travelling wave solutions that climb up or climb down from one phase to another, and kink soliton reaches a constant at infinity. The mentioned model is used for modelling the relationship between the rate of inflation and both real and nominal interest rates, population dynamics in nonlinear media, and logistic population growth models, as well [20, 29, 30]. Fisher’s model has been investigated by a numerical technique which is the q-homotopy analysis transform method (q-HATM) in [31]. They considered the time-fractional Fisher’s model in Caputo’s sense. Besides, they assumed special values of the coefficients in the model. The main advantage of the proposed method is the derived solutions include many other analytical techniques. According to new results and all figures, it has been observed that this method is a powerful tool for obtaining analytical solutions of nonlinear partial differential equations such as governing models. We hope that the provided solutions may be useful for scientists in mathematical biology, neurophysiology, chemical reactions, and economy.

Declarations

Consent for publication

Not applicable

Conflicts of interest

The authors declare that they have no conflict of interest.

Funding

Not applicable.

Author's contributions

G.Y.: Conceptualization, Methodology, Software, Writing - Original Draft, M.K.: Conceptualization, Methodology, Writing - Original Draft A.C.: Methodology, Writing - Review and Editing. All authors discussed the results and contributed to the final manuscript.

Acknowledgements

Not applicable.

References

- [1] Cooper, F., Khare, A., Mihaila, B., & Saxena, A. Exact solitary wave solutions for a discrete $\lambda\phi^4$ field theory in (1+1)-dimensions. *Physical Review E*, 72(3), 036605, (2005). [[CrossRef](#)]
- [2] Hirota, R. Exact solution of the Korteweg–de Vries equation for multiple collision of solitons. *Physical Review Letters*, 27(18), 1192–1194, (1971). [[CrossRef](#)]
- [3] Malfliet, W. Solitary wave solutions of nonlinear wave equations. *American Journal of Physics*, 60(7), 650–654, (1992). [[Cross-Ref](#)]
- [4] Fan, E. Extended tanh-function method and its applications to nonlinear equations. *Physics Letters A*, 277(4–5), 212–218, (2000). [[CrossRef](#)]
- [5] Ma, W.X., Huang T., & Zhang, Y. A multiple exp-function method for nonlinear differential equations and its application. *Physica Scripta*, 82(6), 065003, (2010). [[CrossRef](#)]
- [6] Ma, W.X., & Lee, J.H. A transformed rational function method and exact solutions to the (3+1)-dimensional Jimbo–Miwa equation. *Chaos, Solitons & Fractals*, 42(3), 1356–1363, (2009). [[CrossRef](#)]
- [7] Feng, Z.S., & Wang, X.H. The first integral method to the two dimensional Burgers–Korteweg–de Vries equation. *Physics Letters A*, 308(2–3), 173–178, (2003). [[CrossRef](#)]
- [8] Jawad, A.J.A.M., Petkovic, M.D., & Biswas, A. Modified simple equation method for nonlinear evolution equations. *Applied Mathematics and Computation*, 217(2), 869–877, (2010). [[CrossRef](#)]
- [9] Aksan, E.N., Bulut, H., & Kayhan, M. Some wave simulation properties of the (2+1) dimensional breaking soliton equation. *ITM Web Of Conferences*, 13, 01014, (2017). [[CrossRef](#)]
- [10] Bulut, H., Aksan, E.N., Kayhan, M., & Sulaiman, T.A. New solitary wave structures to the (3+1) dimensional Kadomtsev–Petviashvili and Schrödinger equation. *Journal of Ocean Engineering and Science*, 4(4), 373–378, (2019). [[CrossRef](#)]
- [11] Yel, G., Baskonus, H.M., & Bulut, H. Novel archetypes of new coupled Konno–Oono equation by using sine–Gordon expansion method. *Optical and Quantum Electronics*, 49(9), 285, (2017). [[CrossRef](#)]
- [12] Yan, L., Baskonus, H.M., Cattani, C., & Gao, W. Extractions of the gravitational potential and high-frequency wave Perturbation properties of nonlinear (3+1)- dimensional Vakhnenko–Parkes equation via novel approach. *Mathematical Methods in the Applied Sciences*, 1–10, (2022). [[CrossRef](#)]
- [13] Chen, Q., Baskonus, H.M., Gao, W., & Ilhan, E. Soliton theory and modulation instability analysis: The Ivancevic option pricing model in economy. *Alexandria Engineering Journal*, 61(10), 7843–7851, (2022). [[CrossRef](#)]
- [14] Veerasha, P., Yavuz, M., & Bhaishya, C. A computational approach for shallow water forced Korteweg–De Vries equation on critical flow over a hole with three fractional operators. *An International Journal of Optimization and Control: Theories & Applications*, 11(3), 52–67, (2021). [[CrossRef](#)]
- [15] Jayaprakasha, P.C., & Bhaishya, C. Numerical analysis of predator–prey model in presence of toxicant by a novel approach. *Mathematics in Computer Science*, 11(4), 3963–3983, (2021). [[CrossRef](#)]
- [16] Bhaishya, C. A new application of Hermite collocation method. *International Journal of Mathematical, Engineering and Management Sciences*, 14(1), 182–190, (2019). [[CrossRef](#)]
- [17] Bhaishya, C., & Jaipala. Comparative study of homotopy perturbation method and Genocchi polynomial method for first order fractional differential equation. *Journal of Computer and Mathematical Sciences*, 10(1), 197–206, (2019). [[CrossRef](#)]
- [18] Bhaishya, C., & Veerasha, P. Laguerre polynomial-based operational matrix of integration for solving fractional differential equations with non-singular kernel. *Proceedings of the Royal Society A*, 477(2253), 20210438, (2021). [[CrossRef](#)]
- [19] Zhou, Q., Ekici M., Sonmezoglu, A., Manafian, J., Khaleghizadeh, S., & Mirzazadeh, M. Exact solitary wave solutions to the generalized Fisher equation. *Optik*, 127(24), 12085–12092, (2016). [[CrossRef](#)]

- [20] Fisher, R.A. The advance of advantageous genes. *Annals of Eugenics*, 7(4), 355–369, (1937). [[CrossRef](#)]
- [21] Wazwaz, A.M. The extended tanh method for abundant solitary wave solutions of nonlinear wave equations. *Applied Mathematics and Computation*, 187(2), 1131–1142, (2007). [[CrossRef](#)]
- [22] Triki, H., & Wazwaz, A.M. Trial equation method for solving the generalized Fisher equation with variable coefficients. *Physics Letters A*, 380(13), 1260–1262, (2016). [[CrossRef](#)]
- [23] Matinfar, M., Bahar, S.R., & Ghasemi, M. Solving the Generalized Fisher's equation by differential transform method. *Journal of Applied Mathematics and Informatics*, 30(3–4), 555–560, (2012). [[CrossRef](#)]
- [24] Khalil, R., Al Horani, M., Yousef, A., & Sababheh, M. A new definition of fractional derivative. *Journal of Computational and Applied Mathematics*, 264, 65–70, (2014). [[CrossRef](#)]
- [25] Atangana, A., Baleanu, D., & Alsaedi, A. New properties of conformable derivative. *Open Mathematics*, 13(1), 889–898, (2015). [[CrossRef](#)]
- [26] Yan, L., Yel, G., Baskonus, H.M., Bulut, H., & Gao, W. Newly developed analytical method and its applications of some mathematical models. *International Journal of Modern Physics B*, 36(04), 2250040, (2022). [[CrossRef](#)]
- [27] Yan, L., Yel, G., Kumar, A., Baskonus, H.M., & Gao, W. Newly developed analytical scheme and its applications to the some nonlinear partial differential equations with the conformable derivative. *Fractal and Fractional*, 5(4), 238, 1–15, (2021). [[CrossRef](#)]
- [28] Yamgoué, S.B., Deffo, G.R., & Pelap, F.B. A new rational sine-Gordon expansion method and application to nonlinear wave equations arising in mathematical physics. *The European Physical Journal Plus*, 134(8), 380, (2019). [[CrossRef](#)]
- [29] Tyson, J.J., & Brazhnik, P.K. On travelling wave solutions of Fisher's equation in two spatial dimensions. *SIAM Journal on Applied Mathematics*, 60(2), 371–391, (2000). [[CrossRef](#)]
- [30] Murray, J.D. *Mathematical Biology: I. An Introduction* (3rd Edition). Springer (2002).
- [31] Veerasha, P., Prakasha, D.G., & Baskonus, H.M. Novel simulations to the time fractional Fisher's equation. *Mathematical Sciences*, 13(1), 33–42, (2019). [[CrossRef](#)]

Mathematical Modelling and Numerical Simulation with Applications (MMNSA) (<https://www.mmnsa.org>)



Copyright: © 2022 by the authors. This work is licensed under a Creative Commons Attribution 4.0 (CC BY) International License. The authors retain ownership of the copyright for their article, but they allow anyone to download, reuse, reprint, modify, distribute, and/or copy articles in MMNSA, so long as the original authors and source are credited. To see the complete license contents, please visit (<http://creativecommons.org/licenses/by/4.0/>).



RESEARCH PAPER

On the relations between a singular system of differential equations and a system with delays

Ioannis Dassios  1,*,[†]

¹FRESLIPS, University College Dublin, Dublin, Ireland

*Corresponding Author

[†]ioannis.dassios@ucd.ie, idassios@ed.ac.uk (Ioannis Dassios)

Abstract

In this article, we consider a class of systems of differential equations with multiple delays. We define a transform that reformulates the system with delays into a singular linear system of differential equations whose coefficients are non-square constant matrices, and the number of their columns is greater than the number of their rows. By studying only the singular system, we provide a form of solutions for both systems.

Key words: Delays; differential; singular systems; underdetermined systems

AMS 2020 Classification: 93B30; 93B60; 93C05

1 Introduction

In this article, we consider a class of systems of differential equations with multiple delays and define a transform that reformulates the system with delays into an underdetermined singular linear system of differential equations. The importance of this article is to develop a new idea and method that can bring new insight to researchers between systems with delays and singular systems of differential equations.

We are interested in the following system of differential equations with delays:

$$A_{n+1}x'(t) = A_0x(t) + A_1x(t + \tau_1) + A_2x(t + \tau_2) + \dots + A_nx(t + \tau_n) + V(t), \quad (1)$$

where $\tau_i > 0$ is constant time delay, $V \in \mathbb{C}^{r \times 1}$, $A_i \in \mathbb{C}^{r \times r}$, and $x : [0, +\infty) \rightarrow \mathbb{C}^{r \times 1}$.

Systems of differential equations with delays have become more and more important nowadays. In the past few years, there have been lots of papers concerned with delays, see [18, 25, 26, 30], and their applications in macroeconomics, engineering, etc, see [4, 19, 27, 22, 23, 24, 31, 35].

We now consider the following singular system of differential equations:

$$EY'(t) = AY(t) + V(t), \quad (2)$$

where $E, A \in \mathbb{C}^{r \times m}$, $r < m$, $V \in \mathbb{C}^{r \times 1}$, and $Y : [0, +\infty) \rightarrow \mathbb{C}^{m \times 1}$.

Singular systems of differential equations, see [2, 3, 5, 7, 12, 17, 20], and difference equations, see [8, 21] have attracted the interest of several researchers in the last few decades. Some interesting results have also been obtained for singular systems of equations evolving fractional operators, see [1, 6, 9, 11, 13, 15, 29, 34]. This type of systems appear in control theory, see [3, 10, 33], and in several applications in electrical engineering such as the modeling of electrical circuits, see [20], electricity markets, see [14], and power system dynamics, see [28, 32].

The article provides mainly two results. For the first result we consider the system with delays (1) and construct an equivalent singular system with a singular pencil without delays in the form of (2). This result can also be seen as a transform that connects these two systems. In the second result we consider the singular system (2) and by using matrix theory we provide a form of its solutions. Then, by using this formula and by taking into account that (2) is equivalent to (1), without any further computations we obtain a form of solutions also for the system with delays (1). Through this method we aim to connect two systems of different nature and have an alternative way to discuss and study the system with delays (1).

2 Main results

We, firstly, state the following theorem:

Theorem 1 Consider a system with delays in the form of (1). Then there exists a singular system of differential equations in the form of (2) that is equivalent to (1).

Proof 1 System (1) has the form

$$A_{n+1}x'(t) = A_0x(t) + A_1x(t + \tau_1) + A_2x(t + \tau_2) + \dots + A_nx(t + \tau_n) + V(t).$$

We adopt the following notation:

$$\begin{aligned} y_1(t) &= x(t), \\ y_2(t) &= x(t - \tau_1), \\ y_3(t) &= x(t - \tau_2), \\ &\vdots \\ y_n(t) &= x(t - \tau_n). \end{aligned}$$

Furthermore

$$\begin{aligned} y'_1(t) &= x'(t), \\ y'_2(t) &= x'(t - \tau_1), \\ y'_3(t) &= x'(t - \tau_2), \\ &\vdots \\ y'_n(t) &= x'(t - \tau_n). \end{aligned}$$

Equivalently, we get:

$$\begin{bmatrix} A_{n+1} & 0_{r,r} & 0_{r,r} & \dots & 0_{r,r} \end{bmatrix} \begin{bmatrix} y'_1(t) \\ y'_2(t) \\ y'_3(t) \\ \vdots \\ y'_n(t) \end{bmatrix} = \begin{bmatrix} A_0 & A_1 & A_2 & \dots & A_n \end{bmatrix} \begin{bmatrix} y_1(t) \\ y_2(t) \\ y_3(t) \\ \vdots \\ y_n(t) \end{bmatrix} + V(t),$$

or, equivalently, in matrix form

$$EY'(t) = AY(t) + V(t),$$

where $m = r \cdot n$, $Y = \begin{bmatrix} y_1(t) \\ y_2(t) \\ y_3(t) \\ \vdots \\ y_n(t) \end{bmatrix}$, and $E = \begin{bmatrix} A_{n+1} & 0_{r,r} & 0_{r,r} & \dots & 0_{r,r} \end{bmatrix}$, $A = \begin{bmatrix} A_0 & A_1 & A_2 & \dots & A_n \end{bmatrix}$.

The proof is completed. ■

The importance of Theorem 1 is that we may study a system in the form of (1) which has delays through a system that may be singular and underdetermined, but it is linear and without delays. This system has a pencil that is singular because the matrix coefficients are non-square with $r < m$.

Despite several studies, most articles in the literature deal with singular systems that have regular pencils. The regularity of the pencil means that the matrices are square $r = m$, while the pencil formed has a determinant not identically equal to zero. Focus is then given in studying the solutions and stability of such a system through the eigenvalues of this pencil.

Singular systems with singular pencils are usually avoided. There are two types of singular pencils. A first case is the matrix coefficients of the system to be square but with a pencil that has a determinant identically zero. Meaning that the pencil is not invertible, something that is crucial for the existence of solutions of the system that appears in the frequency domain after the Laplace transform is applied to the system in the time domain. The other type of singular pencil is the matrix coefficients to be

non-square. In this case, the determinant of the pencil cannot be defined.

In this article, as already mentioned, we study the system with delays (1) through the system (2) which is a singular underdetermined system of linear differential equations. The pencil of this type of system is singular. Unlike the regular pencil which may have finite eigenvalues & an infinite eigenvalue, a singular pencil has additional invariants the minimal column and row minimal indices. This type of invariant for such a pencil is not always easy to be obtained. It becomes even more complicated when dealing with large-scale systems. Another important characteristic of this case considered is that the existence of solutions for a system with a singular pencil is not automatically satisfied. This is very important for many applications for which the model is significant only for a certain range of its parameters. In these cases, a careful interpretation of results or even a redesign of the system may be needed.

In general, the pencil of (2) is characterized by a uniquely defined element, known as the complex Kronecker canonical form, see [3], [16], specified by the complete set of invariants of the singular pencil $sE - A$. This is the set of the finite-infinite eigenvalues and the minimal column-row indices. In the case of $r < m$ there exist only column minimal indices. Let \mathcal{N}_r be the right null space of a matrix respectively. Then the equations $(sE - A)U(s) = 0_{r,1}$, have solutions in $V(s)$, which are vectors in the rational vector spaces $\mathcal{N}_r(sE - A)$. The binary vectors $U(s)$ express dependence relationships among the rows of $sE - A$. Note that $U(s) \in \mathbb{C}^{r \times 1}$ are polynomial vectors. Let $d = \dim \mathcal{N}_r(sE - A)$. It is known, that $\mathcal{N}_r(sE - A)$ as rational vector spaces, are spanned by minimal polynomial bases of minimal degrees

$$\epsilon_1 = \epsilon_2 = \dots = \epsilon_g = 0 < \epsilon_{g+1} \leq \dots \leq \epsilon_{g+h},$$

which is the set of *column minimal indices* of $sE - A$. This means there are $g + h = d$ column minimal indices. We are interested only in the h non-zero minimal indices. To sum up the invariants of a singular pencil with $r < m$ is the finite - infinite eigenvalues of the pencil and the minimal column indices as described above. Following the above given analysis, there exist non-singular matrices P, Q with $P \in \mathbb{C}^{r \times r}, Q \in \mathbb{C}^{m \times m}$, such that

$$\begin{aligned} PEQ &= E_K = I_p \oplus H_q \oplus E_\epsilon, \\ PAQ &= A_K = J_p \oplus I_q \oplus A_\epsilon, \end{aligned} \tag{3}$$

where J_p is the Jordan matrix for the finite eigenvalues, H_q is a nilpotent matrix with index q_* which is actually the Jordan matrix of the zero eigenvalues of the pencil $sA - E$. The matrices E_ϵ, A_ϵ are defined as

$$E_\epsilon = \text{blockdiag} \{ L_{\epsilon_{g+1}}, L_{\epsilon_{g+2}}, \dots, L_{\epsilon_d} \}, \tag{4}$$

where $L_\epsilon = \begin{bmatrix} I_\epsilon & \vdots & 0_{\epsilon,1} \end{bmatrix}$, for $\epsilon = \epsilon_{g+1}, \dots, \epsilon_d$

$$A_\epsilon = \text{blockdiag} \{ \tilde{L}_{\epsilon_{g+1}}, \tilde{L}_{\epsilon_{g+2}}, \dots, \tilde{L}_{\epsilon_d} \},$$

where $\tilde{L}_\epsilon = \begin{bmatrix} 0_{\epsilon,1} & \vdots & I_\epsilon \end{bmatrix}$, for $\epsilon = \epsilon_{g+1}, \dots, \epsilon_d$. Finally, the matrices P, Q can be written as

$$P = \begin{bmatrix} P_1 \\ P_2 \\ P_3 \end{bmatrix}, \quad Q = \begin{bmatrix} Q_p & Q_q & Q_\epsilon \end{bmatrix}, \tag{5}$$

and by substituting the transformation $Y(t) = QZ(t)$ into (2) we obtain

$$EY'(t)QZ(t) = AQZ(t) + V(t),$$

whereby, multiplying by P , using (3)-(5) and setting $Z(t) = \begin{bmatrix} Z_p(t) \\ Z_q(t) \\ Z_\epsilon(t) \end{bmatrix}$, we arrive at at the subsystems

$$Z'_p(t) = J_p Z_p(t) + P_1 V(t), \tag{6}$$

$$H_q Z'_q(t) = Z_q(t) + P_2 V(t), \tag{7}$$

and

$$E_\epsilon Z'_\epsilon(t) = A_\epsilon Z_\epsilon(t) + P_3 V(t). \tag{8}$$

The subsystems (6), (7) have the following solutions, respectively:

$$Z_p(t) = e^{Jp t} c + \int_0^\infty e^{Jp(t-u)} P_1 V(u) du,$$

and

$$Z_q(t) = - \sum_{i=0}^{q_*-1} H_q^i P_2 \frac{d^i}{dt^i} V(t).$$

The third subsystem has infinite solutions which can be taken arbitrarily as $Z_\epsilon = C(t)$. This can be proved as follows:

Let $P_3 V = \begin{bmatrix} V_{\epsilon_{g+1}} \\ V_{\epsilon_{g+2}} \\ \vdots \\ V_{\epsilon_d} \end{bmatrix}$. If we set $Z_\epsilon = \begin{bmatrix} Z_{\epsilon_{g+1}} \\ Z_{\epsilon_{g+2}} \\ \vdots \\ Z_{\epsilon_d} \end{bmatrix}$, then we get

$$[L_{\epsilon_{g+1}} \oplus \dots \oplus L_{\epsilon_d}] \begin{bmatrix} Z'_{\epsilon_{g+1}} \\ Z'_{\epsilon_{g+2}} \\ \vdots \\ Z'_{\epsilon_d} \end{bmatrix} = [\tilde{L}_{\epsilon_{g+1}} \oplus \dots \oplus \tilde{L}_{\epsilon_d}] \begin{bmatrix} Z_{\epsilon_{g+1}} \\ Z_{\epsilon_{g+2}} \\ \vdots \\ Z_{\epsilon_d} \end{bmatrix} + \begin{bmatrix} V_{\epsilon_{g+1}} \\ V_{\epsilon_{g+2}} \\ \vdots \\ V_{\epsilon_d} \end{bmatrix}.$$

For the non-zero blocks, an arbitrary equation can be written as

$$L_{\epsilon_i} Z'_{\epsilon_i} = \tilde{L}_{\epsilon_i} Z_{\epsilon_i} + V_{\epsilon_i}, \quad i = g + 1, g + 2, \dots, d,$$

or, equivalently,

$$\begin{bmatrix} I_{\epsilon_i} & \vdots & 0_{\epsilon_i,1} \end{bmatrix} Z'_{\epsilon_i} = \begin{bmatrix} 0_{\epsilon_i,1} & \vdots & I_{\epsilon_i} \end{bmatrix} Z_{\epsilon_i} + V_{\epsilon_i},$$

or, equivalently,

$$\begin{bmatrix} 1 & 0 & \dots & 0 & 0 \\ 0 & 1 & \dots & 0 & 0 \\ \vdots & \vdots & \dots & \vdots & \vdots \\ 0 & 0 & \dots & 1 & 0 \end{bmatrix} \begin{bmatrix} Z'_{\epsilon_i,1} \\ Z'_{\epsilon_i,2} \\ \vdots \\ Z'_{\epsilon_i,\epsilon_i} \\ Z'_{\epsilon_i,\epsilon_i+1} \end{bmatrix} = \begin{bmatrix} 0 & 1 & \dots & 0 & 0 \\ 0 & 0 & \dots & 0 & 0 \\ \vdots & \vdots & \dots & \vdots & \vdots \\ 0 & 0 & \dots & 0 & 1 \end{bmatrix} \begin{bmatrix} Z_{\epsilon_i,1} \\ Z_{\epsilon_i,2} \\ \vdots \\ Z_{\epsilon_i,\epsilon_i} \\ Z_{\epsilon_i,\epsilon_i+1} \end{bmatrix} + \begin{bmatrix} V_{\epsilon_i,1} \\ V_{\epsilon_i,2} \\ \vdots \\ V_{\epsilon_i,\epsilon_i} \\ V_{\epsilon_i,\epsilon_i+1} \end{bmatrix},$$

or, equivalently,

$$\begin{aligned} Z'_{\epsilon_i,1} &= Z_{\epsilon_i,2} + V_{\epsilon_i,1}, \\ Z'_{\epsilon_i,2} &= Z_{\epsilon_i,3} + V_{\epsilon_i,2}, \\ &\vdots \\ Z'_{\epsilon_i,\epsilon_i} &= Z'_{\epsilon_i,\epsilon_i+1} + V_{\epsilon_i,\epsilon_i}. \end{aligned}$$

It is clear from the above analysis that there is the number of unknown functions is $\epsilon_i + 1$ while the number of equations is ϵ_i . Hence by setting $C := C(t)$, the solutions of Z_ϵ can only be taken arbitrary as:

$$Z_\epsilon = C.$$

To conclude, in the case of a singular pencil with $r < m$, system (2) has the solution

$$Y(t) = QZ(t) = \begin{bmatrix} Q_p & Q_q & Q_\epsilon \end{bmatrix} \begin{bmatrix} Z_p(t)\Phi_0(t)C + \int_0^\infty \Phi(t-\tau)V(\tau)d\tau \\ - \sum_{i=0}^{q_*-1} H_q^i P_2 V^{(i)}(t) \\ Z_\epsilon \end{bmatrix},$$

or, equivalently,

$$Y(t) = Q_p \left[\Phi_0(t)C + \int_0^\infty \Phi(t-\tau)V(\tau)d\tau \right] - Q_q \sum_{i=0}^{q_*-1} H_q^i P_2 V^{(i)}(t) + Q_\epsilon Z_\epsilon. \tag{9}$$

To sum up, the solution of (2) can be written in the form:

$$Y(t) = QZ(t),$$

or, equivalently,

$$Y = \begin{bmatrix} Q_p & Q_q & Q_\epsilon \end{bmatrix} \begin{bmatrix} Z_p(t) \\ Z_q(t) \\ Z_\epsilon(t) \end{bmatrix},$$

or, equivalently,

$$Y = Q_p [e^{Jp t} c + \int_0^\infty e^{Jp(t-u)} P_1 V(u) du] - Q_q \left[\sum_{i=0}^{q_*-1} H_q^i P_2 \frac{d^i}{dt^i} V(t) \right] + Q_\epsilon C(t),$$

or, equivalently,

$$Y = Q_p e^{Jp t} c + QK(t),$$

where

$$K(t) = \begin{bmatrix} \int_0^\infty e^{Jp(t-u)} P_1 V(u) du \\ -Q_q \left[\sum_{i=0}^{q_*-1} H_q^i P_2 \frac{d^i}{dt^i} V(t) \right] \\ Q_\epsilon C(t) \end{bmatrix},$$

and $Q_p \in \mathbb{C}^{m \times p}$, and $Q \in \mathbb{C}^{m \times m}$. Hence by setting

$$Q_p = \begin{bmatrix} Q_p^1 \\ Q_p^2 \end{bmatrix}, \quad Q = \begin{bmatrix} Q^1 \\ Q^2 \end{bmatrix},$$

where $Q_p^1 \in \mathbb{C}^{r \times p}$, and $Q^1 \in \mathbb{C}^{r \times m}$, we arrive at the solution of the system with delays (1):

$$x(t) = Q_p^1 e^{Jp t} c + Q^1 K(t).$$

3 Conclusions

In this article, we considered a class of systems with delays in the form of (1). We proved that the system with delays can be studied through an equivalent singular system of differential equations whose coefficients are non-square constant matrices and the number of their columns is greater than the number of their rows. By taking into consideration that the relevant pencil is singular, we provided a formula for solutions. The importance of this result is that we may study system (1) which has delays through system (2), which may be singular and underdetermined, but it is linear and without delays.

As a future direction, we aim to further extend these theoretical results and examine relevant applications where delays appear, i.e. dynamics of electrical power systems, macroeconomic models, electricity market models, etc. In addition, we aim to extend our results to other types of systems where the memory effect appears such as systems of fractional differential equations, and systems of fractional nabla difference equations. For all this, there is already some research in progress.

Declarations

Consent for publication

Not applicable.

Conflicts of interest

The author declares that he has no conflict of interest.

Funding

Not applicable.

Author's contributions

The research was carried out by the author and he accepts that the contributions and responsibilities belong to the author.

Acknowledgements

This work was supported by the Sustainable Energy Authority of Ireland (SEAI), by funding Ioannis Dassios under Grant No. RDD/00681.

References

- [1] Batiha, I., El-Khazali, R., AlSaedi, A., & Momani, S. The general solution of singular fractional-order linear time-invariant continuous systems with regular pencils. *Entropy*, 20(6), 400, (2018). [[CrossRef](#)]
- [2] Campbell, S.L. *Singular systems of differential equations*, Pitman, San Francisco, Vol. 1, 1980; Vol. 2, (1982).
- [3] Dai, L. *Singular Control Systems*, Lecture Notes in Control and Information Sciences Edited by M.Thoma and A.Wyner (1988).
- [4] Dassios, I.K., Zimbidis, A., & Kontzalis, C.P. The delay effect in a stochastic multiplier–accelerator model. *Journal of Economic Structures*, 3(7), 1–24, (2014).
- [5] Dassios, I., Tzounas, G., & Milano, F. The Möbius transform effect in singular systems of differential equations. *Applied Mathematics and Computation*, 361, 338–353, (2019). [[CrossRef](#)]
- [6] Dassios, I. Stability and robustness of singular systems of fractional nabla difference equations. *Circuits, Systems and Signal Processing*, 36(1), 49–64, (2017). [[CrossRef](#)]
- [7] Dassios, I., Tzounas, G., & Milano, F. Participation factors for singular systems of differential equations. *Circuits, Systems and Signal Processing*, 39(1), 83–110, (2020). [[CrossRef](#)]
- [8] Dassios, I., & Kalogeropoulos, G. On a non-homogeneous singular linear discrete time system with a singular matrix pencil. *Circuits, Systems, and Signal Processing*, 32(4), 1615–1635, (2013). [[CrossRef](#)]
- [9] Dassios, I.K., & Baleanu, D.I. Caputo and related fractional derivatives in singular systems. *Applied Mathematics and Computation*, 337, 591–606, (2018). [[CrossRef](#)]
- [10] Dassios, I., Tzounas, G., & Milano, F. Generalized fractional controller for singular systems of differential equations. *Journal of Computational and Applied Mathematics*, 378, 112919, (2020). [[CrossRef](#)]
- [11] Dassios, I., & Milano, F. Singular dual systems of fractional-order differential equations. *Mathematical Methods in the Applied Sciences*, 1–18, (2021). [[CrossRef](#)]
- [12] Dassios, I., Tzounas, G., & Milano, F. Robust stability criterion for perturbed singular systems of linearized differential equations. *Journal of Computational and Applied Mathematics*, 381, 113032, (2021). [[CrossRef](#)]
- [13] Dassios, I.K., Baleanu, D.I., & Kalogeropoulos, G.I. On non-homogeneous singular systems of fractional nabla difference equations. *Applied Mathematics and Computation*, 227, 112–131, (2014). [[CrossRef](#)]
- [14] Dassios, I., Kerci, T., Baleanu, D., & Milano, F. Fractional-order dynamical model for electricity markets. *Mathematical Methods in the Applied Sciences*, 1– 13, (2021). [[CrossRef](#)]
- [15] Dassios, I., Tzounas, G., Liu, M., & Milano, F. Singular over-determined systems of linear differential equations. *Mathematics and Computers in Simulation*, 197, 396–412, (2022). [[CrossRef](#)]
- [16] Gantmacher, R.F. *The Theory of Matrices*(Vol.1 and Vol.2). Chelsea, New York, (1959).
- [17] Duan, G. R. *The Analysis and Design of Descriptor Linear Systems*(Vol.23). Springer, (2011).
- [18] Fu, P., Niculescu, S.I., & Chen, J. Stability of linear neutral time–delay systems: Exact conditions via matrix pencil solutions. *IEEE Transactions on Automatic Control*, 51(6), 1063–1069, (2006). [[CrossRef](#)]
- [19] Kitano, M., Nakanishi, T., & Sugiyama, K. Negative group delay and superluminal propagation: An electronic circuit approach. *IEEE Journal of selected Topics in Quantum electronics*, 9(1), 43–51, (2003). [[CrossRef](#)]
- [20] Lewis, F. L. A survey of linear singular systems. *Circuits, Systems and Signal Processing*, 5(1), 3–36, (1986). [[CrossRef](#)]
- [21] Liu, Y., Wang, J., Gao, C., Gao, Z., & Wu, X. On stability for discrete-time non-linear singular systems with switching actuators via average dwell time approach. *Transactions of the Institute of Measurement and Control*, 39(12), 1771–1776, (2017). [[CrossRef](#)]
- [22] Liu, M., Dassios, I., & Milano, F. Delay margin comparisons for power systems with constant and time-varying delays. *Electric Power Systems Research*, 190, 106627, (2021). [[CrossRef](#)]
- [23] Liu, M., Dassios, I., & Milano, F. On the stability analysis of systems of neutral delay differential equations. *Circuits, Systems, and Signal Processing*, 38(4), 1639–1653, (2019). [[CrossRef](#)]
- [24] Liu, M., Dassios, I., Tzounas, G., & Milano, F. Model-independent derivative control delay compensation methods for power systems. *Energies*, 13(2), 342, (2020). [[CrossRef](#)]
- [25] Michiels, W., & Niculescu, S.I. *Stability and stabilization of time-delay systems: an eigenvalue-based approach*. Society for Industrial and Applied Mathematics(SIAM), Philadelphia, (2007).
- [26] Michiels, W., & Niculescu, S.I. Characterization of delay-independent stability and delay interference phenomena. *SIAM journal on control and optimization*, 45(6), 2138–2155, (2007). [[CrossRef](#)]
- [27] Milano, F., & Dassios, I. Small-signal stability analysis for non-index 1 Hessenberg form systems of delay differential-algebraic equations. *IEEE Transactions on Circuits and Systems I: Regular Papers*, 63(9), 1521–1530, (2016). [[CrossRef](#)]
- [28] Milano, F., & Dassios, I. Primal and dual generalized eigenvalue problems for power systems small-signal stability analysis. *IEEE Transactions on Power Systems*, 32(6), 4626–4635, (2017). [[CrossRef](#)]
- [29] Naim, M., Sabbar, Y., Zahri, M., Ghanbari, B., Zeb, A., Gul, N., Djilali, S., & Lahmidi, F. The impact of dual time delay and Caputo fractional derivative on the long-run behavior of a viral system with the non-cytolytic immune hypothesis. *Physica Scripta*, 97(12), 124002, (2022). [[CrossRef](#)]
- [30] Santra, S.S., Ghosh, A., & Dassios, I. Second-order impulsive differential systems with mixed delays: Oscillation theorems. *Mathematical Methods in the Applied Sciences*, 45(18), 12184–12195, (2022). [[CrossRef](#)]
- [31] Tzounas, G., Dassios, I., & Milano, F. Small-signal stability analysis of implicit integration methods for power systems with delays. *Electric Power Systems Research*, 211, 108266, (2022). [[CrossRef](#)]
- [32] Tzounas, G., Dassios, I., & Milano, F. Modal participation factors of algebraic variables. *IEEE Transactions on Power Systems*, 35(1), 742–750, (2019). [[CrossRef](#)]

- [33] Tzounas, G., Dassios, I., Murad, M.A.A., & Milano, F. Theory and implementation of fractional order controllers for power system applications. *IEEE Transactions on Power Systems*, 35(6), 4622–4631, (2020). [[CrossRef](#)]
- [34] Wei, Y., Peter, W.T., Yao, Z., & Wang, Y. The output feedback control synthesis for a class of singular fractional order systems. *ISA transactions*, 69, 1–9, (2017). [[CrossRef](#)]
- [35] Yu, X., & Jiang, J. Analysis and compensation of delays in field bus control loop using model predictive control. *IEEE Transactions on Instrumentation and Measurement*, 63(10), 2432–2446, (2014). [[CrossRef](#)]

Mathematical Modelling and Numerical Simulation with Applications (MMNSA) (<https://www.mmnsa.org>)



Copyright: © 2022 by the authors. This work is licensed under a Creative Commons Attribution 4.0 (CC BY) International License. The authors retain ownership of the copyright for their article, but they allow anyone to download, reuse, reprint, modify, distribute, and/or copy articles in MMNSA, so long as the original authors and source are credited. To see the complete license contents, please visit (<http://creativecommons.org/licenses/by/4.0/>).



RESEARCH PAPER

Dynamics of a fractional-order COVID-19 model under the nonsingular kernel of Caputo–Fabrizio operator

Saeed Ahmad^{1,†}, Dong Qiu^{2,3,†} and Mati ur Rahman^{4,†,*}

¹Department of Mathematics, University of Malakand, Chakdara Dir (L), KP, Pakistan, ²School of Mathematics and Information Science, Guangxi University, No. 100, East University Road, Nanning, 530004, P.R. China, ³College of Science, Chongqing University of Posts and Telecommunications, Nanan, 400065, Chongqing, China, ⁴School of Mathematical Science, Shanghai Jiao Tong University, P.R. China

*Corresponding Author

†saeedahmad@uom.edu.pk (Saeed Ahmad); qiudong@cqupt.edu.cn (Dong Qiu); mati-maths_374@sjtu.edu.cn (Mati ur Rahman)

Abstract

For the sake of human health, it is crucial to investigate infectious diseases including HIV/AIDS, hepatitis, and others. Worldwide, the recently discovered new coronavirus (COVID-19) poses a serious threat. The experimental vaccination and different COVID-19 strains found around the world make the virus' spread unavoidable. In the current research, fractional order is used to study the dynamics of a nonlinear modified COVID-19 SEIR model in the framework of the Caputo–Fabrizio fractional operator with order b . Fixed point theory has been used to investigate the qualitative analysis of the solution respectively. The well-known Laplace transform method is used to determine the approximate solution of the proposed model. Using the COVID-19 data that is currently available, numerical simulations are run to validate the necessary scheme and examine the dynamic behavior of the various compartments of the model. In order to stop the pandemic from spreading, our findings highlight the significance of taking preventative steps and changing one's lifestyle.

Key words: COVID-19 model; theoretical analysis; Laplace transform; Caputo–Fabrizio fractional operator; numerical simulations

AMS 2020 Classification: 37N25; 34A25; 44A10

1 Introduction

Since December 2019, the whole globe has been facing the dangerous and contagious new infection COVID-19. The infection has caused a lot of health, mental, economic, and unemployment problems throughout the globe. According to recent reports, over fifty million individuals are infected, and nearly four and a half million people have died from the said infection [1]. Pakistan has also been severely affected by COVID-19, with approximately 23,000 citizens dying and 1.5 million contracting the infection. Due to these circumstances, each and every country develops its own policy for controlling the pandemic. For this reason, they ban overcrowding in air transportation services, bus services, and various educational institutions. Different immigration services among the countries are also banned by the policymakers of each country. The big cause of this infection is the meeting of

infectious people with an uninfected population. Therefore keeping masks is also the cry of the day for reducing the transmission of COVID-19. Beyond this, some other precautionary measures are also taken by different countries [2].

The said pandemic is a cause of fear for humanity throughout the world, as most people are aware of past pandemics from which a considerable number of the population faced death. Technology advances over time, allowing for the cure and treatment of various epidemics. To overcome an epidemic, vaccines are prepared in the laboratory. Each related field of science plays a role in the establishment of control strategies, and among them is mathematical modeling. Mathematical modeling gives a prediction of various diseases by using past and future data. For the first time, a real-world problem had been studied via mathematical expressions in the eighteenth century. Following that, mathematical modelling has made significant contributions to the investigation of a wide range of real-world problems [3, 4, 5, 6].

Recently, the pandemic of COVID-19 has attracted the focus of many researchers in various fields as can be seen in [7, 8, 9, 10]. Mathematicians also played a role in the investigation of the said pandemic. The said disease has been transformed into mathematical expressions, and future predictions have been reported. Useful information about the past and present of the disease has been reported, which is advantageous in establishing control strategies for its eradication from society. In this regard, valuable work can be found in [11, 12, 13, 14, 15, 16]. The formation of a mathematical formula consists of conditions regarding the parameters involved in the problem under consideration. Various mathematical models exist in the literature that are helpful in understanding the spread of COVID-19 and suggest the adoption of policies necessary to control (optimize) the spread of the infection in an effective way. One of such remarkable models has been reported by [17]. The authors classified the total population into six categories. These includes the susceptible class \mathbb{S} , the latently infected compartment \mathbb{E} , the infected class \mathbb{I} , the class of recovered population \mathbb{R} , the demised class \mathbb{D} and \mathbb{M} is the COVID-19 filthy materials or surfaces in the atmosphere. The model reported in [17] has been expressed in the form of the following system of autonomous differential equations:

$$\begin{aligned}
 \frac{d\mathbb{S}}{dt} &= \Pi - (\tau + \alpha_1 + \beta q)\mathbb{S}, \\
 \frac{d\mathbb{E}}{dt} &= \beta q\mathbb{S} - (\vartheta + (1 - \kappa)\tau + \alpha_1)\mathbb{E}, \\
 \frac{d\mathbb{I}}{dt} &= \tau\mathbb{S} + (1 - \kappa)\tau\mathbb{E} - (\rho + \alpha_1 + \nu)\mathbb{I}, \\
 \frac{d\mathbb{R}}{dt} &= \vartheta\mathbb{E} + \nu\mathbb{I} - \alpha_1\mathbb{R}, \\
 \frac{d\mathbb{D}}{dt} &= \rho\mathbb{I} - \alpha_2\mathbb{D}, \\
 \frac{d\mathbb{M}}{dt} &= \sigma\mathbb{E} + \zeta\mathbb{I} - \varphi\mathbb{M},
 \end{aligned}
 \tag{1}$$

In model (1), the parameter description has been given in Table 1.

Parameters	values
Π	The rate of recruitment of susceptible class
α_1	Natural death rate except for dead population
α_2	Burning the carcass of dead population
ρ	The demise rate due to virus
ϑ	The rate of recovery from the infection
κ	The rate of average effectiveness of prevailing self-precautionary measures
φ	The rate of decay of \mathbb{M}
ζ	The transfer rate from \mathbb{I} to environment
τ	The rate of force of infection
β	The dissemination rate of susceptible class
q	The rate of change of behavior function
ν	The rate of recovered persons fro exposed class
σ	The shedding rate from \mathbb{E} to environment

Table 1. Description of the given parameters

Fractional calculus (FC), which has a wide range of applications in the modelling of physical processes, has grown in popularity among scholars over the past few decades. The ideas of classical calculus are made more universal by FC. Riemann–Liouville and Caputo conducted the initial investigation into the generalization of the ordinary integral and differential operators into fractional derivatives (FD) [18, 19]. After that, the fractional operator has been used by several researchers in a variety of sectors of science, engineering, and real-world issues [20, 21, 22]. In order to explore real-world issues including viscoelasticity systems, signal processing, diffusion processes, and control processing, fractional order differential equations provided a suitable framework, interested readers are directed to [23, 24, 25, 26]. Recently, in 2015 Caputo and Fabrizio introduced a new concept of fractional order derivative which has a non-singular kernel [27]. Several researchers have published many articles on this new concept of fractional derivatives; for instance, see [28, 29, 30]. The subject has been handled from a variety of angles, including quantitative analysis that considers existence, uniqueness, and regularity, as well as a numerical, analytical method, and the Laplace transform method to evaluate and interpret the data [31, 32, 33].

FC operators have more widespread advantages than the integer order operator since their nonlocal kernels are defined. The memory and history of any physical process are preserved by the fractional operators (FOs). The convolution of the kernels is a

topic of interest to many FOs. Numerous research publications have demonstrated the advantages of FOs over traditional operators. We go over some uses of FOs for the mathematical modelling of actual physical issues. According to the authors in [34], research was done on the COVID-19 pandemic disease’s fractional-order mathematical model, which was based on actual data. Authors in [35], based on actual clinical data, examined the human liver in fractional order. The authors in [36], examined three different fractional operators on the blood ethanol model. For modelling bacterial infections, specifically, researchers also employ FOs. The authors in [37] assessed the Salmonella bacterial infection using fractional operators. The authors in [38] using nonsingular fractional operators, the risky bacterial infection (Dengue fever) was studied. A significant amount of work has been done by researchers in the applications of FC and applied sciences [39, 40, 41, 42].

The motivation and novelty of our work are inspired by the above literature, we study a system of COVID-19 using Caputo–Fabrizio fractional derivative with the exponential kernel. We develop the theoretical results of the considered system. To observe the dissimilarity among the results of the fractional-order and classical models, we compare the concerning results. The obtained results reveal that the analysis obtained from the innovative fractional derivative is more conclusive compared with the analysis of classical derivatives.

The structure of this manuscript is as follows. In Section 2 we recall basic results and notations from FC. In Section 3, we develop the qualitative results for the system under investigation. In section 4, using the well-known Laplace transform together with the integral of Laplace, we find the numerical solution of the model under study. Taking into account the data available in the literature, we carry out numerical simulations in Section 5 and represent simulations graphically. At the end, we conclude our findings in Section 6.

2 Preliminaries

Here, we present some basic definitions from the literature.

Definition 1 [27] Let a function be $g \in H^1[0, T]$, where $T > 0$, and $b \in (0, 1)$, then the fractional Caputo-Fabrizio CF derivative is given by

$${}^{CF}D_t^b[g(\beta)] = \frac{\mathcal{N}(b)}{1-b} \int_0^t g'(\beta) \exp\left[-b \frac{t-\rho}{1-b}\right] d\beta,$$

where $\mathcal{N}(0) = \mathcal{N}(1) = 1$ is known as normalization function. Also for $g \in H^1[0, T]$, the the CF can be described by

$${}^{CF}D_t^b[g(\beta)] = \frac{\mathcal{N}(b)}{1-b} \int_0^t (g(\beta) - g(\rho)) \exp\left[-b \frac{t-\rho}{1-b}\right] d\rho,$$

Definition 2 Let g be a function, then the fractional integral of CF with order $b \in (0, 1)$ is given as

$${}^{CF}I_t^b[g(\beta)] = \frac{1-b}{\mathcal{N}(b)} + \frac{b}{\mathcal{N}(b)} \int_0^t g(\beta) d\beta, \quad t \geq 0.$$

Definition 3 [43] The Laplace transform for the CF derivative can be defined as

$$[{}^{CF}D_t^b g(\beta)] = \frac{\sigma[g(\beta)] - g(0)}{\sigma + b(1-\sigma)}, \quad \sigma \geq 0.$$

3 Theoretical results

In this part, we will convert the considered model (1) into fractional form. By using the fractional operator in the framework of CF by including order b such that $0 < b \leq 1$ is given as:

$$\begin{cases} {}^{CF}D_t^b \tilde{S}(t) = \Pi + \alpha_1 - (\tau + \beta q) \tilde{S}, \\ {}^{CF}D_t^b \tilde{E}(t) = \beta q \tilde{S} - (\alpha_1 + \vartheta + (1-\kappa)\tau) \tilde{E}, \\ {}^{CF}D_t^b \tilde{I}(t) = \tau \tilde{S} + \tau(1-\kappa) \tilde{E} - (\nu + \alpha_1 + \rho) \tilde{I}, \\ {}^{CF}D_t^b \tilde{R}(t) = \vartheta \tilde{E} - \alpha_1 \tilde{R} + \nu \tilde{I}, \\ {}^{CF}D_t^b \tilde{D}(t) = \rho \tilde{I} - \alpha_2 \tilde{D}, \\ {}^{CF}D_t^b \tilde{M}(t) = \sigma \tilde{E} + \zeta \tilde{I} - \varphi \tilde{M}, \end{cases} \tag{2}$$

with initial conditions

$$\tilde{S}_0 = \tilde{S}(0), \quad \tilde{E}_0 = \tilde{E}(0), \quad \tilde{I}_0 = \tilde{I}(0), \quad \tilde{R}_0 = \tilde{R}(0), \quad \tilde{D}_0 = \tilde{D}(0), \quad \tilde{M}_0 = \tilde{M}(0).$$

In this part of the manuscript, we first determine whether the solution to the problem under investigation really exists or not. We exploit the approach of fixed point theory to determine the existence along with the uniqueness of the model. To develop the existence theory we will apply Picard’s operator technique. In order to make mathematical analysis more efficient, we assume

that $\alpha_1 = \alpha_2 = \alpha$. To do this, we re-write the suggested model as

$$\begin{aligned}
 {}^{CF}D_t^b \tilde{S}(t) &= \mathbf{V}_1(t, \tilde{S}) = \Pi - (\tau + \alpha + \beta q)\tilde{S}, \\
 {}^{CF}D_t^b \tilde{E}(t) &= \mathbf{V}_2(t, \tilde{E}) = \beta q\tilde{S} - (\vartheta + (1 - \kappa)\tau + \alpha)\tilde{E}, \\
 {}^{CF}D_t^b \tilde{I}(t) &= \mathbf{V}_3(t, \tilde{I}) = \tau\tilde{S} + \tau(1 - \kappa)\tilde{E} - (\alpha + \nu + \rho)\tilde{I}, \\
 {}^{CF}D_t^b \tilde{R}(t) &= \mathbf{V}_4(t, \tilde{R}) = \vartheta\tilde{E} - \alpha\tilde{R} + \nu\tilde{I}, \\
 {}^{CF}D_t^b \tilde{D}(t) &= \mathbf{V}_5(t, \tilde{D}) = \rho\tilde{I} - \alpha\tilde{D}, \\
 {}^{CF}D_t^b \tilde{M}(t) &= \mathbf{V}_6(t, \tilde{M}) = \sigma\tilde{E} + \zeta\tilde{I} - \varphi\tilde{M}.
 \end{aligned}
 \tag{3}$$

In the following we set

$$F_j = \sup_{C[d, b_j]} \|\mathbf{V}_j(t, \tilde{S})\|, \quad \text{for } 1 \leq j \leq 6,
 \tag{4}$$

where

$$C[w, h_j] = [t - w, t + w] \times [u - c_j, u + c_j] = W \times W_j, \quad \text{for } j = 1, 2, \dots, 6.
 \tag{5}$$

Further, to demonstrate the existence as well as uniqueness of the concerned solution we define the norm on $C[w, h_j]$ where $1 \leq j \leq 6$ as follows

$$\|\tilde{\cup}\|_\infty = \sup_{t \in [t-w, t+h]} |\Phi(t)|.
 \tag{6}$$

The Picard operator is described by the expression

$$\mathbf{A} : C(W, W_1, W_2, W_3, W_4, W_5, W_6) \rightarrow C(W, W_1, W_2, W_3, W_4, W_5, W_6).
 \tag{7}$$

Applying ${}^{CF}I^b$ to all Eqns. of the considered system (2) and using (3), we obtain

$$\begin{cases}
 \tilde{S}(t) = \tilde{S}(0) + {}^{CF}I^b [\mathbf{V}_1(t, \tilde{S})], \\
 \tilde{E}(t) = \tilde{E}(0) + {}^{CF}I^b [\mathbf{V}_2(t, \tilde{E})], \\
 \tilde{I}(t) = \tilde{I}(0) + {}^{CF}I^b [\mathbf{V}_3(t, \tilde{I})], \\
 \tilde{R}(t) = \tilde{R}(0) + {}^{CF}I^b [\mathbf{V}_4(t, \tilde{R})], \\
 \tilde{D}(t) = \tilde{D}(0) + {}^{CF}I^b [\mathbf{V}_5(t, \tilde{D})], \\
 \tilde{M}(t) = \tilde{M}(0) + {}^{CF}I^b [\mathbf{V}_6(t, \tilde{M})].
 \end{cases}
 \tag{8}$$

Simplifying the RHS of the above equation we have

$$\Omega(t) = \Omega_0(t) + [\gamma(t, \Omega(t)) - \gamma_0(t)] \frac{1-b}{\mathcal{N}(b)} + \frac{b}{\mathcal{N}(b)} \int_0^t \gamma(x, \Omega(x)) dx,
 \tag{9}$$

where

$$\begin{cases}
 \Omega(t) = (\tilde{S}, \tilde{E}, \tilde{I}, \tilde{R}, \tilde{D}, \tilde{M})^T, \\
 \Omega_0(t) = (\tilde{S}_0, \tilde{E}_0, \tilde{I}_0, \tilde{R}_0, \tilde{D}_0, \tilde{M}_0)^T, \\
 \gamma(t, \Omega(t)) = (\mathbf{V}_i(t, \tilde{S}, \tilde{E}, \tilde{I}, \tilde{R}, \tilde{D}, \tilde{M}))^T, \quad 1 \leq i \leq 6.
 \end{cases}
 \tag{10}$$

Using Eq. (9) and Eq. (10), the operator defined in (7) can be expressed in the form

$$\mathbf{A}\Omega(t) = \Omega_0(t) + [\gamma(t, \Omega(t)) - \gamma_0(t)] \frac{1-b}{\mathcal{N}(b)} + \frac{b}{\mathcal{N}(b)} \int_0^t \gamma(\beta, \Omega(\beta)) d\beta.
 \tag{11}$$

In the next step, we will assume that the considered system satisfies the following

$$\|\Omega\| \leq \max\{w_1, w_2, w_3, w_4, w_5, w_6\}.
 \tag{12}$$

In this scenario, one may write

$$\begin{aligned}
 \|\mathbf{A}\Omega - \Omega_0(t)\| &= \sup_{t \in D} \left| \gamma(t, \Omega(t)) \frac{1-b}{\mathcal{N}(b)} + \frac{b}{\mathcal{N}(b)} \int_0^t \gamma(\beta, \Omega(\beta)) d\beta \right|, \\
 &\leq \frac{1-b}{\mathcal{N}(b)} \sup_{t \in D} |\gamma(t, \Omega(t))| + \frac{b}{\mathcal{N}(b)} \sup_{t \in D} \int_0^t |\gamma(\beta, \Omega(\beta))| d\beta, \\
 &\leq \frac{1+t_0}{\mathcal{N}(b)} \mathcal{K}, \quad \mathcal{K} = \max\{\mathcal{K}_j\} \quad \text{for } j = 1, 2, \dots, 6 \\
 &< \mathcal{K}w \leq \max\{w_1, w_2, w_3, w_4, w_5, w_6\} = \bar{w}, \quad t_0 = \sup\{t : t \in W\}.
 \end{aligned}
 \tag{13}$$

In the above Eq. (13), let us define $w = \frac{1+t_0}{\mathcal{N}(b)}$, we obtain

$$w < \frac{\bar{w}}{\mathcal{K}}.$$

Next, the given equality can be evaluated as

$$\|\mathbf{A}\Omega_1 - \mathbf{A}\Omega_2\| = \sup_{t \in W} |\Omega_1 - \Omega_2|, \tag{14}$$

we make the use of (9) and write

$$\begin{aligned}
 \|\mathbf{A}\Omega_1 - \mathbf{A}\Omega_2\| &= \sup_{t \in W} \left| \frac{1-b}{\mathcal{N}(b)} (\gamma(t, \Omega_1(t)) - \gamma(t, \Omega_2(t))) \right. \\
 &+ \left. \frac{b}{\mathcal{N}(b)} \int_0^t (\gamma(\beta, \Omega_1(\beta)) - \gamma(\beta, \Omega_2(\beta))) d\beta \right| \\
 &\leq \frac{1-b}{\mathcal{N}(b)} k \sup_{t \in W} |\Omega_1(t) - \Omega_2(t)| + \frac{bk}{\mathcal{N}(b)} \sup_{t \in W} \int_0^t |\Omega_1(\beta) - \Omega_2(\beta)| d\beta, \quad \text{where } k < 1 \\
 &\leq \left[\frac{1+t_0}{\mathcal{N}(b)} \right] k \|\Omega_1 - \Omega_2\| \\
 &\leq wk \|\Omega_1 - \Omega_2\|.
 \end{aligned}
 \tag{15}$$

Since Υ is a contraction, it follows that $wk < 1$. This reflects that the operator \mathbf{A} is a contraction as well. Consequently one may conclude the uniqueness of the solution of the system under study.

4 Analytical algorithm for the proposed model

In the following, we focus our attention on finding the general series solution of the model. With the help of Laplace transform, the given system may be transformed into the form

$$\begin{aligned}
 [\tilde{\mathcal{S}}(t)] &= \frac{\tilde{\mathcal{S}}(0)}{\sigma} + \frac{\sigma + b(1-\sigma)}{\sigma} [\Pi + \alpha - (\tau + \beta q)\tilde{\mathcal{S}}], \\
 [\tilde{\mathcal{E}}(t)] &= \frac{\tilde{\mathcal{E}}(0)}{\sigma} + \frac{\sigma + b(1-\sigma)}{\sigma} [\beta q \tilde{\mathcal{S}} - (\vartheta + (1-\kappa)\tau + \alpha)\tilde{\mathcal{E}}], \\
 [\tilde{\mathcal{I}}(t)] &= \frac{\tilde{\mathcal{I}}(0)}{\sigma} + \frac{\sigma + b(1-\sigma)}{\sigma} [\tau \tilde{\mathcal{S}} + \tau(1-\kappa)\tilde{\mathcal{E}} - (\alpha + \nu + \rho)\tilde{\mathcal{I}}], \\
 [\tilde{\mathcal{R}}(t)] &= \frac{\tilde{\mathcal{R}}(0)}{\sigma} + \frac{\sigma + b(1-\sigma)}{\sigma} [\vartheta \tilde{\mathcal{E}} - \alpha \tilde{\mathcal{R}} + \nu \tilde{\mathcal{I}}], \\
 [\tilde{\mathcal{D}}(t)] &= \frac{\tilde{\mathcal{D}}(0)}{\sigma} + \frac{\sigma + b(1-\sigma)}{\sigma} [\rho \tilde{\mathcal{I}} - \alpha \tilde{\mathcal{D}}], \\
 [\tilde{\mathcal{M}}(t)] &= \frac{\tilde{\mathcal{M}}(0)}{\sigma} + \frac{\sigma + b(1-\sigma)}{\sigma} [\sigma \tilde{\mathcal{E}} + \zeta \Pi - \varphi \tilde{\mathcal{M}}].
 \end{aligned}
 \tag{16}$$

Using the following series solution as

$$\begin{aligned}
 \tilde{\mathcal{S}}(t) &= \sum_{z=0}^{\infty} \tilde{\mathcal{S}}_z(t), \quad \tilde{\mathcal{E}}(t) = \sum_{z=0}^{\infty} \tilde{\mathcal{E}}_z(t), \quad \tilde{\mathcal{I}}(t) = \sum_{z=0}^{\infty} \tilde{\mathcal{I}}_z(t), \quad \tilde{\mathcal{R}}(t) = \sum_{z=0}^{\infty} \tilde{\mathcal{R}}_z(t), \\
 \tilde{\mathcal{D}}(t) &= \sum_{z=0}^{\infty} \tilde{\mathcal{D}}_z(t), \quad \tilde{\mathcal{M}}(t) = \sum_{z=0}^{\infty} \tilde{\mathcal{M}}_z(t).
 \end{aligned}
 \tag{17}$$

Using equations (17), the system (16) has the following form:

$$\begin{aligned}
 \left[\sum_{z=0}^{\infty} \tilde{S}_z(t) \right] &= \frac{\tilde{S}(0)}{\sigma} + \frac{\sigma + b(1 - \sigma)}{\sigma} \left[\Pi - (\tau + \beta q + \alpha) \sum_{z=0}^{\infty} \tilde{S}_z \right], \\
 \left[\sum_{z=0}^{\infty} \tilde{E}_z(t) \right] &= \frac{\tilde{E}(0)}{\sigma} + \frac{\sigma + b(1 - \sigma)}{\sigma} \left[\beta q \sum_{z=0}^{\infty} \tilde{S}_z - (\vartheta + \alpha + (1 - \kappa)\tau) \sum_{z=0}^{\infty} \tilde{E}_z \right], \\
 \left[\sum_{z=0}^{\infty} \tilde{I}_z(t) \right] &= \frac{\tilde{I}(0)}{\sigma} + \frac{\sigma + b(1 - \sigma)}{\sigma} \left[\tau \sum_{z=0}^{\infty} \tilde{S}_z + (1 - \kappa)\tau \sum_{z=0}^{\infty} \tilde{E}_z - (\alpha + \rho + \nu) \sum_{z=0}^{\infty} \tilde{I}_z \right], \\
 \left[\sum_{z=0}^{\infty} \tilde{R}_z(t) \right] &= \frac{\tilde{R}(0)}{\sigma} + \frac{\sigma + b(1 - \sigma)}{\sigma} \left[\vartheta \sum_{z=0}^{\infty} \tilde{E}_z + \nu \sum_{z=0}^{\infty} \tilde{I}_z - \alpha \sum_{z=0}^{\infty} \tilde{R}_z \right], \\
 \left[\sum_{z=0}^{\infty} \tilde{D}_z(t) \right] &= \frac{\tilde{D}(0)}{\sigma} + \frac{\sigma + b(1 - \sigma)}{\sigma} \left[\rho \sum_{z=0}^{\infty} \tilde{I}_z - \alpha \sum_{z=0}^{\infty} \tilde{D}_z \right], \\
 \left[\sum_{z=0}^{\infty} \tilde{M}_z(t) \right] &= \frac{\tilde{M}(0)}{\sigma} + \frac{\sigma + b(1 - \sigma)}{\sigma} \left[\sigma \sum_{z=0}^{\infty} \tilde{E}_z + \zeta \sum_{z=0}^{\infty} \tilde{I}_z - \varphi \sum_{z=0}^{\infty} \tilde{M}_z \right].
 \end{aligned}
 \tag{18}$$

Comparing similar terms on both sides of (18), we may arrive at

$$\begin{aligned}
 [\tilde{S}_0(t)] &= \frac{\tilde{S}_0}{\sigma}, \quad [\tilde{E}_0(t)] = \frac{\tilde{E}_0}{\sigma}, \quad [\tilde{I}_0(t)] = \frac{\tilde{I}_0}{\sigma}, \quad [\tilde{R}_0(t)] = \frac{\tilde{R}_0}{\sigma}, \\
 [\tilde{D}_0(t)] &= \frac{\tilde{D}_0}{\sigma}, \quad [\tilde{M}_0(t)] = \frac{\tilde{M}_0}{\sigma}, \\
 [\tilde{S}_1(t)] &= \frac{\sigma + b(1 - \sigma)}{\sigma} \left[\Pi - (\tau + \beta q + \alpha)\tilde{S}_0 \right], \\
 [\tilde{E}_1(t)] &= \frac{\sigma + b(1 - \sigma)}{\sigma} \left[\beta q\tilde{S}_0 - (\vartheta + \alpha + (1 - \kappa)\tau)\tilde{E}_0 \right], \\
 [\tilde{I}_1(t)] &= \frac{\sigma + b(1 - \sigma)}{\sigma} \left[\tau\tilde{S}_0 + (1 - \kappa)\tau\tilde{E}_0 - (\alpha + \rho + \nu)\tilde{I}_0 \right], \\
 [\tilde{R}_1(t)] &= \frac{\sigma + b(1 - \sigma)}{\sigma} \left[\vartheta\tilde{E}_0 + \nu\tilde{I}_0 - \alpha\tilde{R}_0 \right], \\
 [\tilde{D}_1(t)] &= \frac{\sigma + b(1 - \sigma)}{\sigma} \left[\rho\tilde{I}_0 - \alpha\tilde{D}_0 \right], \\
 [\tilde{M}_1(t)] &= \frac{\sigma + b(1 - \sigma)}{\sigma} \left[\sigma\tilde{E}_0 + \zeta\tilde{I}_0 - \varphi\tilde{M}_0 \right], \\
 [\tilde{S}_2(t)] &= \frac{\sigma + b(1 - \sigma)}{\sigma} \left[\Pi - (\tau + \beta q + \alpha)\tilde{S}_1 \right], \\
 [\tilde{E}_2(t)] &= \frac{\sigma + b(1 - \sigma)}{\sigma} \left[\beta q\tilde{S}_1 - (\vartheta + \alpha + (1 - \kappa)\tau)\tilde{E}_1 \right], \\
 [\tilde{I}_2(t)] &= \frac{\sigma + b(1 - \sigma)}{\sigma} \left[\tau\tilde{S}_1 + (1 - \kappa)\tau\tilde{E}_1 - (\alpha + \rho + \nu)\tilde{I}_1 \right], \\
 [\tilde{R}_2(t)] &= \frac{\sigma + b(1 - \sigma)}{\sigma} \left[\vartheta\tilde{E}_1 + \nu\tilde{I}_1 - \alpha\tilde{R}_1 \right], \\
 [\tilde{D}_2(t)] &= \frac{\sigma + b(1 - \sigma)}{\sigma} \left[\rho\tilde{I}_1 - \alpha\tilde{D}_1 \right], \\
 [\tilde{M}_2(t)] &= \frac{\sigma + b(1 - \sigma)}{\sigma} \left[\sigma\tilde{E}_1 + \zeta\tilde{I}_1 - \varphi\tilde{M}_1 \right], \\
 &\vdots \\
 [\tilde{S}_{q+1}(t)] &= \frac{\sigma + b(1 - \sigma)}{\sigma} \left[\Pi - (\tau + \beta q + \alpha)\tilde{S}_z \right], \\
 [\tilde{E}_{q+1}(t)] &= \frac{\sigma + b(1 - \sigma)}{\sigma} \left[\beta q\tilde{S}_z - (\vartheta + \alpha + (1 - \kappa)\tau)\tilde{E}_z \right], \\
 [\tilde{I}_{q+1}(t)] &= \frac{\sigma + b(1 - \sigma)}{\sigma} \left[\tau\tilde{S}_z + (1 - \kappa)\tau\tilde{E}_z - (\alpha + \rho + \nu)\tilde{I}_z \right], \\
 [\tilde{R}_{q+1}(t)] &= \frac{\sigma + b(1 - \sigma)}{\sigma} \left[\vartheta\tilde{E}_z + \nu\tilde{I}_z - \alpha\tilde{R}_z \right], \\
 [\tilde{D}_{q+1}(t)] &= \frac{\sigma + b(1 - \sigma)}{\sigma} \left[\rho\tilde{I}_z - \alpha\tilde{D}_z \right], \\
 [\tilde{M}_{q+1}(t)] &= \frac{\sigma + b(1 - \sigma)}{\sigma} \left[\sigma\tilde{E}_z + \zeta\tilde{I}_z - \varphi\tilde{M}_z \right].
 \end{aligned}
 \tag{19}$$

On computing the Laplace transform of Eq. (19), we have

$$\begin{aligned}
 \tilde{S}_0(t) &= N_1, \quad \tilde{E}_0(t) = N_2, \quad \tilde{I}_0(t) = N_3, \quad \tilde{R}_0(t) = N_4, \quad \tilde{D}_0(t) = N_5, \quad \tilde{M}_0(t) = N_6, \\
 \tilde{S}_1(t) &= \left[\Pi - (\tau + \beta q + \alpha)N_1 \right] (1 + b(t - 1)), \\
 \tilde{E}_1(t) &= \left[\beta q N_1 - (\alpha + \vartheta + (1 - \kappa)\tau)N_2 \right] (1 + b(t - 1)), \\
 \tilde{I}_1(t) &= \left[\tau N_1 + \tau(1 - \kappa)N_2 - (\rho + \alpha + \nu)N_3 \right] (1 + b(t - 1)), \\
 \tilde{R}_1(t) &= \left[\vartheta N_2 + \nu N_3 - \alpha N_4 \right] (1 + b(t - 1)), \\
 \tilde{D}_1(t) &= \left[\rho N_3 - \alpha N_5 \right] (1 + b(t - 1)), \\
 \tilde{M}_1(t) &= \left[\sigma N_2 + \zeta N_3 - \varphi N_6 \right] (1 + b(t - 1)), \\
 \tilde{S}_2(t) &= \Pi(1 + b(t - 1)) \left[-(\tau + \beta q + \alpha)s_{11} \right] \left(\frac{1}{2}b^2t^2 - 2b^2t + 2bt + (b - 1)^2 \right), \\
 \tilde{E}_2(t) &= \left[\beta qs_{11} - (\vartheta + \alpha + (1 - \kappa)\tau)e_{11} \right] \left(\frac{1}{2}b^2t^2 - 2b^2t + 2bt + (b - 1)^2 \right), \\
 \tilde{I}_2(t) &= \left[\tau s_{11} + \tau(1 - \kappa)e_{11} - (\rho + \alpha + \nu)u_{11} \right] \left(\frac{1}{2}b^2t^2 - 2b^2t + 2bt + (b - 1)^2 \right), \\
 \tilde{R}_2(t) &= \left[\vartheta e_{11} + \nu u_{11} - \alpha r_{11} \right] \left(\frac{1}{2}b^2t^2 - 2b^2t + 2bt + (b - 1)^2 \right), \\
 \tilde{D}_2(t) &= \left[\rho u_{11} - \alpha d_{11} \right] \left(\frac{1}{2}b^2t^2 - 2b^2t + 2bt + (b - 1)^2 \right), \\
 \tilde{M}_2(t) &= \left[\sigma e_{11} + \zeta u_{11} - \varphi m_{11} \right] \left(\frac{1}{2}b^2t^2 - 2b^2t + 2bt + (b - 1)^2 \right).
 \end{aligned} \tag{20}$$

Correspondingly, the series solution for the next terms may be computed. Further, the unknown terms in the above equation (20) are as

$$\begin{aligned}
 s_{11} &= \Pi - (\tau + \beta q + \alpha)N_1, \\
 e_{11} &= \beta q N_1 - (\alpha + \vartheta + \tau(1 - \kappa))N_2, \\
 u_{11} &= \tau N_1 + \tau(1 - \kappa)N_2 - (\rho + \alpha + \nu)N_3, \\
 r_{11} &= \vartheta N_2 + \nu N_3 - \alpha N_4, \\
 d_{11} &= \rho N_3 - \alpha N_5, \\
 m_{11} &= \sigma N_2 + \zeta N_3 - \varphi N_6.
 \end{aligned} \tag{21}$$

5 Results and discussion

This particular section of the manuscript is devoted to the numerical simulations of the proposed model. Parameters of the model are assigned values given in Table 2 which are taken from [17]. The description of initial population of the compartments for the proposed model is $\tilde{S} = 220.89857$, $\tilde{E} = 220.812$, $\tilde{I} = 0.0008555$, $\tilde{R} = 0.00003208$, $\tilde{D} = 0.0007777$, $\tilde{M} = 80.000706$ million.

Parameters	values	Parameters	values
Π	0.80	β	0.000761
α	0.0080	τ	0.00073
ρ	0.00039	q	1
ϑ	0.00064	σ	0.0075
κ	0.5998	ζ	0.0023
φ	0.07862	ν	0.000236

Table 2. Parameter values used in numerical simulation

We simulate the six classes of the model under consideration for available data described in Table 2 using the series solution technique of Laplace transform. Figure 1 is the representation of the susceptible class showing sudden decay with the passing of time. This is due to the fact that various contaminated constituents of COVID-19 are absorbed by the said class and jump to the other classes of the system. At the early stage, they decrease and afterward the class becomes stable for distinct fractional-order b . Fractional order behavior is compared with integer order. In Figure 2 one can see the representation of exposed cases for different fractional-order b along with a comparison with integer-order. Like susceptible the exposed population also decreases as they transfer to other compartments. Figure 3 shows that the infection class reaches the maximum value. This class then slowly and gradually decreases and attains stability at various fractional orders. Due to the robust immunity and self-defense, there are

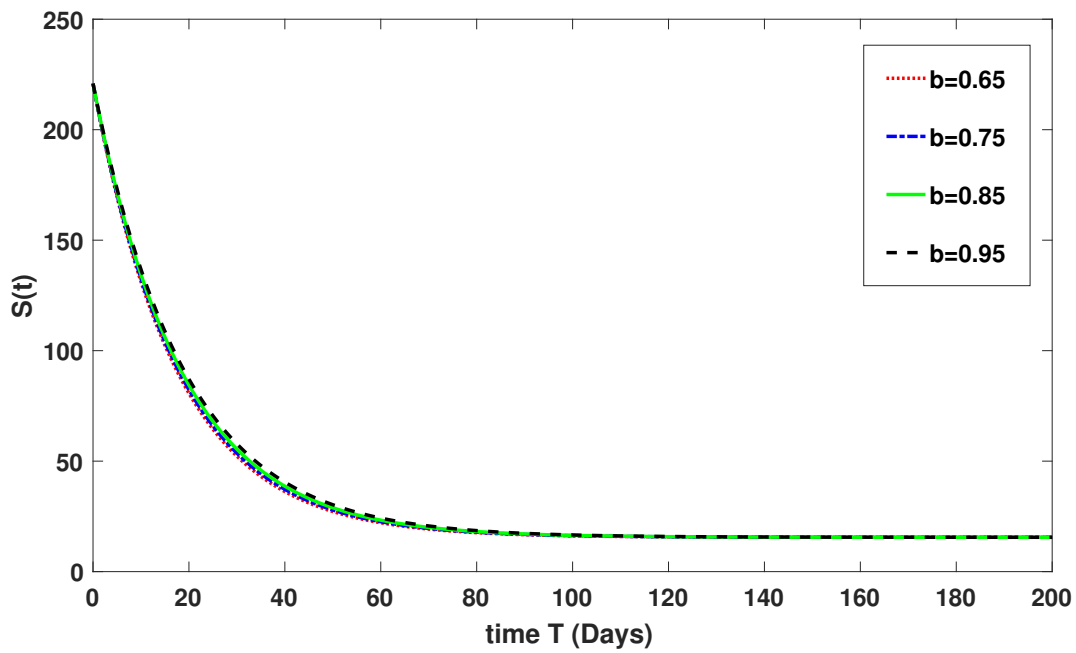


Figure 1. Dynamical behavior of \tilde{S} at various order b .

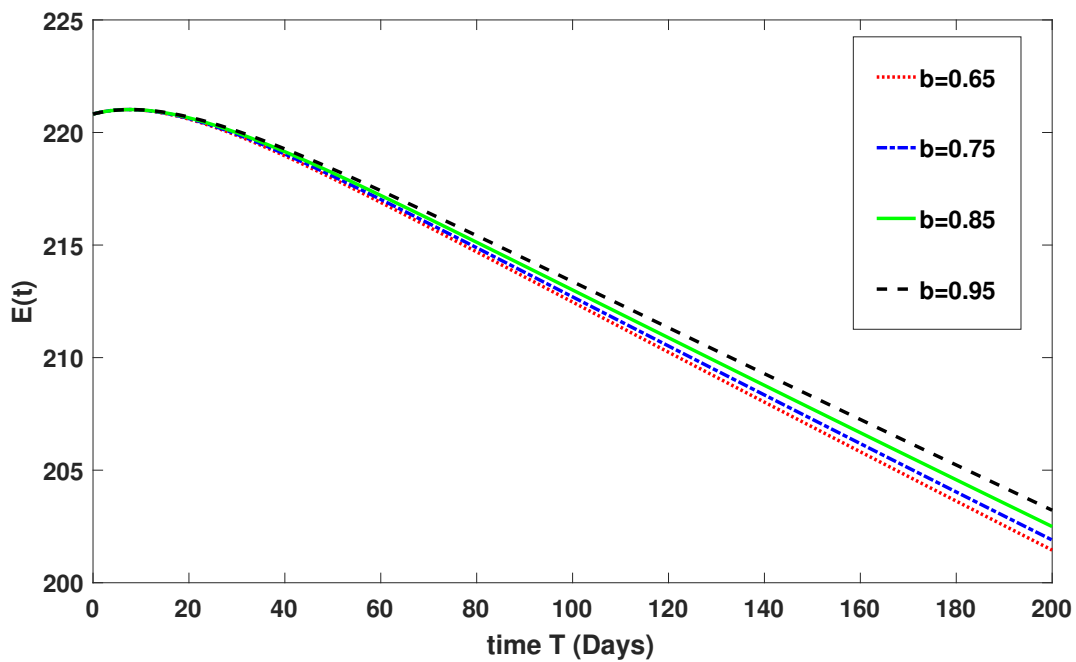


Figure 2. Dynamical behavior of \tilde{E} at various order b .

reductions and stability in the infection. Once more, we have provided an integer-order comparison. The recovery rate increases over time as the infection class increases. The maximum attained value for the recovered class is 1.5. After that, the recovery class also becomes stable as shown in Figure 4. We have observed in all the graphical representations that by increasing the values of fractional order, the dynamics will converge to the integer-order value 1. The stability was attained rapidly at low fractional-order and vice versa. Figure 5 represents the dynamics of demised class caused due to COVID-19. We note that the maximum value of this compartment is attained at 0.01. The class then declines and approaches the stability in distinct fractional orders. The decline

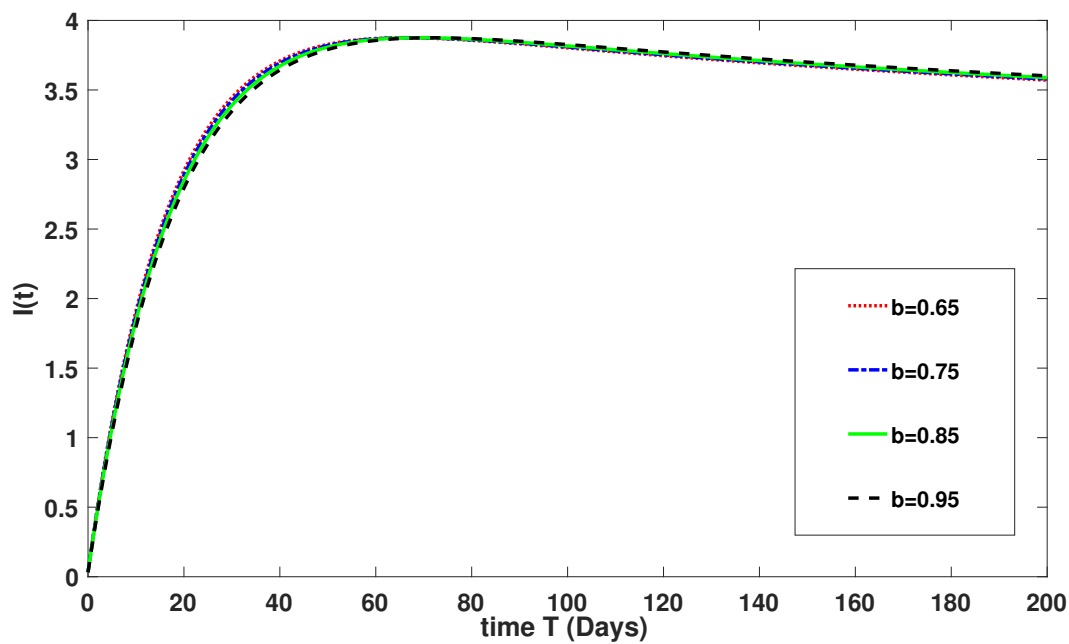


Figure 3. Dynamical behavior of \tilde{I} at various order b .

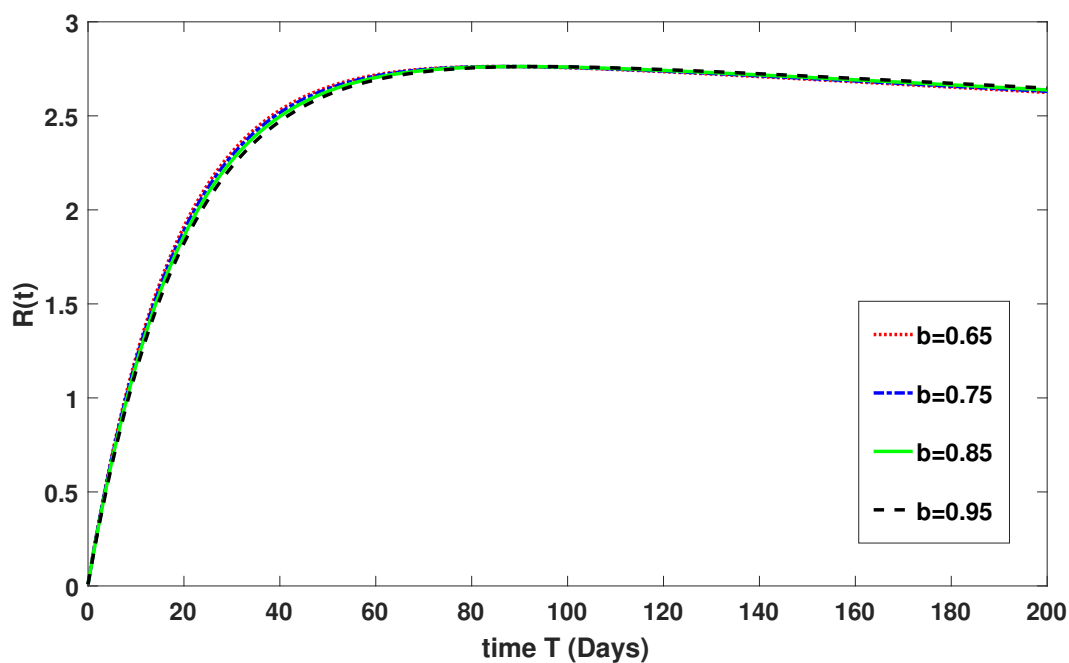


Figure 4. Dynamical behavior of \tilde{I} at various order b .

and stability gained in the demised class are due to the decrease in infection and the adoption of some precautionary measures for cleaning society. This obviously decreases the contaminated constituents $\tilde{M}(t)$ as depicted in Figure 6. In Figures 7–12, we take another set of initial data as $\tilde{S} = 220$, $\tilde{E} = 150.892$, $\tilde{I} = 0.4555$, $\tilde{R} = 0.013208$, $\tilde{D} = 0.7777$, $\tilde{M} = 80.000706$ million. The behavior of all six compartments is slightly changed and converging on different fractional orders. In this case, we also compare the dynamics of fractional orders with integer orders.

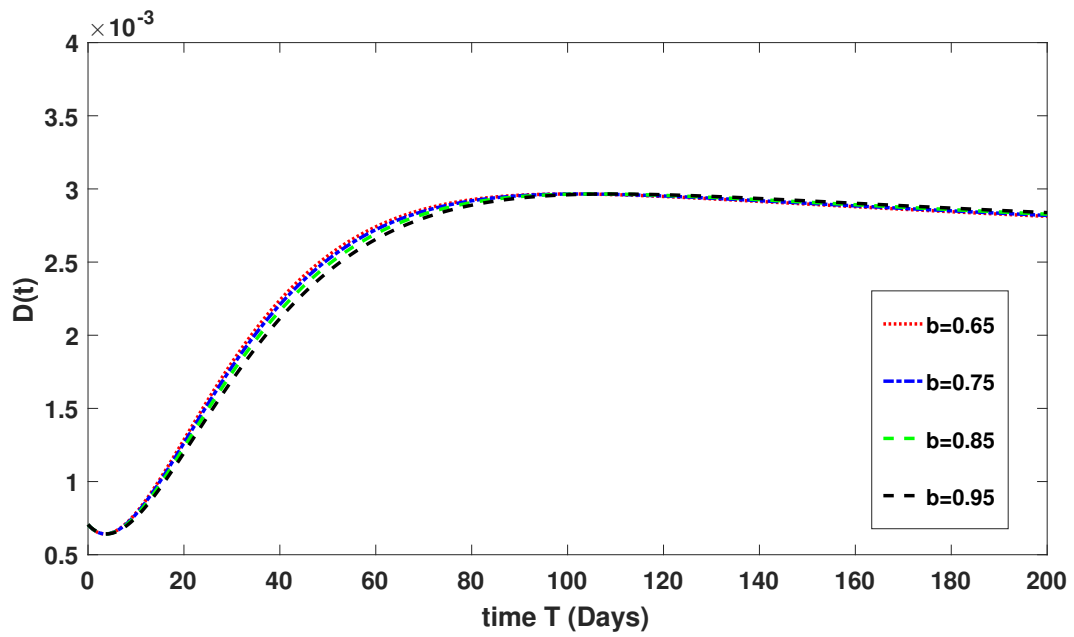


Figure 5. Dynamical behavior of \tilde{D} at various order b .

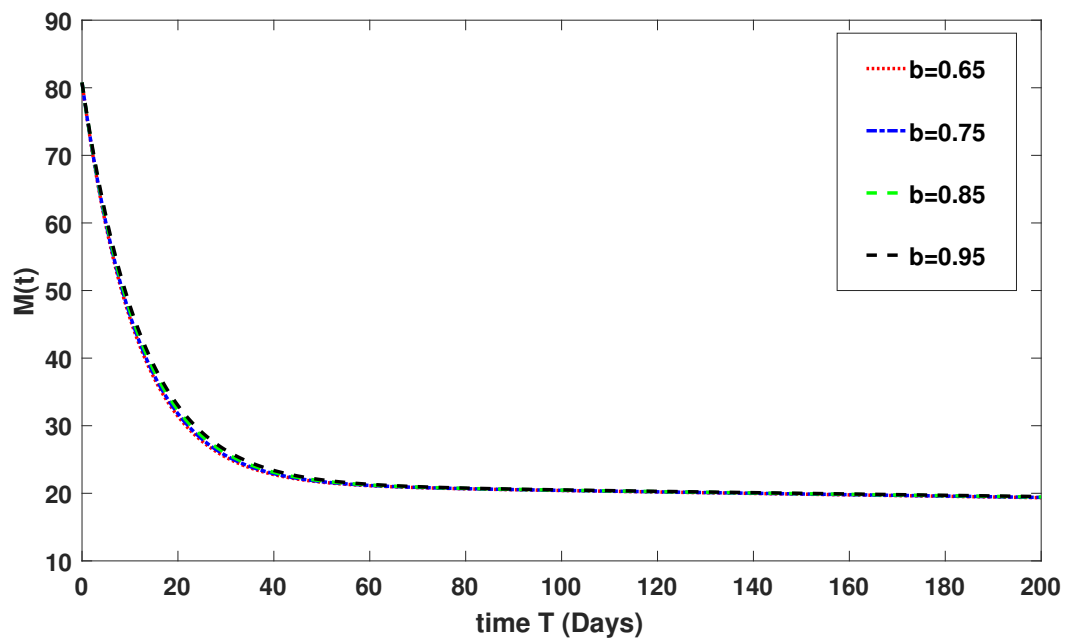


Figure 6. Dynamical behavior of \tilde{M} at various order b .

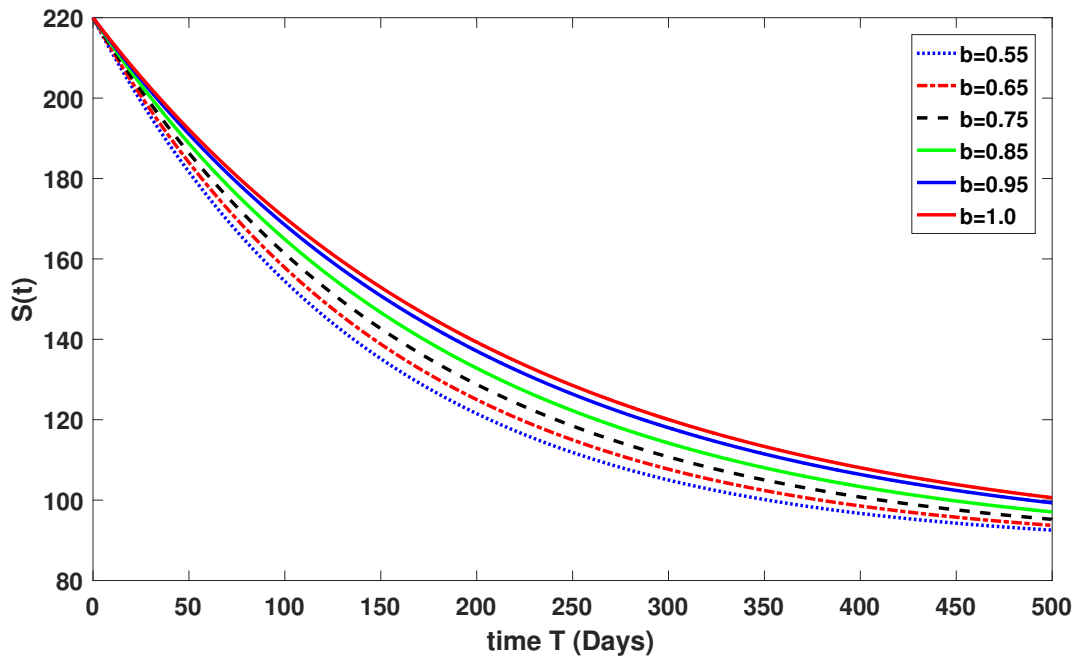


Figure 7. Dynamical behavior of \tilde{S} at various order b .

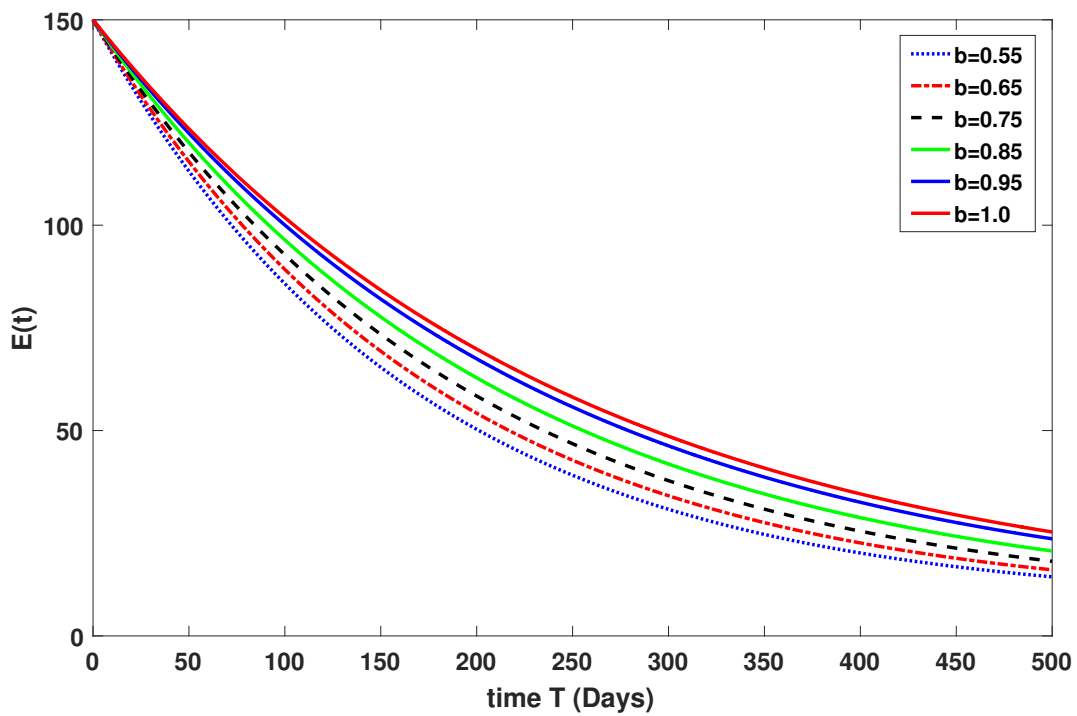


Figure 8. Dynamical behavior of \tilde{E} at various order b .

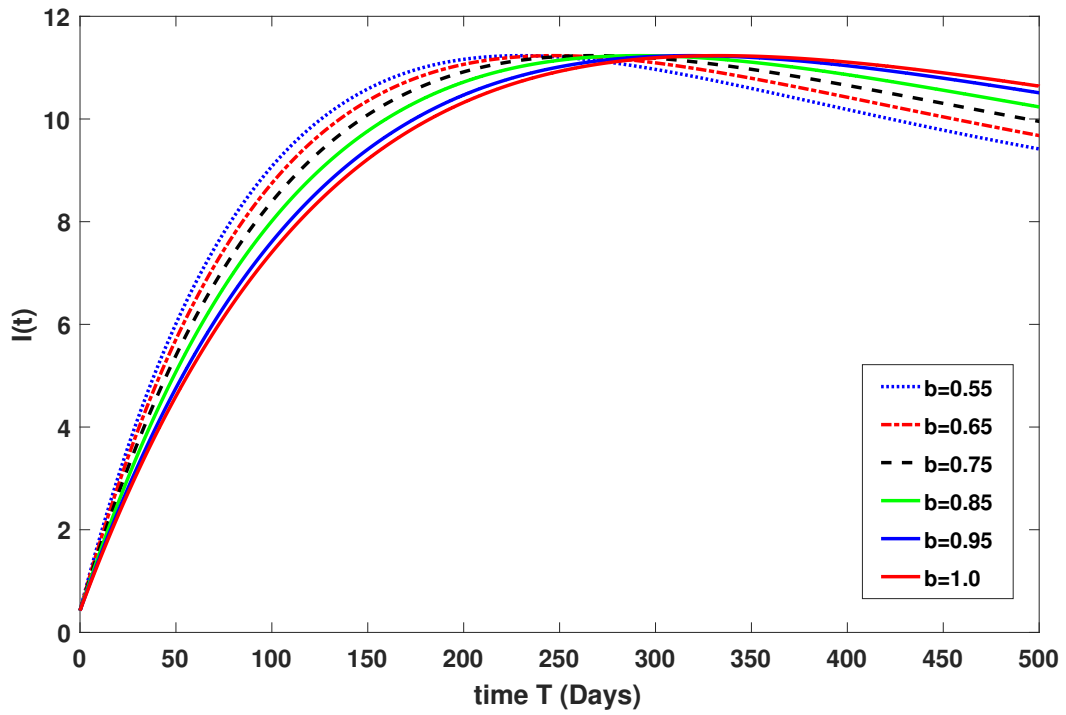


Figure 9. Dynamical behavior of \bar{I} at various order b .

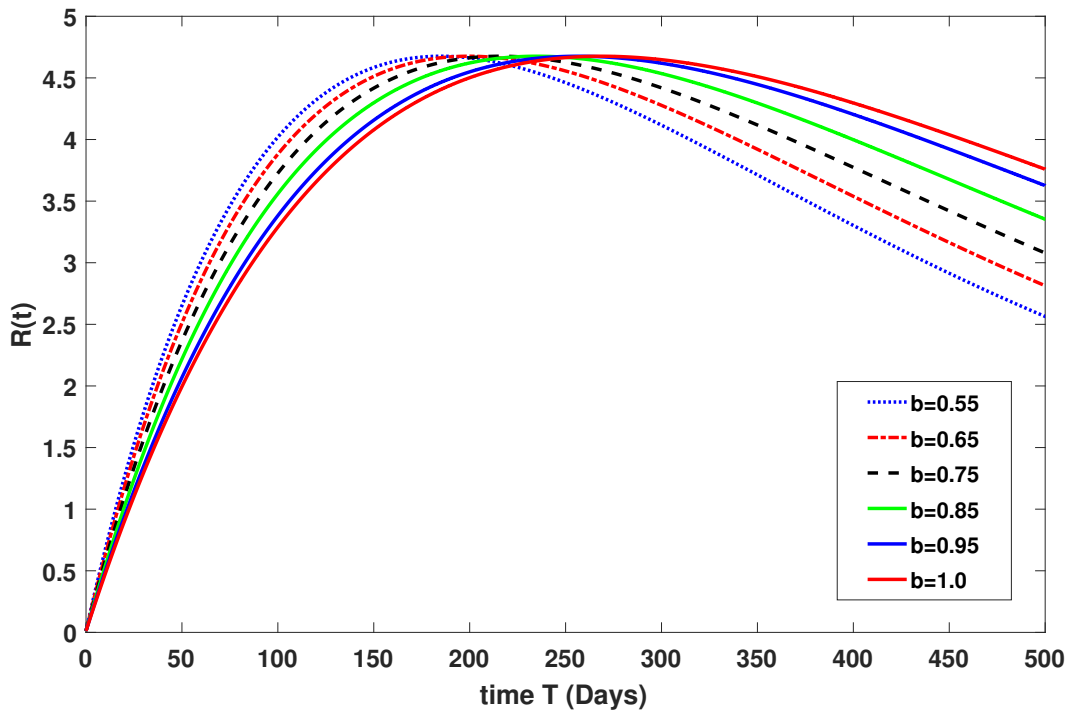


Figure 10. Dynamical behavior of \bar{R} at various order b .

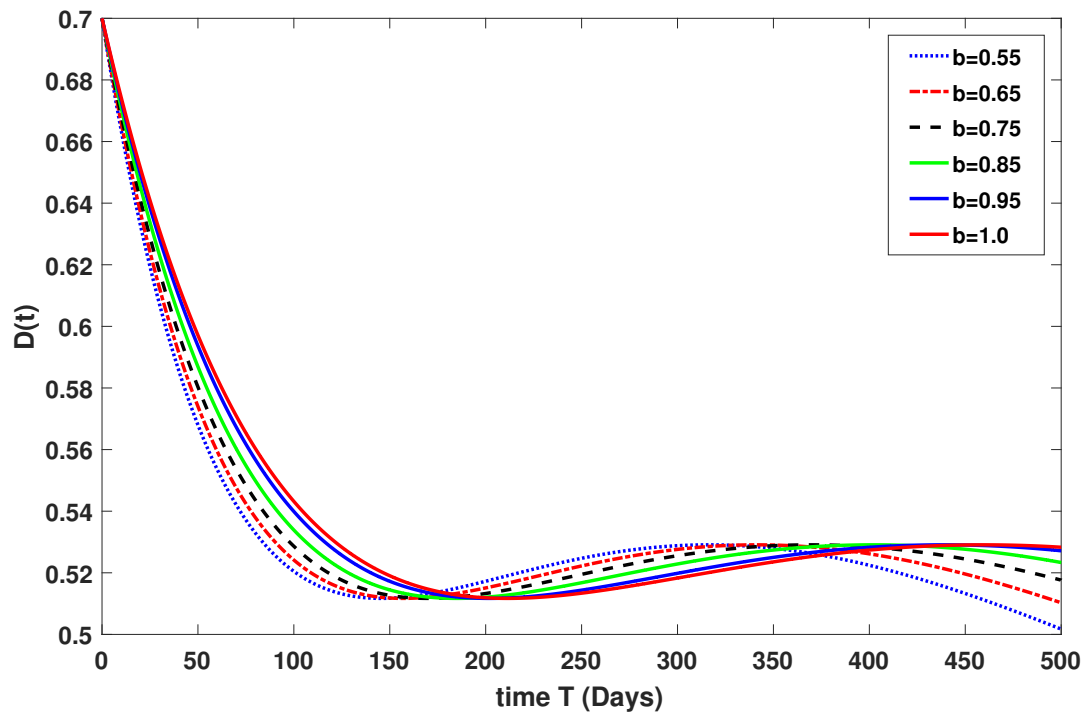


Figure 11. Dynamical behavior of \hat{D} at various order b .

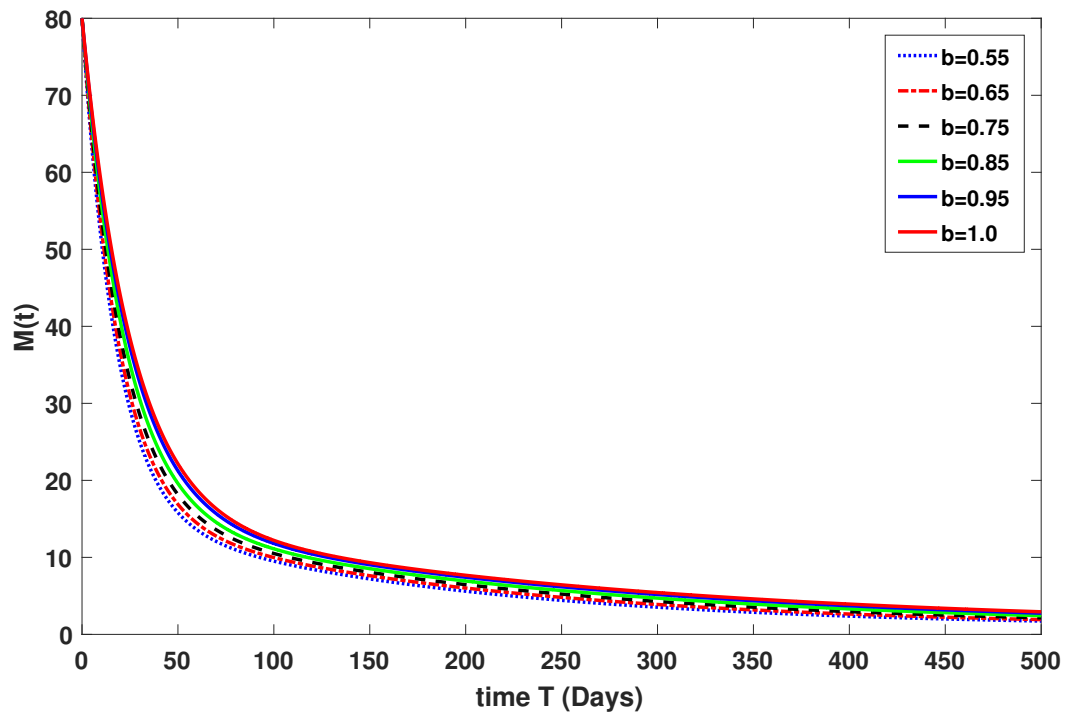


Figure 12. Dynamical behavior of \hat{M} at various order b .

6 Conclusion

In this paper, we have examined the dynamics of a fractionally-order modified non-linear SEIR type system using the Caputo-Fabrizio derivative operator of the non-singular kernel. Our study suggested a strategy to overcome the spread of COVID-19 and how to stabilize it. We have carried out the qualitative analysis with the help of the findings from the nonlinear functional analysis. The numerical solutions have been obtained with the aid of the Laplace transform of series solutions. All the small quantities are then added together to obtain an approximate solution for each quantity. The said technique has been simulated for the first few terms on different fractional orders along with a comparison with integer orders to validate the required scheme. This dynamic is caused by viruses or microorganisms present in the human body and throat, therefore, the nano-technical dynamics of the pandemic model are very effective in the sense of fractional derivative. Therefore, our study has strongly recommended that an individual strictly follow the SOPs of the WHO in order to control the spread of the infection. It is also essential to raise awareness and disseminate information in society in order to keep the populace safe from the virus and possibly prevent the infection from spreading to a pandemic level. Our research predicts the future spread and controls of the COVID-19 dynamics in the form of a fractional Caputo-Fabrizio derivative for dynamics ranging from 0 to 1.

Declarations

Consent for publication

Not applicable.

Conflicts of interest

The authors declare that they have no conflict of interest.

Funding

Not applicable.

Author's contributions

S.A.: Writing-Original Draft, Methodology, Formal Analysis. D.Q.: Software, Formal Analysis, Conceptualization. M.U.R.: Writing-Review & Editing, Methodology, Formal Analysis. All authors discussed the results and contributed to the final manuscript.

Acknowledgements

This work was supported by the National Natural Science Foundation of China (Grant no. 12171065).

References

- [1] World Health Organization, Coronavirus disease 2019 (COVID-19) Situation Report-62 https://www.who.int/docs/default-source/coronaviruse/situation-reports/20200322-sitrep-62-covid-19.pdf?sfvrsn=f7764c462_2020.
- [2] Lu, H., Stratton, C.W., & Tang, Y.W. Outbreak of pneumonia of unknown etiology in Wuhan, China: The mystery and the miracle. *Journal of Medical Virology*, 92(4), 401-402, (2020). [[CrossRef](#)]
- [3] Uçar, S. Analysis of hepatitis B disease with fractal-fractional Caputo derivative using real data from Turkey. *Journal of Computational and Applied Mathematics*, 419, 114692, (2023). [[CrossRef](#)]
- [4] Uçar, E., Özdemir, N., & Altun, E. Qualitative analysis and numerical simulations of new model describing cancer. *Journal of Computational and Applied Mathematics*, 422, 114899, (2023). [[CrossRef](#)]
- [5] Evirgen, F. Transmission of Nipah virus dynamics under Caputo fractional derivative. *Journal of Computational and Applied Mathematics*, 418, 114654, (2023). [[CrossRef](#)]
- [6] Özköse, F., Yavuz, M., Şenel, M.T., & Habbireeh, R. Fractional order modelling of omicron SARS-CoV-2 variant containing heart attack effect using real data from the United Kingdom. *Chaos, Solitons & Fractals*, 157, 111954, (2022). [[CrossRef](#)]
- [7] Joshi, H., Jha, B.K., & Yavuz, M. Modelling and analysis of fractional-order vaccination model for control of COVID-19 outbreak using real data. *Mathematical Biosciences and Engineering*, 20(1), 213-240, (2023). [[CrossRef](#)]
- [8] Allegrretti, S., Bulai, I.M., Marino, R., Menandro, M.A., & Parisi, K. Vaccination effect conjoint to fraction of avoided contacts for a Sars-Cov-2 mathematical model. *Mathematical Modelling and Numerical Simulation with Applications*, 1(2), 56-66, (2021). [[CrossRef](#)]
- [9] Haq, I.U., Ali, N., & Nisar, K.S. An optimal control strategy and Grünwald-Letnikov finite-difference numerical scheme for the fractional-order COVID-19 model. *Mathematical Modelling and Numerical Simulation with Applications*, 2(2), 108-116, (2022). [[CrossRef](#)]
- [10] He, F., Deng, Y., & Li, W. Coronavirus disease 2019: What we know?. *Journal of medical virology*, 92(7), 719-725, (2020). [[CrossRef](#)]
- [11] Tian, X., Li, C., Huang, A., Xia, S., Lu, S., Shi, Z., ... & Ying, T. Potent binding of 2019 novel coronavirus spike protein by a SARS coronavirus-specific human monoclonal antibody. *Emerging microbes & infections*, 9(1), 382-385, (2020). [[CrossRef](#)]
- [12] Riou, J., & Althaus, C.L. Pattern of early human-to-human transmission of Wuhan 2019 novel coronavirus (2019-nCoV), December 2019 to January 2020. *Eurosurveillance*, 25(4), 2000058, (2020). [[CrossRef](#)]

- [13] Li, B., Liang, H., & He, Q. Multiple and generic bifurcation analysis of a discrete Hindmarsh–Rose model. *Chaos, Solitons & Fractals*, 146, 110856, (2021). [[CrossRef](#)]
- [14] Eskandari, Z., Avazzadeh, Z., Khoshsiar Ghaziani, R., & Li, B. Dynamics and bifurcations of a discrete-time Lotka–Volterra model using nonstandard finite difference discretization method. *Mathematical Methods in the Applied Sciences*, (2022). [[Cross-Ref](#)]
- [15] Li, B., Liang, H., Shi, L., & He, Q. Complex dynamics of Kopel model with nonsymmetric response between oligopolists. *Chaos, Solitons & Fractals*, 156, 111860, (2022). [[CrossRef](#)]
- [16] Qu, H., Rahman, M.U., Wang, Y., Arfan, M., & Adnan. Modeling Fractional–Order Dynamics of Mers–Cov via Mittag–Leffler Law. *Fractals*, 30(1), 2240046, (2022). [[CrossRef](#)]
- [17] Mekonen, K.G., Habtemicheal, T.G., & Balcha, S.F. Modeling the effect of contaminated objects for the transmission dynamics of COVID-19 pandemic with self protection behavior changes. *Results in Applied Mathematics*, 9, 100134, (2021). [[CrossRef](#)]
- [18] Kilbas, A.A., Srivastava, H.M., & Trujillo, J.J. *Theory and applications of fractional differential equations* (Vol.204). Elsevier, (2006).
- [19] Samko, S.G., Kilbas, A.A., & Marichev, O.I. *Fractional integrals and derivatives: theory and applications* (Vol.1). Switzerland: Gordon and Breach Science Publishers, Yverdon, (1993).
- [20] Haq, I.U., Yavuz, M., Ali, N., & Akgül, A. A SARS–CoV-2 fractional–order mathematical model via the modified Euler method. *Mathematical and Computational Applications*, 27(5), 82, (2022). [[CrossRef](#)]
- [21] Ucar, S., Evirgen, F., Özdemir, N., & Hammouch, Z. Mathematical analysis and simulation of a giving up smoking model within the scope of non–singular derivative. *Proceeding of the Institute of Mathematics and Mechanics*, 48, 84–99, (2022). [[Cross-Ref](#)]
- [22] Uçar, E., Uçar, S., Evirgen, F., & Özdemir, N. A fractional SAIDR model in the frame of Atangana–Baleanu derivative. *Fractal and Fractional*, 5(2), 32, (2021). [[CrossRef](#)]
- [23] Hilfer, R. (Ed.). *Applications of fractional calculus in physics*. World scientific, (2000).
- [24] Uçar, S. Existence and uniqueness results for a smoking model with determination and education in the frame of non–singular derivatives. *Amer Inst Mathematical Sciences-AIMS*, 14(7), 2571–2589, (2021). [[CrossRef](#)]
- [25] Sene, N. Theory and applications of new fractional–order chaotic system under Caputo operator. *An International Journal of Optimization and Control*, 12(1), 20–38, (2022). [[CrossRef](#)]
- [26] Zhang, L., ur Rahman, M., Haidong, Q., & Arfan, M. Fractal–fractional Anthroponotic Cutaneous Leishmania model study in sense of Caputo derivative. *Alexandria Engineering Journal*, 61(6), 4423–4433, (2022). [[CrossRef](#)]
- [27] Caputo, M., & Fabrizio, M. A new definition of fractional derivative without singular kernel. *Progress in Fractional Differentiation & Applications*, 1(2), 73–85, (2015). [[CrossRef](#)]
- [28] Atangana, A., & Alkahtani, B.S.T. Analysis of the Keller–Segel model with a fractional derivative without singular kernel. *Entropy*, 17(6), 4439–4453, (2015). [[CrossRef](#)]
- [29] Koca, I. Analysis of rubella disease model with non–local and non–singular fractional derivatives. *An International Journal of Optimization and Control: Theories & Applications (IJOCTA)*, 8(1), 17–25, (2018). [[CrossRef](#)]
- [30] Baleanu, D., Mohammadi, H., & Rezapour, S. A mathematical theoretical study of a particular system of Caputo–Fabrizio fractional differential equations for the Rubella disease model. *Advances in Difference Equations*, 2020(1), 1–19, (2020). [[Cross-Ref](#)]
- [31] Abro, K.A., & Atangana, A. A comparative analysis of electromechanical model of piezoelectric actuator through Caputo–Fabrizio and Atangana–Baleanu fractional derivatives. *Mathematical Methods in the Applied Sciences*, 43(17), 9681–9691, (2020). [[CrossRef](#)]
- [32] Morales–Delgado, V.F., Gómez–Aguilar, J.F., Saad, K., & Escobar Jiménez, R.F. Application of the Caputo–Fabrizio and Atangana–Baleanu fractional derivatives to mathematical model of cancer chemotherapy effect. *Mathematical Methods in the Applied Sciences*, 42(4), 1167–1193, (2019). [[CrossRef](#)]
- [33] Chasreechai, S., Sitthiwiratham, T., El–Shorbagy, M.A., Sohail, M., Ullah, U., & ur Rahman, M. Qualitative theory and approximate solution to a dynamical system under modified type Caputo–Fabrizio derivative. *AIMS Mathematics*, 7(8), 14376–14393, (2022). [[CrossRef](#)]
- [34] Nisar, K.S., Ahmad, S., Ullah, A., Shah, K., Alrabaiah, H., & Arfan, M. Mathematical analysis of SIRD model of COVID-19 with Caputo fractional derivative based on real data. *Results in Physics*, 21, 103772, (2021). [[CrossRef](#)]
- [35] Ameen, I.G., Sweilam, N.H., & Ali, H.M. A fractional–order model of human liver: Analytic–approximate and numerical solutions comparing with clinical data. *Alexandria Engineering Journal*, 60(5), 4797–4808, (2021). [[CrossRef](#)]
- [36] Xu, C., Ur Rahman, M., Fatima, B., & Karaca, Y. Theoretical and numerical investigation of complexities in fractional–order chaotic system having torus attractors, *Fractals*, 30(07), 2250164, (2022). [[CrossRef](#)]
- [37] Shah, K., Ali, A., Zeb, S., Khan, A., Alqudah, M.A., & Abdeljawad, T. Study of fractional order dynamics of nonlinear mathematical model. *Alexandria Engineering Journal*, 61(12), 11211–11224, (2022). [[CrossRef](#)]
- [38] Shah, K., Jarad, F., & Abdeljawad, T. On a nonlinear fractional order model of dengue fever disease under Caputo–Fabrizio derivative. *Alexandria Engineering Journal*, 59(4), 2305–2313, (2020). [[CrossRef](#)]
- [39] Liu, X., ur Rahman, M., Ahmad, S., Baleanu, D., & Nadeem Anjam, Y. A new fractional infectious disease model under the non–singular Mittag–Leffler derivative. *Waves in Random and Complex Media*, 1–27, (2022). [[CrossRef](#)]
- [40] Rahman, M.U., Arfan, M., Deebani, W., Kumam, P., & Shah, Z. Analysis of time–fractional Kawahara equation under Mittag–Leffler Power Law. *Fractals*, 30(1), 2240021, (2022). [[CrossRef](#)]
- [41] Rahman, M.U., Althobaiti, A., Riaz, M.B., & Al–Duais, F.S. A theoretical and numerical study on fractional order biological models with Caputo–Fabrizio derivative. *Fractal and Fractional*, 6(8), 446, (2022). [[CrossRef](#)]
- [42] Rashid, S., Hammouch, Z., Aydi, H., Ahmad, A. G., & Alsharif, A.M. Novel computations of the time–fractional Fisher’s model via generalized fractional integral operators by means of the Elzaki transform. *Fractal and Fractional*, 5(3), 94, (2021). [[CrossRef](#)]
- [43] Losada, J., & Nieto, J.J. Properties of a new fractional derivative without singular kernel. *Progress in Fractional Differentiation & Applications*, 1(2), 87–92, (2015). [[CrossRef](#)]

Mathematical Modelling and Numerical Simulation with Applications (MMNSA) (<https://www.mmnsa.org>)



Copyright: © 2022 by the authors. This work is licensed under a Creative Commons Attribution 4.0 (CC BY) International License. The authors retain ownership of the copyright for their article, but they allow anyone to download, reuse, reprint, modify, distribute, and/or copy articles in MMNSA, so long as the original authors and source are credited. To see the complete license contents, please visit (<http://creativecommons.org/licenses/by/4.0/>).



RESEARCH PAPER

Mathematical modelling of a glucose–insulin system for type 2 diabetic patients in Chad

Adam Hassan Adoum^{1,†}, Mahamat Saleh Daoussa Haggar^{2,†} and Jean Marie Ntaganda^{3,‡,*}

¹Department of Mathematics, University Adam Barka d'Abeche, Faculty of Sciences and Techniques (FAST), Chad, ²Laboratory of Modeling, Mathematics, Computer Science, Applications and Simulation (L2MIAS), Department of Mathematics, Faculty of Exact and Applied Sciences, University of N'djamena, Chad, ³Department of Mathematics, College of Science and Technology, School of Science, University of Rwanda, Rwanda

*Corresponding Author

†adamhassan2009@yahoo.fr (Adam Hassan Adoum); msdhaggag@gmail.com (Mahamat Saleh Daoussa Haggar); jmnta@yahoo.fr (Jean Marie Ntaganda)

Abstract

In this paper, we focus on modelling the glucose–insulin system for the purpose of estimating glucagon, insulin, and glucose in the liver in the internal organs of the human body. A three-compartmental mathematical model is proposed. The model parameters are estimated using a nonlinear inverse optimization problem and data collected in Chad. In order to identify insulin and glucose in the liver for type 2 diabetic patients, the Sampling Importance Resampling (SIR) particle filtering algorithm is used and implemented through discretization of the developed mathematical model. The proposed mathematical model allows further investigation of the dynamic behavior of hepatic glucose, insulin, and glucagon in internal organs for type 2 diabetic patients. During periods of hyperglycemia (i.e., after meal ingestion), whereas insulin secretion is increased, glucagon secretion is reduced. The results are in agreement with empirical and clinical data and they are clinically consistent with physiological responses.

Key words: Mathematical model; Type 2 diabetes patients; glucose; insulin; estimation; internal organs

AMS 2020 Classification: 92B05; 37N25; 34A45; 65L05

1 Introduction

Diabetes is a disease that cannot be cured (chronic) but can be treated. It is due to an abnormal increase in glucose [1]. This disease has become a major world health problem, particularly in Chad. Like all developing countries, Chad is paying heavy consequences due to this disease. Chad, the second largest country and the third most overcrowded country in Central Africa, is in the midst of a transition from this disease [2]. According to the report of the International Diabetes Federation, 425 million people worldwide were living with the disease in 2015 and this number may increase to an estimated 622 million in 2040 [3]. In 2013, 231290 Chadians had diabetes [4], this number may be significant in the future. All these results make diabetes a real public health problem. There are two main types of diabetes: type 1 diabetes, which affects 10 percent of the affected population and type 2 diabetes, which affects the remaining percent [5, 6]. Type 2 diabetes is therefore important in terms of severity. Consequently, many researchers are trying to find methods to diagnose and treat this disease. Generally, disease dynamics is investigated throughout the application of the mathematical models [7, 8, 9]. One approach is to find a mathematical model that can describe

the dynamics of the glucose–insulin system in order to analyze, interpret and predict the results. One of the approaches used is to find a mathematical model capable of describing the dynamics of the glucose–insulin system in order to predict, analyze and interpret the results. In literature, much effort has been made recently to analyze [10] and to develop mathematical models of type 2 diabetes [11, 12, 13, 14]. The objective of this paper is to propose a mathematical model of the glucose–insulin system suitable for type 2 diabetic patients in Chad. The glucagon, insulin, and hepatic glucose in internal human organs are estimated using Sampling Importance Resampling (SIR) algorithm. The mathematical model parameters are estimated using a nonlinear inverse optimization problem and data collected in Chad.

This paper is structured as follows: Materials and methods are presented in Section 2. It deals with data sources and mathematical model equations. Section 3 focuses on the estimation of the parameters of the model. The numerical tests are given in Section 4 while concluding remarks are presented in Section 5.

2 Materials and methods

Data set

The data are collected in the laboratory of the hematology department at regional Abéché hospital in Chad for a period of one month from 23, January 2019 to end 23, February 2019. Moreover, 900 exams should be done, but we faced some challenge including lack of material such as glucose meter, lower number of enumerators and financial means to organize the transport of participants who live so far from the hospital to come early morning in a fasting state. Consequently, the data have been collected only for 96 participants and 75 among them have type 2 diabetes.

Model equations

More multiple pancreatic hormones are involved in glucose homeostasis [15], but the potent hormone regulators of both glucose appearance and disappearance in the circulation are insulin and glucagon. Indeed, insulin is the key regulatory hormone of glucose disappearance, and glucagon is a major regulator of glucose appearance. Consequently, the deficiency of these hormones is the main cause of type 2 diabetes. During the fed state, the rate of gastric emptying is the major determinant source of circulating glucose and other sources of how glucose appears in the circulation are derived from hepatic processes. Glucagon plays a major role in sustaining plasma glucose during fasting conditions by stimulating hepatic glucose production. During the first 8–12 hours of fasting, glucagon facilitates this process and thus promotes glucose appearance in the circulation throughout the glycogenolysis mechanism [16]. Over longer periods of fasting, glucose, produced by gluconeogenesis, glucose is released from the liver which is the sole source of endogenous glucose production. Most tissues have the ability to hydrolyze glycogen and glucose removal into skeletal muscle and adipose tissue is driven mainly by insulin in the immediate post–feeding state [16]. In addition, insulin contributes to augmenting glucose uptake in peripheral tissues and in the liver by affecting the activity of different enzymes. The peripheral insulin resistance and relative insulin deficiency in type 2 diabetic patients have resulted in low glucose uptake rates by muscle cells and adipose tissue cells [17]. The studies show that insulin-induced stimulation effects on hepatic glucose uptake and hepatic glucose production rate are impaired in type 2 diabetic patients. This leads to reduced hepatic glucose uptake [18]. A type 2 diabetic patient is experienced with postprandial β -cell action that becomes abnormal due to the loss of immediate insulin response to a meal [19]. Therefore, hyperglycemia in type 2 diabetic patients is caused by the resistance of peripheral insulin resistance coupled with progressive β -cell failure and decreased availability of insulin and other hormones that is amylin (a neuroendocrine hormone coexpressed and consecrated with insulin by pancreatic β -cells in response to nutrient stimuli, and GLP-1 (more potent incretin hormone secreted in greater concentrations and is more physiologically relevant in humans) [20]. Due to high glucose level that can induce vascular endothelial cell dysfunction and affect blood viscosity and arterial wall tension, type 2 diabetes patients are at higher risk for the development of vascular complications than non-diabetic persons [21]. Due to such a high demand for understanding the blood flow characteristics in type 2 diabetic patients, in this study, we develop the mathematical model of type 2 diabetes patients.

We propose a three-compartmental mathematical model where the compartments are the vascular and tissues compartment, liver compartment and pancreas compartment. The state variables are are glucagon (Γ), insulin (I_p), hepatic glucose (G_L), glucose (G). Taking into consideration the diagram model illustrated in Figure 1.

The model equations are as follows:

$$\begin{cases} V^\Gamma \frac{d\Gamma(t)}{dt} = n_\Gamma G^\alpha I_p - p_1 \Gamma, \\ V^{I_p} \frac{dI_p(t)}{dt} = n_{I_p} G^\delta - p_2 I_p, \\ V^{G_L} \frac{dG_L(t)}{dt} = n_{G_L} \Gamma^\beta - p_3 G_L + p_4 G + R_{PGL}, \\ V^G \frac{dG(t)}{dt} = p_3 G_L + n_G I_p^\gamma - p_5 G + R_{meal}, \end{cases} \quad (1)$$

where n_i denotes the rate of blood coming indirectly in compartment i ($i = \Gamma, I_p, G_L, G$) from vascular circulation. α, β, γ and δ are the constants to be estimated and refer to the non-linearity of the corresponding determinant variable. The parameters and variables are described in Table 1.

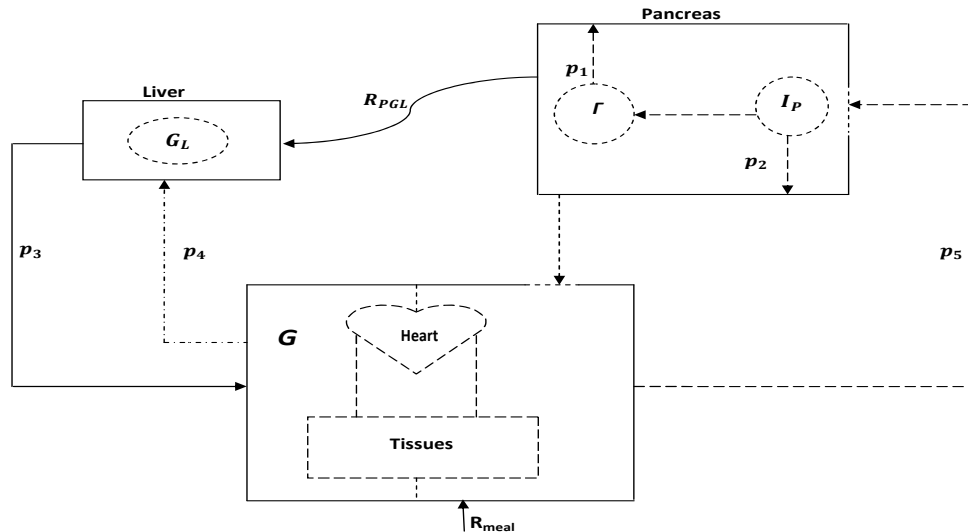


Figure 1. Diagram of the mathematical model. The dash lines notify that a certain quantity of mass flows non-linearly from one compartment/sub-compartment to another. The dashed dot line between the heart-tissues compartment means that a small quantity of glucose is transmitted to the liver compartment.

Parameter/Variable	Description	Unit
Variables		
Γ	Number of glucagon secreted by the α -cells to release glucose stored in the liver	pg/ml
I_p	Concentration of the insulin secreted by the beta (β)-cells and poured into blood to make penetrate and store in the liver the surplus of the glucose level found in the blood	$\mu U/dl$
G	Glucose concentration in the heart and tissues	mg/dl
G_L	Glucose concentration in the liver	mg/dl
Parameter to be estimated (Rate)		
n_Γ	Rate of blood coming to glucagon sub-compartment in the pancreas	$(dl)^2 / \mu U.min$
n_{I_p}	Rate of blood coming to insulin sub-compartment in the pancreas	dl. $\mu U/mg.min$
n_{G_L}	Rate of blood coming to in the liver	dl/min
n_G	Rate of blood in heart and tissues	$\mu U.mg/dl.min$
p_1	Rate of glucagon from the pancreas to the blood	dl/min
p_2	Rate of insulin from the pancreas to the blood	dl/min
p_3	Rate of glucose from the liver to the heart and tissues	dl/min
p_4	Rate of glucose from the blood to liver (Few quantity)	dl/min
p_5	Rate of glucose from the blood to pancreas	dl/min
R_{meal}	Rate of glucose in human body after meal	mg/min
R_{PGL}	Rate of insulin from pancreas to the blood through the liver	mg/min
Parameter from literature		
V^Γ	Volume of glucagon in glucagon sub-compartment	dl
V^{I_p}	Volume of insulin in insulin sub-compartment	dl
V^{G_L}	Volume of glucose in the liver compartment	dl
V^G	Volume of glucose in the heart and tissues	dl

Table 1. Description of variables and parameters of the mathematical model

3 Estimation of parameters

We consider that the volumes are obtained from literature and they are presented in Table 2 [14].

Parameter	Value	Parameter	Value
V^G	11.6	V^Γ	113.1
V^{G_L}	25.1	V^{I_p}	67.4

Table 2. Parameters used from the literature [14]

To estimate other parameters, let

$$\mu = (n_\Gamma, n_{I_p}, n_{G_L}, n_G, p_1, p_2, p_3, p_4, p_5, R_{meal}, \alpha, \beta, \gamma, \delta, R_{PGL})'$$

be a vector of parameters to be estimated. We fix a positive parameter and we consider the following discretisation of the interval

$[0, T_{\max}]$,

$$t_k = \frac{kT_{\max}}{N},$$

where T_{\max} denotes a positive time parameter. For a positive integer parameter N and $G^\sigma(t_k)$ corresponding data measurement of real values $G(t_k)$ at time t_k we take

$$\underline{G}^\sigma = (G^\sigma(t_1), \dots, G^\sigma(t_N))'. \tag{2}$$

The superscript σ is the perturbation parameter due to some imprecision on measured data [22]. The identification of parameters can be done by formulating nonlinear inverse problem which is solved using regularization techniques [23]. Let \underline{G} be vector solutions in \mathbb{R}^N at time grid points of the system (1) depending of the parameter vector u . We want to solve the coefficient identification problem

$$J(\mu) = \|\underline{G} - \underline{G}^\sigma\|^2,$$

where \underline{G}^σ is given by (2).

This inverse problem can be formulated as follows. Find $\mu^* = (n_\Gamma^*, n_p^*, n_{G_L}^*, n_G^*, p_1^*, p_2^*, p_3^*, p_4^*, p_5^*, R_{meal}^*, \alpha^*, \beta^*, \gamma^*, \delta^*, R_{PGL}^*)'$ such that

$$\mu^* = \arg \min_{\mu} J(\mu), \tag{3}$$

subject to (1). We should notify that the (3) is not linear inverse problem and it is ill-posed. This means that little perturbation on data produces a solution that is very different of the original ones. Furthermore, the solution μ does not depend continuously on the data. To find the regularization of the problem (3), we use Tikhonov techniques (See [23] for details). Therefore, this problem becomes Taking $\omega = (n_\Gamma, n_p, n_{G_L}, n_G, p_1, p_2, p_3, p_4, p_5, R_{meal}, \alpha, \beta, \gamma, \delta, R_{PGL})'$, find $\underline{\mu}^\theta$ solution of

$$J(\underline{\mu}^\theta) = \min_{\omega} J^\theta(\omega), \tag{4}$$

subject to (1) where we have set

$$J^\theta(\omega) = \|\underline{G} - \underline{G}^\sigma\|^2 + \theta \|\mathcal{L}\omega\|^2, \tag{5}$$

for good θ such that $\underline{\mu}^\theta$ converges to the solution $\underline{\mu}$ as $\theta \rightarrow 0$. Here \mathcal{L} is an operator used for stabilization (i.e., \mathcal{L} is the identity, a differentiation operator, etc.). The solution of (4) subject to (1) is obtained using the Least square method and the data collected in Chad. The numerical simulations are carried out using Matlab built-in function *fmincon* which allows solving constrained optimization problems. The parameters estimated are shown in Table 3.

Estimated parameter	Value
n_Γ	0.6005
n_p	1.1938
n_{G_L}	1.3845
n_G	0.5479
p_1	1.0343
p_2	1.5477
p_3	1.3693
p_4	0.7866
p_5	1.9521
R_{meal}	101.4078
α	0.0506
β	0.5151
γ	0.0545
δ	0.0505
R_{PGL}	0.5539

Table 3. Estimated model parameters

4 Numerical tests

The measurement of glucose and insulin from different parts of the body needs to take blood samples to determine their concentration. However, to take blood samples from many internal body organs for instance heart and the liver is clinically impossible. We solve this problem, we can estimate concentrations of these parameters using measurements from peripheral tissues along with a mathematical model and a filtering algorithm. Sampling Importance Resampling (SIR) algorithm is one of the methods that can give the estimated solution. For more details about the SIR algorithm, we refer the readers to [24, 25]. The data collected

in Chad is the glucose measured in the tissues of patients. In our simulation we estimate glucose in the liver, insulin and glucagon in the pancreas by taking this measured glucose as measurements. We assume that noisy measurements of glucose in tissues and the heart are available measured data. To apply the SIR algorithm, we consider a fixed-step backward difference approximation by

$$\frac{dX}{dt} \approx \frac{X_k - X_{k-1}}{\Delta t}, \quad 0 \leq t \leq T_{\max}, \tag{6}$$

where

$$X_k = (\Gamma_k, I_{p,k}, G_{L,k}, G_k)^t, \tag{7}$$

and

$$X_k = X(t_k).$$

If M denotes the total number of discretization intervals we have

$$X_k = X_{k-1} + \Delta t,$$

where $\Delta t = \frac{T_{\max}}{M}$ is step.

Let set

$$F_{k-1}(X_{k-1}) = (F_1(X_{k-1}), F_2(X_{k-1}), F_3(X_{k-1}), F_4(X_{k-1}))^t,$$

which refers to the dynamic equations with

$$\begin{aligned} F_1(X_{k-1}) &= \left(1 - \frac{\Delta t}{V\Gamma} p_1\right) \Gamma_{k-1} + \frac{\Delta t}{V\Gamma} n_{\Gamma} G_{k-1}^{\alpha} I_{p,k-1}, \\ F_2(X_{k-1}) &= \left(1 - \frac{\Delta t}{V I_p} p_1\right) I_{p,k-1} + \frac{\Delta t}{V I_p} n_{I_p} G_{k-1}^{\delta}, \\ F_3(X_{k-1}) &= \left(1 - \frac{\Delta t}{V G_L} p_3\right) G_{L,k-1} + \frac{\Delta t}{V G_L} (n_{G_L} \Gamma_{k-1}^{\beta} + p_4 G_{k-1} + R_{PGL}), \\ F_4(X_{k-1}) &= \left(1 - \frac{\Delta t}{V G} p_5\right) G_{k-1} + \frac{\Delta t}{V G} (p_3 G_{L,k-1} + n_G I_{p,k-1}^{\gamma} + R_{meal}). \end{aligned} \tag{8}$$

Using (8) our state dynamic model (1) is estimated recursively by the following compact form

$$\begin{cases} X_k = F_{k-1}(X_{k-1}) + v_{k-1}, \\ Y_k = P X_k + e_{k-1}, \end{cases} \tag{9}$$

where we set $Y_k = G_k$ that is measurement of glucose in tissues, v_{k-1} and e_{k-1} are the stochastic process and measurement noise, respectively and they are independent and identically distributed (i.i.d.). P denotes the matrix from the equations modelling the sensors referred to as the measurement model given as

$$P = (0, 0, 0, 1)^t.$$

In numerical simulation, we consider $M = 100$, $T_{\max} = 300$ minutes, $N = 1000$ particles and we assume that the state X_0 and state measurement noises have a Gaussian probability density function that is $X_0 \sim \mathcal{N}(0, 5)$, $v_k \sim \mathcal{N}(0, 20)$ and $e_k \sim \mathcal{N}(0, 1)$ where \mathcal{N} means normal distribution. The numerical results are illustrated in the Figure 2, 3 and 4.

Figure 2 shows the concentration of glucagon in the pancreas using SIR implemented on the mathematical model. There is not a significant variation of this parameter that plays a crucial role in the regulation of blood glucose. This means that blood glucose is not regulated for a type 2 diabetic patient. The pancreatic insulin decreases as shown in the Figure 3. Therefore, there is no role of both insulin and glucagon as regulators of blood glucose. During periods of hyperglycemia (i.e., after meal ingestion), whereas insulin secretion is increased, glucagon secretion is reduced. All those results are justified by the increase of glucose in the liver (See Figure 4). Hence, the liver affects insulin concentrations, since about 50% of insulin is extracted at first passage, and this fraction may be reduced in the insulin-resistant liver, leading to hyperinsulinemia [26]. The elevated rate of hepatic glucose production (HGP) is a major cause of fasting hyperglycemia and a lack of suppression of HGP may contribute to postprandial hyperglycemia. Through an increased secretion of triglyceride, the liver may also contribute to peripheral insulin resistance and thereby further increase postprandial hyperglycemia [26].

5 Concluding remarks

The mechanical behaviour of the glucose–insulin system depends on the type of mathematical model that describes its dynamics. The simple mathematical model should describe accurately this system vis-a-vis the diseases that affect it. In this work, we have proposed a three-compartmental mathematical model for type 2 diabetic patients that describes the variation of glucose and insulin in Chad context based on data collected at Abéché hospital. To estimate the dynamics of glucagon, insulin and hepatic glucose in internal organs of the human body, the Sampling Importance Resampling (SIR) particle filtering algorithm is used and implemented using the developed mathematical model. Numerical results show that the new glucose–insulin system model

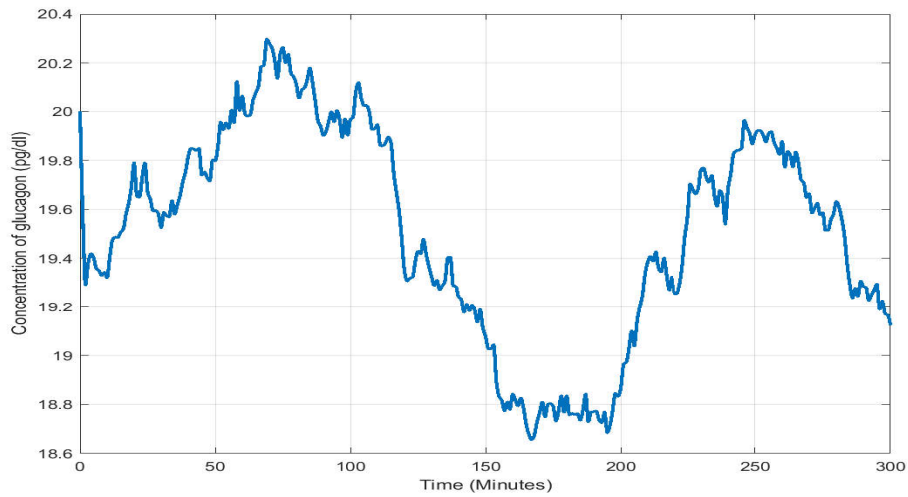


Figure 2. Variation of glucagon in the pancreas

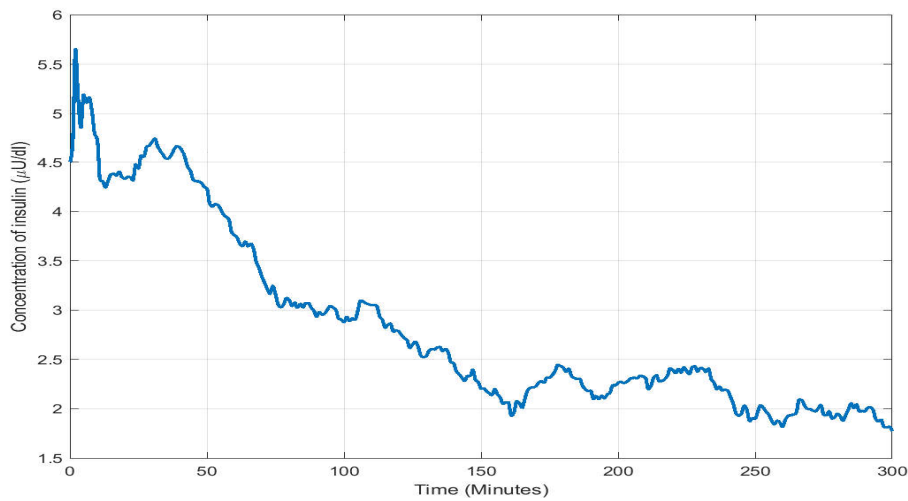


Figure 3. Variation of insulin in the pancreas

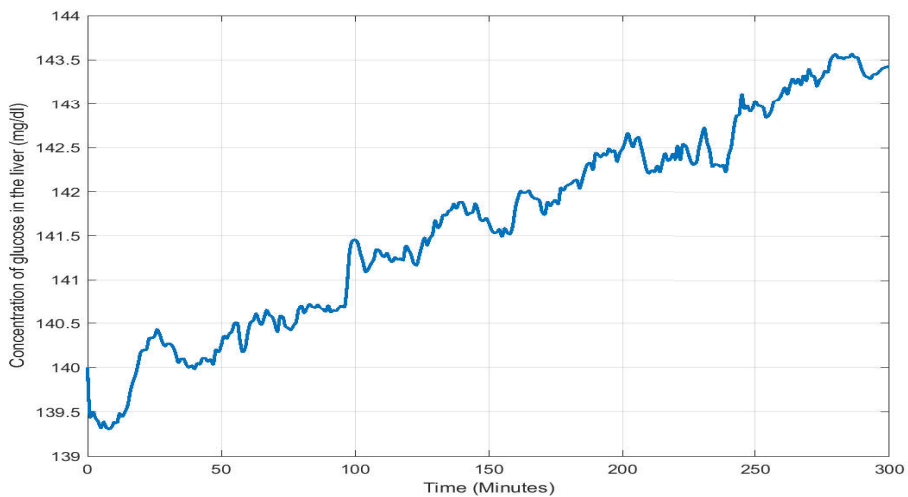


Figure 4. Variation of glucose in the liver

introduced fits with the clinical data and they are clinically consistent with physiological responses. Indeed, insulin secretion increases while glucagon secretion reduces due to periods of hyperglycemia. The proposed mathematical model can also be used by physiologists and other experts in medicine for monitoring the glucose-insulin system.

Declarations

Consent for publication

Not applicable.

Conflicts of interest

The authors declare that they have no conflict of interest.

Funding

Not applicable.

Author's contributions

A.H.A.: Conceptualization, Investigation, Methodology, Software, Writing – Original Draft, M.S.D.H.: Investigation, Methodology, Writing – Original Draft, J.M.N.: Methodology, Supervision, Validation, Writing – Review and Editing. All authors discussed the results and contributed to the final manuscript.

Acknowledgements

Not applicable.

References

- [1] Tolić, I.M., Mosekilde, E., & Sturis, J. Modeling the insulin–glucose feedback system: the significance of pulsatile insulin secretion. *Journal of Theoretical Biology*, 207(3), 361–375, (2000). [[CrossRef](#)]
- [2] <https://fr.wikipedia.org/wiki/Afriquecentrale>, 2022, Access Date: 15th May 2022.
- [3] International Diabetes Federation (IDF), Atlas, Seventh edition, 2015, Access Date: 15th May 2022.
- [4] International Diabetes Federation (IDF), Atlas, Sixth edition, 2013, Access Date: 5th June 2022.
- [5] <https://www.diabete.qc.ca/fr/comprendre-le-diabete/tout-sur-le-diabete/types-de-diabete/le-diabete-de-type-2>, Access Date: 5th June 2022.
- [6] Lin, C.W. Modeling glucose–insulin kinetics and development of type 2 diabetes in offspring of diabetic parents. Ph.D. Thesis, University of Iowa, (2011). [[CrossRef](#)]
- [7] Joshi, H., & Jha, B. K. Chaos of calcium diffusion in Parkinson's infectious disease model and treatment mechanism via Hilfer fractional derivative. *Mathematical Modelling and Numerical Simulation with Applications*, 1(2), 84–94, (2021). [[CrossRef](#)]
- [8] Joshi, H., Jha, B.K., & Yavuz, M. Modelling and analysis of fractional-order vaccination model for control of COVID-19 outbreak using real data. *Mathematical Biosciences and Engineering*, 20(1), 213–240, (2023). [[CrossRef](#)]
- [9] Durai, P., Xavier, F., Zubair, B., & Fuqian, S. Fractional Reaction–Diffusion Model for Parkinson's Disease. In: Pandian, D., Fernando, X., Baig, Z., Shi, F. (eds) Proceedings of the International Conference on ISMAC in Computational Vision and Bio-Engineering 2018 (ISMAC-CVB). ISMAC 2018. Lecture Notes in Computational Vision and Biomechanics, vol 30. Springer, Cham. [[CrossRef](#)]
- [10] Uçar, S., Özdemir, N., Koca, İ., & Altun, E. Novel analysis of the fractional glucose–insulin regulatory system with non-singular kernel derivative. *The European Physical Journal Plus*, 135(5), 414, (2020). [[CrossRef](#)]
- [11] Vahidi, O., Kwok, K.E., Gopaluni, R.B., & Sun, L. Development of a physiological model for patients with type diabetes mellitus. In Proceedings of 2010, *American Control Conference*, pp.2027–2032, Mariott Waterfront, Baltimore, MD, USA, (2010). [[CrossRef](#)]
- [12] Vahidi, O. Dynamic Modeling of Glucose Metabolism for the Assessment of Type II Diabetes Mellitus. Ph.D. Thesis, The University of British Columbia, (2013).
- [13] Vahidi, O., Kwok, K.E., Gopaluni, R.B., & Sun, L. Developing a physiological model for type II diabetes mellitus. *Biochemical Engineering Journal*, 55(1), 7–16, (2011). [[CrossRef](#)]
- [14] Sorensen, J.T. A physiologic model of glucose metabolism in man and its use to design and assess improved insulin therapies for diabetes. Ph.D. Thesis, USA: Massachusetts Institute of Technology, (1985).
- [15] Moore, C.X., & Cooper, G.J. Co-secretion of amylin and insulin from cultured islet β -cells: modulation by nutrient secretagogues, islet hormones and hypoglycemic agents. *Biochemical and Biophysical Research Communications*, 179(1), 1–9, (1991). [[CrossRef](#)]
- [16] Aronoff, S.L., Berkowitz, K., Shreiner, B., & Want, L. Glucose metabolism and regulation: beyond insulin and glucagon. *Diabetes Spectrum*, 17(3), 183–190, (2004). [[CrossRef](#)]
- [17] Basu, A., Basu, R., Shah, P., Vella, A., Johnson, C.M., Nair, K.S., Jensen, M.D., Schwenk, W.F. & Rizza, R.A. Effects of type 2 diabetes on the ability of insulin and glucose to regulate splanchnic and muscle glucose metabolism: evidence for a defect in hepatic glucokinase activity. *Diabetes*, 49(2), 272–283, (2000). [[CrossRef](#)]
- [18] Iozzo, P., Hallsten, K., Oikonen, V., Virtanen, K.A., Kemppainen, J., Solin, O., Ferrannini, E., Knuuti, J., & Nuutila, P. Insulin-mediated hepatic glucose uptake is impaired in type 2 diabetes: evidence for a relationship with glycemic control. *The Journal of Clinical Endocrinology & Metabolism*, 88(5), 2055–2060, (2003). [[CrossRef](#)]

- [19] Kahn, S.E. The importance of the beta cell in the pathogenesis of type 2 diabetes mellitus. *The American Journal of Medicine*, 108(6), 2–8, (2000). [[CrossRef](#)]
- [20] Toft-Nielsen, M.B., Damholt, M.B., Madsbad, S., Hilsted, L.M., Hughes, T.E., Michelsen, B.K., & Holst, J.J. Determinants of the impaired secretion of glucagon-like peptide-1 in type 2 diabetic patients. *The Journal of Clinical Endocrinology & Metabolism*, 86(8), 3717–3723, (2001). [[CrossRef](#)]
- [21] Igari, K., Kudo, T., Uchiyama, H., Toyofuku, T., & Inoue, Y. Quantitative evaluation of microvascular dysfunction in peripheral neuropathy with diabetes by indocyanine green angiography. *Diabetes Research and Clinical Practice*, 104(1), 121–125, (2014). [[CrossRef](#)]
- [22] Ntaganda, J.M., Niyobuhungiro, J., Banzi, W., Mpinganzima, L., Minani, F., Gahutu, J.B., Dusabejambo, V., & Kambutse, I. Mathematical modelling of human cardiovascular-respiratory system responses to exercise in Rwanda. *International Journal of Mathematical Modelling and Numerical Optimisation*, 9(3), 287–308, (2019). [[CrossRef](#)]
- [23] Hanke, M. (2000). Iterative regularization techniques in image reconstruction. In *Surveys on solution methods for inverse problems* (pp. 35–52). Springer, Vienna. [[CrossRef](#)]
- [24] Arulampalam, M.S., Maskell, S., Gordon, N., & Clapp, T. A tutorial on particle filters for online nonlinear/non-Gaussian Bayesian tracking. *IEEE Transactions on Signal Processing*, 50(2), 174–188, (2002). [[CrossRef](#)]
- [25] Doucet, A., Godsill, S., & Andrieu, C. On sequential Monte Carlo sampling methods for Bayesian filtering. *Statistics and Computing*, 10(3), 197–208, (2000). [[CrossRef](#)]
- [26] Staehr, P., Hother-Nielsen, O., & Beck-Nielsen, H. The role of the liver in type 2 diabetes. *Reviews in Endocrine & Metabolic Disorders*, 5(2), 105–110, (2004). [[CrossRef](#)]

Mathematical Modelling and Numerical Simulation with Applications (MMNSA) (<https://www.mmnsa.org>)



Copyright: © 2022 by the authors. This work is licensed under a Creative Commons Attribution 4.0 (CC BY) International License. The authors retain ownership of the copyright for their article, but they allow anyone to download, reuse, reprint, modify, distribute, and/or copy articles in MMNSA, so long as the original authors and source are credited. To see the complete license contents, please visit (<http://creativecommons.org/licenses/by/4.0/>).